

Providing Bipartite GNN Explanations with PGExplainer

Tristan Marten Lewin Schulz

Bachelor of Science

May 19, 2025

Supervisors:
Prof. Dr. Stefan Harmeling
Lukas Schneider

Artificial Intelligence (VIII)
Department of Computer Science
TU Dortmund University

Abstract

The recent advances in deep learning (DL) have lead to machine learning (ML) approaches for solving the boolean satisfiability problem (SAT), commonly represented as a bipartite graph problem, with NeuroSAT being a prominent example utilizing a graph neural network (GNN). However, models like these often suffer from a lack of natural proofs or explanations of their predictions, hindering the trustworthiness as well as practical cross-domain applicability. In this work, we explore a method that provides instance explanations with a global view of the GNN, thus seeking to generally explain a model's predictions. We reimplement the parameterized explainer for graph neural networks (PGExplainer) using PyTorch Geometric, testing its generalizability in the inductive setting and extending it to the domain of NeuroSAT.

While our replication showed that the framework succeeds in generating inductive explanations for structurally similar node instances, it struggles with generalizing these across different node instances of a motif. At the same time, general explanations for graph instances showed promising results. To apply the PGExplainer on NeuroSAT and generate explanations for SAT instances, we interpret unsatisfiable SAT instances using minimal unsatisfiable subsets (MUSes) - small unsatisfiable cores - as ground truth (GT). Though we were unable to generate favorable explanations that consistently align with these, our findings indicate potential measures for future work and highlight the need for more robust and generalizable methods.

Contents

Abstract	iii
List of Figures	vii
List of Tables	ix
List of Acronyms	xi
1 Introduction	1
2 Theoretical Background	3
2.1 Deep Learning	3
2.2 Graph Theory	9
2.3 Information Theory	11
2.4 Graph Neural Networks	13
2.5 Boolean Satisfiability Problem	17
3 Related Work	20
3.1 Explainability in GNNs	20
3.2 Explainer Models	23
3.3 Graph Model Lacking Explanations	24
4 Methodology	25
4.1 Theoretical Foundations of PGExplainer	25
4.2 Extension to Application on NeuroSAT	32
4.3 Implementation Details	34
5 Experiments and Results	46
5.1 Replication of PGExplainer	46
5.2 Generating Bipartite Explanations for NeuroSAT	59
6 Discussion	64
6.1 Generalizability of PGExplainer	64
6.2 Explanations for Unsatisfiable SAT Problems	64

7 Conclusion	66
Bibliography	67
A Supplementary Material	73
A.1 Material from original PGExplainer	73
A.2 Data Visualization	75
A.3 Replication Hyperparameter Searches	76
A.4 Multiple Explanation Visualizations	79
A.5 NeuroSAT Explainer Hyperparameter Searches	85
A.6 Satisfiability of a Hard Constraint Explanation	86
Affidavit	88

List of Figures

2.1	A simple MLP with one hidden layer	5
2.2	Example of an undirected graph	11
2.3	Example of a bipartite graph	11
2.4	Common applications of GNNs	14
2.5	k -hop neighborhood visualization	16
2.6	Message passing	18
2.7	Bipartite graph in LCG	19
3.1	General pipeline of perturbation-based explainability methods	22
4.1	Black-box target model in PGExplainer context	29
4.2	Pipeline of PGExplainer	31
4.3	Visualization of used target models	38
5.1	The different motifs used in the datasets	48
5.2	Validation metrics for Tree-Cycles	53
5.3	Validation metrics for BA-2Motif	56
5.4	Explanations for a singular instance of each dataset.	59
5.5	Visualization of the best soft constraint explanation	61
5.6	Visualization of the best hard constraint explanation	63
A.1	Visualization of original PGExplainer datasets	75
A.2	Grid of BA-Shapes explanations (top-6 edges)	79
A.3	Grid of BA-Community explanations (top-6 edges)	80
A.4	Grid of Tree-Cycles explanations (top-6 edges)	81
A.5	Grid of Tree-Grid explanations (top-6 edges)	82
A.6	Grid of BA-2Motif explanations (top-6 edges)	83
A.7	Grid of MUTAG explanations (top-6 edges)	84
A.8	Grid search results of soft constraint explainer	86

List of Tables

5.1	Statistics of PGExplainer datasets	48
5.2	Statistics of motif instances per dataset	49
5.3	Accuracies of adapted target GNN	50
5.4	Optimal explainer parameter values for all replication datasets	52
5.5	Baseline PGExplainer and RE-PGExplainer	52
5.6	Inductive performance of our reimplementation	54
5.7	Collective performance of our reimplementation	55
5.8	Inductive performance with more training instances	55
5.9	Inductive performance on BA-2Motif with inverted ground truth	56
5.10	Statistics of adapted motif node instances	57
5.11	Inductive performance using all motif nodes for training	58
5.12	Inductive performance using one motif node for training	58
5.13	Inductive performance of PGExplainer on NeuroSAT	62
A.1	Accuracies of original GNN downstream task	74
A.2	BA-Shapes grid search	76
A.3	BA-Community grid search	76
A.4	Tree-Cycles grid search	77
A.5	Tree-Grid grid search	77
A.6	BA-2Motif grid search	77
A.7	MUTAG grid search	78
A.8	NeuroSAT soft constraint grid search	85
A.9	NeuroSAT hard constraint grid search	85

List of Acronyms

AUC area under the curve

BA Barabási-Albert

CNF conjunctive normal form

CNN convolutional neural network

DL deep learning

GCN graph convolutional network

GNN graph neural network

GT ground truth

LCG literal-clause graph

ML machine learning

MLP multilayer perceptron

MPNN message passing neural network

MUS minimal unsatisfiable subset

PGEExplainer parameterized explainer for graph neural networks

ROC receiver operating characteristic

ROC-AUC/AUROC area under the receiver operating characteristic curve

SAT boolean satisfiability problem

TM target model

Chapter 1

Introduction

Solvers for SAT are one of many applications that have seen progress through the development of DL in recent years. NeuroSAT [64] is one exemplary framework that combines ML with SAT solving. Since SAT instances can naturally be represented as bipartite graphs, GNNs or message passing neural networks (MPNNs) are a logical choice for solving this task. However, NeuroSAT lacks the ability of providing proofs to its predictions of unsatisfiability, which are required to compete with state-of-the-art SAT solvers [5], [16]. This is one example of the general need for explanations that establish trust in the predictions of GNNs [24], [57].

Several approaches have been developed to explain the predictions made by deep graph models. One perturbation-based method is the PGExplainer [43] whose explanations provide a global, generalizable understanding of the underlying trained GNN. It learns approximated discrete edge masks from GNN representations of input graphs to explain instance predictions. Since the masks are sampled from a mask predictor shared across all edges in the dataset, it is able to provide explanations with a global view of the model [43], [73]. Moreover, this allows for the application in an inductive setting, where unexplained test instances can be explained without being used during training, as opposed to the collective setting used in previous works.

We will start this work by introducing the theoretical background, including the concepts of GNNs and explainability in GNNs [73]. After explaining the main concepts of PGExplainer [43] we re-implement the model, as well as the underlying GNNs, using PyTorch Geometric [17] rather than the originally used library TensorFlow [50]. Additionally, we introduce slight changes to the GNN design in regard to bipartite graphs to verify if the explainer, as claimed by the authors, is invariant to changes in model architecture. The generated explanations are evaluated using both qualitative and quantitative metrics, which we further use to optimize the model. We will then compare our results to the baseline of the original paper, as well as a present replication study, while focusing on the application in the inductive setting. [29].

After a successful replication of the baseline experiments we aim to apply the explainer method to NeuroSAT. In doing so, we aim to learn and generate general, retrospective bipartite explanations of unsatisfiable instances that support the predictions of NeuroSAT. Since we require GTs to evaluate the accuracy of explanations, we propose treating MUSes - small unsatisfiable cores - of the instances as expected GT. We justify this with the fact that unsatisfiable SAT instances can be "reduced" to MUSes by perturbing the edges outside the subset, which represent appearances of literals in clauses not included in the subset. Ultimately, our goal is testing whether the explanations provided for NeuroSAT align with "human-understandable" principles, specifically the appointed MUS GT.

Chapter 2

Theoretical Background

In this chapter we define the necessary background for understanding PGExplainer as well as the follow-up work regarding its application on an ML solver for SAT. We start by giving an introduction to DL in Section 2.1, including a specific architecture and regularization techniques. In Section 2.2 we define the necessary graph theory, including bipartite graphs and random graphs. To understand the motivation behind the objective of PGExplainer we outline the relevant concepts of information theory, namely entropy, cross-entropy and mutual information, in Section 2.3. Since the explainer model operates on Graph Neural networks, we introduce the historically relevant GNN model by Scarselli et al. [62] in Section 2.4, as well as three succeeding models. Lastly, in Section 2.5 we describe SAT as the problem that motivates this work.

2.1 Deep Learning

In this chapter we introduce DL in the context of ML and their concepts required for this work. The definitions in this chapter loosely follow Goodfellow et al. [22].

ML algorithms generally learn to perform certain tasks from data that can broadly be divided into supervised and unsupervised learning. In this work, we focus on supervised learning, meaning that the algorithm learns from a dataset containing both features and labels or targets that the algorithm is supposed to predict. In other words, the algorithm learns from a training set of input examples, defined as vectors $\mathbf{x} \in \mathbb{R}^d$ of d features, and output examples y . Its goal is to be able to associate unseen inputs from a set of test data, coming from the same distribution as the training data, with some target output. This process estimates the generalization error of the learner after the training is complete. Common supervised ML tasks include classification, assigning an input to one of k categories, and regression, where the program shall predict a numeric value given some input.

DL entails expanding the size of the model used in our algorithm to allow for representations of functions with increasing complexity. This enables many human-solvable tasks

that consist of mapping an input vector to an output vector to be performed with DL, given sufficiently large models and datasets. Most notably, Krizhevsky et al. [36] achieved record-breaking results by using a large, deep convolutional network for image classification.

However, increasing the size of a model comes with new challenges. Since models become more complex with increasing number of layers, subnetworks and parameters, they are commonly treated as a "black box", as it is difficult to explain their decision-making process [53]. Thus, the need for methods that can explain and interpret such models arises. Furthermore, the increasing number of parameters directly raises the computational complexity, resulting in longer training times and higher hardware requirements. This may also impose limitations when deploying the model on low-resourced end-devices.

In many cases DL involves optimizing an objective function that guides the model, usually by minimizing $f(x)$. This objective function is also referred to as loss function in the context of minimization.

To minimize a function $y = f(x)$, where $y, x \in \mathbb{R}$, we make use of the derivative $f'(x)$ that tells us how to change x in order to get an improvement in y . We can reduce $f(x)$ by moving x in the direction opposite of the sign of its derivative, since $f(x - \epsilon \text{ sign}(f'(x))) < f(x)$ for small enough ϵ . Since we usually want to minimize a function with multiple inputs, we let $\mathbf{x} \in \mathbb{R}^n$ be a vector with n elements. The partial derivative $\frac{\partial}{\partial x_i} f(\mathbf{x})$ is utilized, telling us how f changes when only x_i increases at point \mathbf{x} . To generalize this to a vector, the gradient $\nabla_{\mathbf{x}} f(\mathbf{x})$ of f is defined as the vector containing all partial derivatives. The aforementioned technique used to minimize a function is hence called gradient descent (see Cauchy[9]).

Ultimately, a DL algorithm typically consists of the following components: a dataset, an objective function, an optimization procedure like gradient descent, and a model.

We generally control an ML algorithm by tuning the hyperparameters, which are settings used to control its behavior that are not adapted by the algorithm itself [22]. Settings that are difficult to optimize may be selected as hyperparameters. Common examples are the number of epochs - the iterations over the full training data - and the learning rate, that controls how much the model adjusts the weights at each step. An additional goal is finding the combination of hyperparameter settings that leads to the best performance of our model. This may also be automated with searching or learning algorithms.

To tune the hyperparameters we need a validation set of data that is not directly observed by the training algorithm, since the separate test data may not be used for making decisions about our model. This set estimates the generalization error during training. The training data is therefore commonly split into two disjoint sets, the training set and the validation set, with a standard split being 80/20.

A traditional approach for tuning hyperparameters is the grid search, as described in Liashchynskyi and Liashchynskyi [39]. This method involves defining a subspace of the

complete hyperparameter space and searching for the best-performing training algorithm across all possible combinations within that subspace.

2.1.1 Multilayer Perceptron

A classical DL model is the multilayer perceptron (MLP), first proposed by Rosenblatt [60], with the general goal of approximating a function f^* . In the case of classification we could define a function $y = f^*(\mathbf{x})$ that maps an input vector \mathbf{x} to a label y . The MLP then defines the mapping $y = f(\mathbf{x}; \boldsymbol{\theta})$ and learns the value of the parameters in $\boldsymbol{\theta}$ that best approximate the function. At the start of the training these parameters are initialized randomly or by a smart initialization strategy, like the Glorot/Xavier [21] initialization.

These models are also referred to as feedforward neural networks, as they process information from \mathbf{x} , through the intermediate computations that define f , to the output y without feedback connections that would feed outputs back to itself. The name network is derived from their representation as a composition of multiple different functions, that are described by a directed acyclic graph. An example network is $f(\mathbf{x}) = f^{(2)}(f^{(1)}(\mathbf{x}))$, which processes an input vector \mathbf{x} through a hidden layer $f^{(1)}$, and an output layer $f^{(2)}$ (see Figure 2.1). The length of this chain of functions defines the depth of a model, coining the term "deep learning".

The approximation is achieved by training our network with training data, that consists of approximated examples of $f^*(\mathbf{x})$ at different points in the training, and labels $y \approx f^*(\mathbf{x})$. These training examples dictate the output layer to generate a value close to y for each input \mathbf{x} , or to produce a higher-level representation that can be used for subsequent tasks. The learning algorithm then learns to utilize the other hidden layers, without specified behaviors, to achieve the best approximation. It is to note that the hidden layers are vector-valued with each vector element, referred to as unit, loosely taking the role of a neuron in neuroscience. This comparison is a common analogy to convey the idea of information processing. Models are therefore also referred to as neural networks.

Following [22], an input or intermediate layer for our model could be defined as

$$f^{(i)}(\mathbf{x}; \mathbf{W}, \mathbf{c}) = \mathbf{W}\mathbf{x} + \mathbf{c}, \quad (2.1)$$

where $\mathbf{W} \in \mathbb{R}^{m \times d}$ denotes a weight matrix for m units with d features and $\mathbf{c} \in \mathbb{R}^m$ is a vector of bias terms. To keep the model from strictly learning a linear function of its inputs

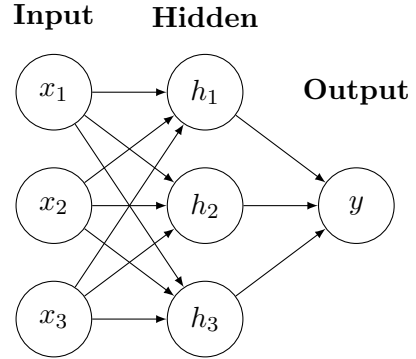


Figure 2.1: A simple MLP with one hidden layer.

we can calculate the vector of hidden units $\mathbf{h} \in \mathbb{R}^m$ by applying an activation function g to the output of the linear layer:

$$\mathbf{h} = g(f^{(i)}(\mathbf{x}; \mathbf{W}, \mathbf{c})). \quad (2.2)$$

The activation function g is typically applied element-wise to describe the features of a hidden layer:

$$h_i = g(\mathbf{W}_{i,:}\mathbf{x} + c_i), \quad (2.3)$$

where $\mathbf{W}_{i,:}$ denotes the i -th row of \mathbf{W} . The hidden units \mathbf{h} can then serve as input to the next hidden layer or directly to the output layer.

An example for a linear output layer that calculates a scalar for an input vector \mathbf{h} is

$$f^{(i+1)}(\mathbf{h}; \mathbf{w}, b) = \mathbf{h}^\top \mathbf{w} + b, \quad (2.4)$$

with weight vector $\mathbf{w} \in \mathbb{R}^m$ and bias $b \in \mathbb{R}$ as parameters. This would define our model consisting of the two defined layers as $f(x; \boldsymbol{\theta})$ with parameters $\boldsymbol{\theta} = (\mathbf{W}, \mathbf{c}, \mathbf{w}, b)$. The learning algorithm would thus adapt the parameters $\boldsymbol{\theta}$ to approximate the target function as close as possible.

The activation function typically maps its input to a real number within a specific range, often between 0 and 1, conceptually imitating the activation of a biological neuron. We try to use activation functions that are continuous differentiable and easily calculated, to minimize computational complexity [41]. Examples are the Sigmoid function

$$\sigma(x) = \frac{1}{1 + e^{-x}}, \quad (2.5)$$

where e denotes the exponential function, and the Rectified Linear Unit (ReLU):

$$\text{ReLU}(x) = \begin{cases} 0 & x \leq 0, \\ 1 & x > 0. \end{cases} \quad (2.6)$$

Backpropagation

The backpropagation algorithm [61] is commonly used during neural network training. It optimizes the network parameters by leveraging gradient descent. It first calculates the values for each unit in the network given the input and a set of parameters in a forward order. Then the error for each variable to be optimized is calculated, and the parameters are updated according to their corresponding partial derivative backwards. These two steps will repeat until reaching the optimization target [22].

2.1.2 Regularization

A central problem of not only DL but ML in general is the creation of an algorithm that generalizes well, therefore performing not only on training data, but also on unseen test

inputs [22]. There exists many strategies that aim to reduce the test error, sometimes at the expense of an increase in training error. These strategies are known as regularization. We introduce a selection of these strategies that are relevant in the course of this work, following Goodfellow et al. [22].

Parameter Norm Penalties

Many regularization approaches in DL restrict the capacity of a model by adding a parameter norm penalty $\Omega(\boldsymbol{\theta})$ to the objective function. Let J be the objective function of our learning algorithm, with training input $\mathbf{X} \in \mathbb{R}^{I \times d}$ and target values $\mathbf{y} \in \mathbb{R}^I$, for I training instances with n features. The regularized objective function is then defined as

$$\tilde{J}(\boldsymbol{\theta}; \mathbf{X}, \mathbf{y}) = J(\boldsymbol{\theta}; \mathbf{X}, \mathbf{y}) + \alpha\Omega(\boldsymbol{\theta}), \quad (2.7)$$

where $\alpha \in [0, \infty)$ is a hyperparameter used to weigh the relative contribution of the norm penalty term $\Omega(\boldsymbol{\theta})$. $\alpha = 0$ results in no regularization, while larger values increase the regularization effect. During training the algorithm will not only minimize the objective function J , but also the regularization measure of the parameters $\boldsymbol{\theta}$, or a subset of these. We usually only regularize the weights \mathbf{w} with Ω , since these specify the interaction of two variables, rather than the bias b that only controls a singular variable [22].

Inherently, different parameter norms Ω can result in different preferred solutions. One common example is the L^2 regularization, known as weight decay. It drives the weights closer to the origin by adding the term

$$\Omega(\boldsymbol{\theta}) = \frac{1}{2}\|\mathbf{w}\|_2^2 = \frac{1}{2}\mathbf{w}^\top \mathbf{w}, \quad (2.8)$$

with $\|\mathbf{x}\|_p = (\sum_i |x_i|^p)^{\frac{1}{p}}$ denoting the L^p norm or size of a vector \mathbf{x} . Specifically, the L^2 norm denotes the Euclidean distance from the origin to the point \mathbf{x} , and the size of a vector \mathbf{x} if squared: $\|\mathbf{w}\|_2^2 = \mathbf{x}^\top \mathbf{x}$.

Another option is the L^1 regularization, defined as

$$\Omega(\boldsymbol{\theta}) = \|\mathbf{x}\|_1 = \sum_i |\mathbf{x}_i|, \quad (2.9)$$

that provides a more sparse solution in comparison, meaning that some parameters have an optimal value of zero.

Early stopping

When training a deep model, a commonly observable problem is the training error steadily decreasing over time, but the validation set error rising after some time, indicating that the model is overfitting to the train data [22]. To obtain a better model we may then return to a parameter setting at an earlier point in the training, where the validation set error was at its lowest. In practice, we store a copy of the model parameters at any point in training where the validation error decreases. Thus, when the training is concluded we

return the stored set of parameters, rather than the latest one. Additionally, we may stop our algorithm early if the validation error does not decrease over a set period of iterations.

Dropout

Dropout [28] is a regularization technique used to prevent a neural network from "overfitting" to the training data, which occurs due to feature detectors of models being highly tuned to the training data, but not to the unseen test data. This is done by randomly omitting each hidden unit from the network with a common probability p for each presentation of each training instance, to avoid hidden units relying on the presence of other hidden units. Usually, to reduce the error on a test set, an average of the predictions of multiple networks is consulted, which requires training many separate networks. Random dropout provides a computationally cheap alternative to this approach. Effectively, at each presentation of each training instance a different network is used, but the present hidden units share the same weights across all these networks.

At test time, the "mean network" is used, that contains all hidden units with their outgoing weights scaled by the factor $\frac{1}{1-p}$, to account for more hidden units being present during this stage.

Batch Normalization

While not strictly a regularization technique, batch normalization [32] often serves a similar purpose in practice by improving generalization. In deep models composed of several layers the gradient tells us how to update each parameter assuming that the other layers do not change. Since in practice all layers are updated simultaneously, this may lead to unexpected results. Batch normalization is an optimization technique that can be applied to any input or hidden layer to reduce the aforementioned problem. We follow the definition by Goodfellow et al. [22].

Let $\mathcal{B} \in \mathbb{R}^{m \times d}$ be a mini-batch design matrix of activations of the layer to normalize, in the form of a design matrix with rows of activations. To normalize \mathcal{B} , it is replaced by

$$\mathcal{B}' = \frac{\mathcal{B} - \boldsymbol{\mu}}{\boldsymbol{\sigma}}, \quad (2.10)$$

where $\boldsymbol{\mu} \in \mathbb{R}^d$ is a vector containing the mean of each unit and $\boldsymbol{\sigma} \in \mathbb{R}^d$ is a vector containing the standard deviation of each unit. Each activation is normalized individually with the $\boldsymbol{\mu}$ and $\boldsymbol{\sigma}$ corresponding to its row. The network processes \mathcal{B}' as functionally equivalent to \mathcal{B} . During training,

$$\boldsymbol{\mu} = \frac{1}{m} \sum_i \mathcal{B}_i \quad (2.11)$$

and

$$\boldsymbol{\sigma} = \sqrt{\delta + \frac{1}{m} \sum_i (\mathcal{B}_i - \boldsymbol{\mu})^2}, \quad (2.12)$$

where δ is a small positive value introduced to avoid \sqrt{z} at $z = 0$ and m is the number of elements in the batch. It is important to note that backpropagation is performed

through all three operations, to prevent the gradient from proposing an operation that solely increases the mean and standard deviation of the output of a layer. Batch normalization therefore reparameterizes the model to include some units that are standardized by definition.

When testing the model, we replace μ and σ with running averages that were collected during training, to enable the evaluation of individual examples outside mini-batches.

2.1.3 Monte Carlo Sampling

In order to best approximate a randomized algorithm we can make use of Monte Carlo methods as described in [22]. A common practice in ML is to draw samples from a probability distribution and using these to form a Monte Carlo estimate of some quantity. This can be used to train a model that can then sample from a probability distribution itself. More specifically, the idea of Monte Carlo sampling is to view a sum of function

evaluations, such as those of a loss function, as if it was an expectation under some probability distribution. This estimate is approximated with a corresponding average. Let X be a discrete random variable with alphabet \mathcal{X} and probability mass function $p(x) = \Pr\{X = x\}$ for $x \in \mathcal{X}$. The sum to estimate is defined as

$$s = \sum_{x \in \mathcal{X}} p(x)f(x) = \mathbb{E}_p[f(X)], \quad (2.13)$$

where \mathbb{E} denotes the expectation. Then s can be approximated by drawing n samples from p and constructing the empirical average

$$\hat{s}_n = \frac{1}{n} \sum_{i=1}^n f(x^{(i)}). \quad (2.14)$$

2.2 Graph Theory

The following definitions loosely follow Liu and Zhou [41]. A graph is a data structure consisting of a set of nodes that are connected via edges, modeling objects and their relationships. It can be represented as $G = (V, E)$ with $V = \{v_1, v_2, \dots, v_n\}$ being the set of n nodes, and $E \subseteq V \times V$ being the set of edges. We adopt the conventions from Diestel [15] to refer to the node and edge set of any graph G with $V(G)$ and $E(G)$ respectively, regardless of the actual names of the sets. Moreover, we refer to G with node set V as "G on V ".

An edge $e = (u, v)$, connects nodes u and v , making them neighbors that are both incident to e . The neighborhood $\mathcal{N}(u)$ of node u in $V(G)$ is defined as

$$\mathcal{N}(u) = \{v \in V(G) \mid (v, u) \in E(G)\}.$$

We denote the set of edges that are incident to u as

$$E(u) = \{(v, u) \in E(G) \mid v \in \mathcal{N}(u)\}.$$

Additionally, we define the k -hop neighborhood of node u in $V(G)$ as

$$\mathcal{N}_k(u) = \{v \in V(G) \mid \text{dist}_G(v, u) \leq k\},$$

where $\text{dist}_G(v, u)$ denotes the distance of nodes v, u in G , defined as the length of the shortest path between the two nodes. Edges are either directed or undirected and lead to directed or undirected graphs if exclusively present.

The degree of a node $v \in V(G)$ is the number of edges connected to v and denoted by $d(v) = |\{(u, v) \in E(G) \mid u \in V(G)\}|$. G can be described by an adjacency matrix $\mathbf{A} \in \mathbb{R}^{n \times n}$, where

$$\mathbf{A}_{ij} = \begin{cases} 1 & \text{if } \{v_i, v_j\} \in E \text{ and } i \neq j, \\ 0 & \text{otherwise.} \end{cases}$$

If G is an undirected Graph the adjacency matrix will be symmetrical, as seen in Figure 2.2. The diagonal degree matrix $D \in \mathbb{R}^{n \times n}$ of G is defined as:

$$D_{ii} = d(v_i).$$

G is called a subgraph of another graph $G' = (V', E')$, denoted as $G' \subseteq G$, if

$$V(G) \subseteq V(G') \text{ and } E(G) \subseteq E(G').$$

The number of nodes $|V|$ in a graph is called its order and the number of edges $|E|$ is its size (see Diestel [15]).

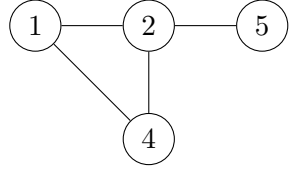
We follow the definition of bipartite graphs given by Asratian et al. [4]: A graph G is bipartite if the set of nodes V can be partitioned into two disjoint sets V_1 and V_2 such that

$$\begin{aligned} V &= V_1 \cup V_2, \quad V_1 \cap V_2 = \emptyset, \quad \text{and} \\ \forall (i, j) \in E(G) : & (i \in V_1 \wedge j \in V_2) \vee (i \in V_2 \wedge j \in V_1). \end{aligned}$$

This formalizes that no two nodes from the same set are adjacent. The sets V_1 and V_2 are called color classes and (V_1, V_2) is a bipartition of G . This means that if a graph is bipartite all nodes in V can be colored by at most two colors so that no two adjacent nodes share the same color. This is visualized in Figure 2.3.

Random Graphs

Gilbert [19] describes the process of generating a random graph of order n by assigning a common probability of existence to each potential edge between any two nodes. For each



$$\mathbf{A} = \begin{bmatrix} 0 & 1 & 1 & 0 \\ 1 & 0 & 1 & 1 \\ 1 & 1 & 0 & 0 \\ 0 & 1 & 0 & 0 \end{bmatrix}$$

Figure 2.2: A simple undirected graph G on V , with $V = \{1, 2, 4, 5\}$ (left), and its adjacency matrix \mathbf{A} (right).

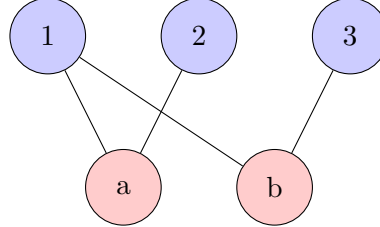


Figure 2.3: A bipartite graph with color classes $V_1 = \{1, 2, 3\}$ (blue) and $V_2 = \{a, b\}$ (red).

of these potential edges an experiment is performed independently to determine whether it shall be included in the resulting graph. Note that this process can be modeled using a Bernoulli distribution.

A random graph is further described by Diestel [15] as follows. Let $V = \{0, \dots, n - 1\}$ be a fixed set of n elements. Say we want to define the set \mathcal{G} of all graphs on V as a probability space, which allows us to ask whether a Graph $G \in \mathcal{G}$ has a certain property. To generate our random graph we then decide from some random experiment whether e shall be an edge of G for each potential $e \in V \times V$. The probability of success - accepting e as edge in G - is defined as $p \in [0, 1]$ for each experiment. This leads to the probability of G being a particular graph G_0 on V with e.g. m edges being equal to $p^m q^{\binom{n}{2}-m}$ with $q := 1 - p$.

2.3 Information Theory

To fully understand the learning objective of PGExplainer it is necessary to define the concepts of entropy and mutual information. We follow the definitions by Cover and Thomas [11] if not stated otherwise.

2.3.1 Entropy

Entropy is used to describe the uncertainty of a random variable. It quantifies the average amount of information produced by the outcomes of said variable. This is commonly

illustrated as the average number of bits needed to encode its possible values if optimal code is used [22]. The entropy $H(X)$, also written as $H(p)$, is defined as

$$H(X) = - \sum_{x \in \mathcal{X}} p(x) \log p(x). \quad (2.15)$$

The log is to the base e and entropy is measured in natural units of information (nats) in our case. We will use the convention from Cover and Thomas [11] that $0 \log 0 = 0$, as terms of zero probability do not change the entropy.

The conditional entropy of Y given X is defined as the expected value of the entropies of the conditional distributions, averaged over the conditioning random variable. Let $(X, Y) \sim p(x, y)$ for a pair of discrete random variables (X, Y) with joint distribution $p(x, y)$. The conditional entropy is then defined as

$$\begin{aligned} H(Y|X) &= - \sum_{x \in \mathcal{X}} p(x) H(Y|X=x) \\ &= - \sum_{x \in \mathcal{X}} \sum_{y \in \mathcal{Y}} p(x, y) \log p(y|x) \\ &= -\mathbb{E} \log p(Y|X). \end{aligned} \quad (2.16)$$

2.3.2 Relative Entropy and Cross-Entropy

The relative entropy between two distributions is a measure of "distance" between the two. It measures the inefficiency of assuming a distribution to be q when the true distribution is p . Note that it is not a true measure of distance as it is not symmetrical. The relative entropy takes a value of 0 only if $p = q$. We define the KL divergence or relative entropy between two probability mass functions $p(x), q(x)$ as

$$D_{KL}(p||q) = \sum_{x \in \mathcal{X}} p(x) \log \frac{p(x)}{q(x)}. \quad (2.17)$$

We adopt the convention from Cover and Thomas [11] that $0 \log \frac{0}{0} = 0$, $0 \log \frac{0}{q} = 0$ and $p \log \frac{p}{0} = \infty$. Suppose we know the true distribution p of our random variable. We could then construct a code with an average description length of $H(p)$. If we used the code for the distribution q instead, we would need $H(p) + D_{KL}(p||q)$ nats to describe the random variable on average. This is also referred to as the cross-entropy (see Goodfellow et al. [22]):

$$H(p, q) = H(p) + D_{KL}(p||q) \quad (2.18)$$

Since this is later applied in the PGExplainer (see Equation 4.6), we derive for the discrete case with mass probability functions p, q defined on the same support \mathcal{X} :

$$\begin{aligned} H(p, q) &= H(p) + D_{KL}(p||q) = - \sum_{x \in \mathcal{X}} p(x) \log p(x) + \sum_{x \in \mathcal{X}} p(x) \log \frac{p(x)}{q(x)} \\ &= - \sum_{x \in \mathcal{X}} p(x) \log p(x) + \sum_{x \in \mathcal{X}} p(x) \log p(x) - \sum_{x \in \mathcal{X}} p(x) \log q(x) \\ &= - \sum_{x \in \mathcal{X}} p(x) \log q(x) \end{aligned} \quad (2.19)$$

2.3.3 Mutual Information

A closely related concept is mutual information. It measures the amount of information that one random variable contains about another or the reduction in uncertainty of said variable due to knowing the other. A high mutual information therefore implies that the information of one variable can be gathered from the other.

Let X and Y be two random variables with the joint probability mass function $p(x, y)$ and marginal probability mass functions $p(x)$ and $p(y)$. Mutual information $MI(X; Y)$ is the relative entropy between the joint distribution and the product distribution $p(x)p(y)$:

$$\begin{aligned} MI(X; Y) &= \sum_{x \in \mathcal{X}} \sum_{y \in \mathcal{Y}} p(x, y) \log \frac{p(x, y)}{p(x)p(y)} \\ &= H(X) - H(X|Y) \end{aligned} \tag{2.20}$$

2.4 Graph Neural Networks

GNNs [62] are a DL-based approach for modeling graph data. Due to their unique non-Euclidean property they find usage in many areas, with common tasks including node classification [18], graph classification [70] and link prediction [75] (see Figure 2.4). Their high interpretability and strong performance have led to GNNs becoming a commonly employed method in graph analysis. Modern GNNs combine the key features of convolutional neural networks (CNNs) [37], such as local connection, shared weights, and multi-layer usage, with the concept of graph embeddings [8] to leverage the power of feature extraction and representation as low-dimensional vectors for graphs (see Liu and Zhou [41]).

Graphs are a common way of representing data in many different fields, including ML. ML applications on graphs can mostly be divided into graph-focused tasks and node-focused tasks. For graph-focused applications our model does not consider specific singular nodes, but rather implements, for example, a classifier on representations of complete graphs. In node-focused applications however the model is dependent on specific nodes, leading to classification tasks that rely on the properties of each node.

The study of GNNs was first introduced in [23] and refined in [62]. Thus, we describe the supervised GNN model by Scarselli et al. [62] that aims to preserve the important, structural information of graphs by encoding their topological relationships among nodes.

A node is naturally defined by its features as well as its related nodes in a graph. The goal of a GNN is to learn state embeddings $\mathbf{h}_v \in \mathbb{R}^s$ for each node v , that map the neighborhood of a node into a representation. These embeddings are used to obtain outputs \mathbf{o}_v , that, e.g., may contain the distribution of a predicted node label. The GNN model proposed by Scarselli et al. [62] uses undirected homogeneous graphs with \mathbf{x}_v describing

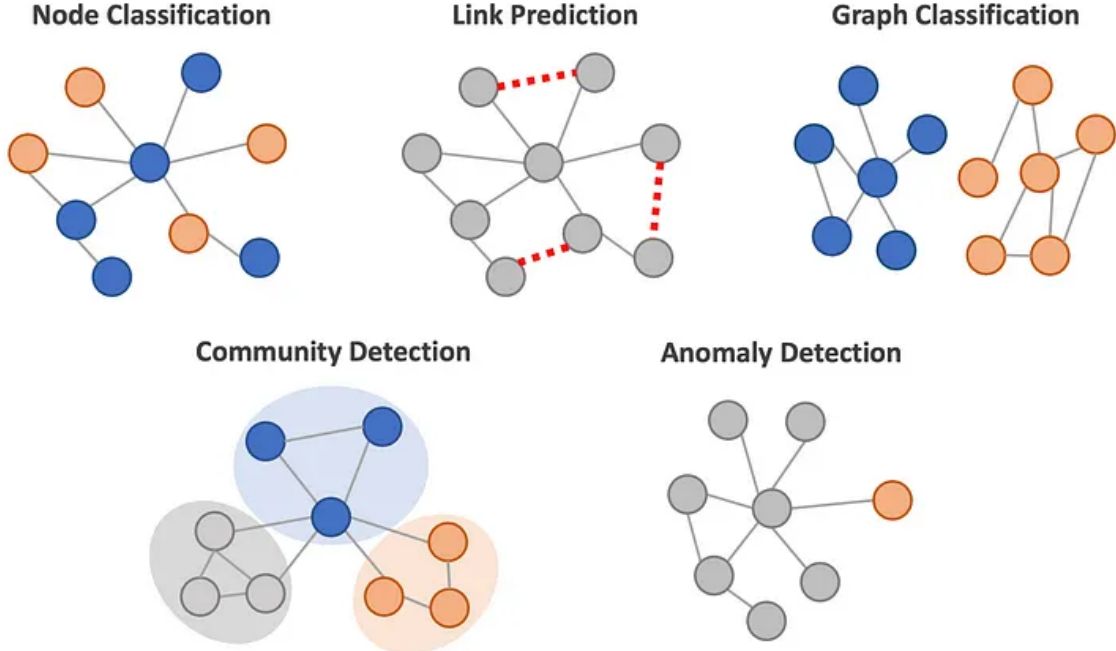


Figure 2.4: Common applications of GNNs. Reprinted from [51].

the d -dimensional features of each node and x_e the optional features of each edge. The model updates the node states according to the input neighborhood with a local transition function f that is shared by all nodes. Additionally, the local output function g is used to produce the output of each node. \mathbf{h}_v and \mathbf{o}_v are therefore defined as

$$\mathbf{h}_v = f(\mathbf{x}_v, \mathbf{x}_{E(v)}, \mathbf{h}_{\mathcal{N}(v)}, \mathbf{x}_{\mathcal{N}(v)}), \quad (2.21)$$

$$\mathbf{o}_v = g(\mathbf{h}_v, \mathbf{x}_v), \quad (2.22)$$

with \mathbf{x} denoting input features and \mathbf{h} the hidden state. $\mathbf{x}_v, \mathbf{x}_{E(v)}, \mathbf{h}_{\mathcal{N}(v)}, \mathbf{x}_{\mathcal{N}(v)}$ denote the features of the node v and of its incident edges, as well as the states and features of its neighboring nodes, respectively. We define $\mathbf{H}, \mathbf{O}, \mathbf{X}$ and \mathbf{X}_N as the matrices that are constructed by stacking all states, outputs, features, and node features, respectively. This allows us to define with the global transition function F and the global output function G , which are stacked versions of their local equivalent for all nodes in a graph:

$$\mathbf{H} = F(\mathbf{H}, \mathbf{X}), \quad (2.23)$$

$$\mathbf{O} = G(\mathbf{H}, \mathbf{X}_N). \quad (2.24)$$

Note that F is assumed to be a contraction map and the value of \mathbf{H} is the fixed point of equation (2.23). To compute the state the iterative scheme

$$\mathbf{H}^{t+1} = F(\mathbf{H}^t, \mathbf{X}) \quad (2.25)$$

is used with \mathbf{H}^t denoting iteration t of \mathbf{H} . The computations of f and g can be understood as the feedforward neural network.

To learn the parameters of this GNN, with target information t_v for a specific node v , the loss is defined as

$$\text{loss} = \sum_{i=1}^p (t_i - \mathbf{o}_i) \quad (2.26)$$

where p are the supervised nodes. A gradient-descent strategy is utilized in the learning algorithm, which consist of the following three steps: the states \mathbf{h}_v^t are updated iteratively using equation (2.21) until time step T . We then obtain an approximate fixed point solution of equation (2.23): $\mathbf{H}(T) \approx \mathbf{H}$. For the next step the gradients of the weights W are calculated from the loss. Finally, the weights W are updated according to the computed gradient. This allows us to train a model for specific supervised or semi-supervised tasks, referred to as downstream task, and get hidden states of nodes in a graph [41].

Though the architecture proposed by Scarselli et al. [62] proved to be powerful for modeling structural data, this initial approach suffers from a few limitations. Most notably, it uses the same parameters in the iteration, while nowadays it is common practice to use different parameters in different layers [41].

Stacking k GNN layers allows each node to aggregate information from nodes within its k -hop neighborhood, represented in Figure 2.5, seeking an increase in performance. It is important to note that this approach may also increase the noisy information spread by the exponentially increasing neighborhood nodes [41].

Another drawback is the computational inefficiency, as hidden states have to be updated T times until reaching the fixed point. A relaxation of the fixed point assumption enables multi-layer GNNs to provide stable representations of the node and its neighborhood [38]. Additionally, this architecture is unable to model informative edge features, which limits its capacity to learn meaningful hidden representations for edges.

Therefore, we briefly present two subsequent models that are used in the course of this work, as well as a more general framework relevant in the context of NeuroSAT.

Graph Convolutional Network

The graph convolutional network (GCN) aims to generalize the convolution operation of CNNs to the graph domain. An example is the model proposed by Kipf and Welling [35] that introduces a simple, layer-wise propagation rule for multi-layer GCNs as

$$\mathbf{H}^{(l+1)} = \sigma(\tilde{\mathbf{D}}^{-\frac{1}{2}} \tilde{\mathbf{A}} \tilde{\mathbf{D}}^{-\frac{1}{2}} \mathbf{H}^{(l)} \mathbf{W}^{(l)}), \quad (2.27)$$

where $\tilde{\mathbf{A}} = \mathbf{A} + \mathbf{I}_N$ is the adjacency matrix of the undirected input graph G with added self-connections. \mathbf{I}_N is the identity matrix, $\tilde{\mathbf{D}}$ is the degree matrix and $\mathbf{W}^{(l)}$ is a layer-specific trainable weight matrix. $\sigma(\cdot)$ denotes an activation function, such as ReLU. $\mathbf{H}^{(l)} \in \mathbb{R}^{n \times D}$ denotes the matrix of node activations in the l -th layer, with layer-specific embedding dimension D , where $\mathbf{H}^{(0)} = X$.

Note that this definition differs from the iterative formulation in Equation 2.25, in the sense that each layer applies a different function $F^{(l)}$, rather than a shared function F .

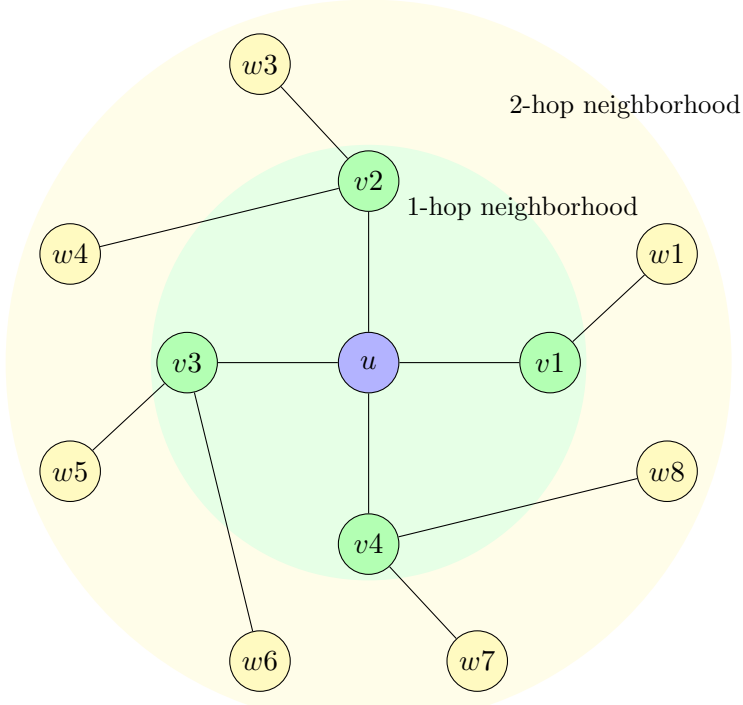


Figure 2.5: Visualization of the k -hop neighborhood of u .

$\tilde{\mathbf{D}}^{-\frac{1}{2}} \tilde{\mathbf{A}} \tilde{\mathbf{D}}^{-\frac{1}{2}}$ describes a normalization of the adjacency matrix, referred to as renormalization trick. This architecture aims to alleviate the problem of overfitting on local neighborhood structures for graphs with very wide node degree distributions [35].

Stacked GNN

Morris et al. [52] propose an implementation for a basic GNN model based on the general study on representation learning on graphs by Hamilton et al. [26]. This model consists of a stacked neural network layers, that each aggregate the local neighborhood information of a node, i.e., features of neighbors, and pass it to the next layer.

This network is defined specifically for graphs that can be partitioned into r color classes and therefore applicable to bipartite graphs. The new features of node i are then computed with:

$$\mathbf{x}_i^{(l)} = \sigma(\mathbf{W}_1^{(l)} \mathbf{x}_i^{(l-1)} + \mathbf{W}_2^{(l)} \cdot \sum_{j \in \mathcal{N}(i)} e_{j,i} \cdot \mathbf{x}_j^{(l-1)}) \quad \in \mathbb{R}^D, \quad (2.28)$$

where $\mathbf{W}_1^{(l)}, \mathbf{W}_2^{(l)} \in \mathbb{R}^{D \times d}$ are two layer-specific trainable weight matrices with embedding dimension D . Note that $e_{j,i}$ denotes an optional edge weight for the edge (j, i) that defaults to 1 in the case without explicit edge weights.

Message Passing Neural Network

The MPNN proposed by Gilmer et al. [20] seeks to unify GNN models, by providing a general framework for supervised learning on GNNs, since many by now existing models operate similarly. Typically, messages derived from node features are passed along edges of a graph to be able to learn meaningful graph and node representations that can be used for downstream tasks [35], [62], [68], [70]. This is visualized in Figure 2.6. Therefore, GNNs may be expressed as MPPNs, where the forward pass consist of a message passing phase and a readout phase. The message passing phase runs for T time steps and is defined by the message function M_t , as well as the node update function U_t . At each time step t , the hidden state \mathbf{h}_v^{t+1} of a node v in the graph G is updated based on the message \mathbf{m}_v^{t+1} , which aggregates information from the previous hidden states of its neighbors according to the message function M_t . Formally, this is defined as

$$\mathbf{m}_v^{t+1} = \sum_{w \in \mathcal{N}(v)} M_t(\mathbf{h}_v^t, \mathbf{h}_w^t, \mathbf{e}_{v,w}) \quad (2.29)$$

$$\mathbf{h}_v^{t+1} = U_t(\mathbf{h}_v^t, \mathbf{m}_v^{t+1}), \quad (2.30)$$

where $\mathbf{e}_{v,w}$ denotes possible edge features of edge (v, w) . In the readout phase a feature vector $\hat{\mathbf{y}}$ is computed for the entire graph from the final node states using a readout function R :

$$\hat{\mathbf{y}} = R(\{\mathbf{h}_v^T \mid v \in G\}). \quad (2.31)$$

Note that the three functions M_t , U_t and R_t are learned and differentiable.

The GCN by Kipf and Welling [35], for example, may also be defined with the following message and update functions:

$$M_t(\mathbf{h}_v^t, \mathbf{h}_w^t) = c_{v,w} \mathbf{h}_w^t, \quad (2.32)$$

$$U_v^t(\mathbf{h}_v^t, \mathbf{m}_w^{t+1}) = \text{ReLU}(\mathbf{W}^t \mathbf{m}_v^{t+1}), \quad (2.33)$$

with $c_{v,w} = (d(v)d(w))^{-\frac{1}{2}} \mathbf{A}_{v,w}$.

2.5 Boolean Satisfiability Problem

We define SAT according to Guo et al. [24]: In propositional logic, a boolean formula is constructed from boolean variables, that only evaluate to True (1) or False (0), parentheses, and the three logic operators: conjunction (\wedge), disjunction (\vee) and negation (\neg). SAT aims to evaluate whether there exists a variable assignment for a formula constructed of said parts so that it evaluates to True. If so, the formula is said to be satisfiable, or unsatisfiable otherwise.

Every propositional formula can be converted into an equivalent formula in conjunctive normal form (CNF), which consists of a conjunction of one or more clauses. These clauses



Figure 2.6: Node features passed along edges. Reprinted from [3].

are enclosed in parentheses and must contain only disjunctions of at least one literal, i.e., a variable or its negation. In this work we consider only formulae in CNF, as NeuroSAT [64] assumes SAT problems to be in CNF. An example of a satisfiable formula in CNF over the set of variables $U = \{x_1, x_2\}$ is

$$\psi(U) = (x_1) \wedge (\neg x_1 \vee x_2) \wedge (\neg x_2 \vee x_2)$$

with satisfying assignment $A : \{x_1 \mapsto 1, x_2 \mapsto 1\}$.

Furthermore, SAT is the first NP-complete problem, meaning that if there exists a deterministic algorithm able to solve SAT in polynomial time, then such an algorithm exists for every NP problem (see Cook [10]). Current state-of-the-art SAT solvers apply searching based methods such as Conflict Driven Clause Learning [49] or Stochastic Local Search [63] with exponential worst-case complexity.

2.5.1 Representation as Bipartite Graph

SAT has extensively been studied in the form of graphs. Guo et al. [24] describe four different types of graph representations for CNF formulae with varying complexity and information compression. Since we want to minimize the loss of information for SAT we adapt the information-richest form of a literal-clause graph (LCG). A LCG is a bipartite graph that separates literals and clauses, with edges connecting literals to the clauses they appear in (see Figure 2.7). The resulting graph G_b can formally be described by a biadjacency matrix \mathbf{B} of shape $L \times C$, with (L, C) being a bipartition of G_b into literals and clauses.

Following Sun et al. [66], let $\mathbf{A} \in \mathbb{R}^{(L+C) \times (L+C)}$ be the adjacency matrix of our bipartite graph. Since for the bipartite case edges exist only between the two color classes L and C , the adjacency matrix can be represented as

$$\mathbf{A}(i, j) = \begin{bmatrix} \mathbf{0}_{L \times L} & \mathbf{B} \\ \mathbf{B}^T & \mathbf{0}_{C \times C} \end{bmatrix}, \quad (2.34)$$

where $\mathbf{0}$ denotes a zero matrix in the shape of their subscript.

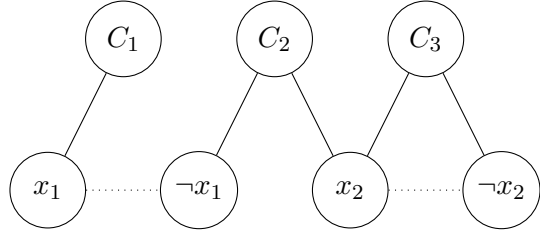


Figure 2.7: LCG representation of $\psi(U)$ with dashed lines representing the connection between complementary literals relevant for the message passing in NeuroSAT.

2.5.2 Unsatisfiable Cores

The core of an unsatisfiable formula in CNF is a subset of the boolean clauses defining the formula that is also unsatisfiable. Every unsatisfiable formula therefore is a core on its own, but can be broken down into smaller cores. The smaller a core the more significance it holds [67].

A minimal unsatisfiable core, also referred to as a MUS, is a unsatisfiable core that becomes satisfiable whenever one of its clauses is removed [14]. It is notable that unsatisfiable SAT formulae can contain multiple MUSes, meaning that an individual MUS may be a local minimum, but not necessarily a global one [40]. SAT solvers like MiniSat [16] are able to compute unsatisfiable cores but do not generally provide a MUS due to high computational cost. However, several deletion-based algorithms exist for computing MUSes (see Torlak et al. [67]).

Chapter 3

Related Work

Yuan et al. [73] performed an extensive taxonomic survey on explainability in graph neural networks. We use this survey to discuss different approaches and motivate the selection of the PGExplainer for our work in Section 3.1. In Section 3.2 we briefly introduce important work related to the PGExplainer, as well as the model itself, since it is the core of our work. Lastly, we refer to NeuroSAT, which we later use to train the PGExplainer to generate explanations for unsatisfiable SAT instances in Section 3.3.

3.1 Explainability in GNNs

Methods in DL have seen growth in performance in many tasks of artificial intelligence, including GNNs, since graphs are able to capture real-world data such as social networks or chemical molecules [71], [46]. However, the interpretability of these models is often limited due to their black-box design [53]. Explainability methods aim to bypass this limitation by designing post-hoc techniques that provide insights into the decision-making process in the form of explanations. Such human-intelligible explanations are crucial for deploying models in real-world applications, especially when applied in interdisciplinary fields [57].

There exist several different approaches for explaining predictions of deep graph models, that can be categorized into instance-level methods and model-level methods (see Yuan et al. [73]). Instance-level methods aim to explain each input-graph by identifying important input features for its prediction, leading to input-dependent explanations. These can further be grouped by their importance score calculation into four branches. Gradients/feature-based methods use gradients as approximations of importance scores. Sensitivity Analysis [6] is an example that directly uses squared values of gradients as importance scores of input features. This enables the scores to be calculated directly with backpropagation.

Perturbation-based approaches like GNNExplainer [72] and PGExplainer [43] study the variation of the output with regard to different input perturbations. The intuition behind

this is that when input information crucial to the prediction is kept, the new prediction should roughly align with the prediction from the original input. PGExplainer aims to improve the GNNExplainer by providing a way of generating explanations with a global understanding of the GNN, significantly improving the computational cost. Another approach is SubgraphX [74], which utilizes Monte Carlo Tree search to generate subgraph-level explanations. This does, however, entail a higher computational cost.

Surrogate methods for deep graph models are inspired by surrogate methods for image data, that rely on neighboring areas of an input. Since graph data usually is concrete and contains topological information it is difficult to define the neighboring regions of an input graph.

The idea is to obtain a local dataset containing neighboring data objects and predictions and fitting a simple, interpretable surrogate model to learn the local dataset. The explanations of the surrogate model are then regarded as the explanations of the original model. GraphLime [30] is an example that considers the N -hop neighboring nodes of a target node as the local dataset, where N may be the number of GNN-layers. The weighted features of a non-linear surrogate model are then regarded as explanations. It is notable that this method only explains node features, rather than the graph structure.

Decomposition methods, also motivated by success in the image domain, aim to measure input feature importance by decomposing the prediction into several terms, regarded as feature dependant importance score. Approaches for deep graph neural networks, like Layer-wise Relevance Propagation [6], decompose the output prediction score to node importance scores. The decomposition rule is based on hidden features and weights, only enabling the study of node importance rather than graph structures.

Model-level methods, on the other hand, aim to explain GNNs without considering specific inputs, leading to input-independent, high-level explanations.

To fully trust the explanations provided by an explainer model, they must satisfy certain criteria, since there often is a mismatch between the optimizable metrics like accuracy and the actual metric of interest, which may not be measurable (see Ribeiro et al. [57]). First and foremost, an explanation should be **interpretable** and therefore provide qualitative, human-understandable interpretations, that also consider the possibility of limited user knowledge. Additionally, **local fidelity** asserts that explanations should be faithful in a local context and consider the models' behavior in the vicinity of predicted instances. Explainers that treat the model to be explained as a black-box are **model-agnostic** and should therefore be able to explain any model. Lastly, a **global perspective** is needed to explain a model fully, allowing us to take sample explanations of individual predictions that serve as representation of the model.

The perturbation-based PGExplainer [43] claims to satisfy all the criteria, while also maintaining reasonable computational cost and being able to explain unseen instances

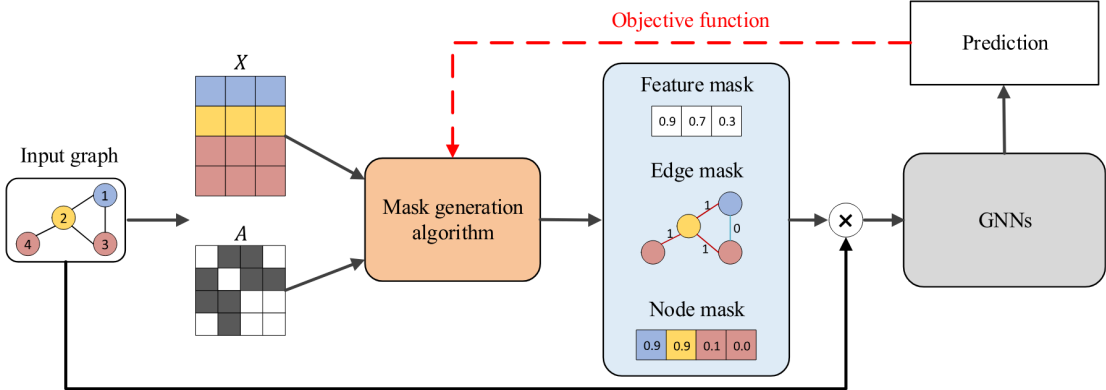


Figure 3.1: General pipeline of perturbation-based methods with a soft mask for node features, a discrete mask for edges, and an approximated discrete mask for nodes. The prediction of the GNN for the masked input graph is used in the objective function to train the generation algorithm and learn explanations. Reprinted from [73].

inductively. Though Yuan et al. [73] note that the PGExplainer performs worse than originally reported, we select this model for the course of this study with regard to its applicability in the inductive setting.

The general pipeline for different perturbation based approaches (see Figure 3.1) can be described as follows: First, the important features from the input graph are converted into a mask by our generation algorithm, depending on the explanation task at hand. These masks are applied to the input graph to highlight said features. Lastly, the masked graph is fed into the trained GNN to evaluate the mask. The mask generation algorithm is updated according to the similarity of the predictions on the original and masked graphs.

These different approaches mostly differ in the specific mask generation algorithm, the type of mask used and the objective function. It is important to distinguish between soft masks, discrete masks and approximated discrete masks. Soft masks take continuous values between $[0, 1]$, which enables the graph algorithm to be updated via backpropagation. A downside of soft masks is that they suffer from the "introduced evidence" problem (see Dabrowski and Gal [12]). Any mask value that is non-zero or non-one may add new semantic meaning or noise to the input graph, since graph edges are by nature discrete. Discrete masks, on the other hand, always rely on non-differentiable operations, e.g., sampling, which hinders the updating the model using backpropagation. Therefore, approximated discrete masks utilize reparameterization tricks to avoid the "introduced evidence" problem while also enabling backpropagation.

Explanations can on the one hand be evaluated by visualizing the graph and considering the "human-comprehensibility". Since this requires a GT, is prone to the subjective un-

derstanding and is usually performed for a few random samples, it is important to apply stable evaluation metrics.

One relevant accuracy metric for synthetic datasets with GTs is the area under the receiver operating characteristic curve (ROC-AUC or AUROC) (see Richardson et al. [58]). The receiver operating characteristic (ROC) curve plots the false positive rate on the x-axis against the true positive rate, across different classification thresholds. The area under the curve (AUC) is calculated for said curve, resulting in the AUROC. It is important to note, that a score of 0.5 equals random guessing, while a score of 1.0 indicates perfect classification. Other metrics include the fidelity, which measures the difference in accuracy between the original prediction and the prediction after important features have been masked [73]. Note that we do not consider the fidelity in the course of this work.

3.2 Explainer Models

GNNEExplainer

Ying et al. proposed the GNNEExplainer [72] - the first general, model-agnostic explainer for graph neural networks on any graph-based machine learning task. It is able to identify a concise subgraph structure and a subset of node features, that play a crucial role in the prediction of the underlying graph neural network. This is generally understood as an explanation. The work by Ying et al. serves as the main baseline for the PGExplainer, that seeks to improve its predecessor. Many concepts, experiments and specifications of PGExplainer were adapted from the GNNEExplainer, which we seek to process in our work.

Parameterized Explainer for Graph Neural Network

The Parameterized Explainer for Graph Neural Network (PGExplainer) by Lou et al. [43] is the main subject of our work. The idea of the framework is to collectively explain a set of instances using the instance predictions of a GNN, while at the same time being able to generalize the explainer model to unexplained instances in an inductive setting. To achieve this, the method utilizes a deep neural network to parameterize the generation process of explanations.

A secondary study on the inductive performance was also performed by the authors, which we want to extend by applying it on a graph neural network with a slightly different architecture, testing whether the explainer proves to be model-agnostic.

[Re] Parameterized Explainer for Graph Neural Network

Holdijk et al. [29] performed a replication study on the PGExplainer that focuses on reimplementing the method in PyTorch, testing whether the claims with respect to the GNNEExplainer hold and discussing whether the used evaluation method makes sense. They highlight a large discrepancy between the paper and codebase, making a replication

that includes the evaluation method from the paper alone impossible. With help of the codebase, the authors are able to replicate the experiments and verify the main claims of the original paper. However, they express some concerns regarding the evaluation setup and note a large difference between the originally noted AUC scores and their results for most of the datasets. Additionally, they question the general approach for evaluating graph data with GTs, as done in GNNExplainer and PGExplainer. This replication study serves as an additional baseline.

3.3 Graph Model Lacking Explanations

NeuroSAT

Proposed by Selsam et al., NeuroSAT [64] is a machine learning approach for solving SAT using a message passing neural network. It is able to detect satisfying assignments, but lacks proofs of unsatisfiability. The authors performed a small study on the detection of unsatisfiable cores, revealing that the NeuroUNSAT model is able to detect unsatisfiable cores if the unsatisfiable problems contain a specific core. This is expected to be due to the model memorizing the cores, rather than generalizing to any unsatisfiable core.

Chapter 4

Methodology

In this chapter we present the Methodology of our work, including the detailed theory of the explainer model used in our approach. Thus, we start by presenting the concepts of the PGExplainer [43] in Section 4.1.

In Section 4.2 we present our idea of training the PGExplainer on the NeuroSAT framework to generate post-hoc explanations for a machine learning SAT-solving approach and comparing these to the "human-understandable" concept of unsatisfiable cores.

We then describe our implementation in detail (see Section 4.3), including the changes made and difficulties during the process, as well as the adaptations for the application on NeuroSAT.

4.1 Theoretical Foundations of PGExplainer

In the following subchapter, we introduce the PGExplainer by Luo et al. [43]. The idea is to generate explanations in the form of edge distributions or soft masks for input graphs using a probabilistic generative model for graph data. The explainer uncovers the concise underlying structures of the graphs, believed to have the biggest impact on the prediction of a GNN, as explanations. This approach may be applied to any trained GNN-based model, henceforth referred to as target model (TM).

By utilizing a deep neural network to parameterize the generation process, the explainer learns to collectively explain multiple target instances. Since the parameters of the neural network are shared across the population of explained instances, PGExplainer provides "model-level explanations for each instance with a global view of the GNN model" [43]. Therefore, this approach cannot only be used in a collective setting, but also in an inductive setting, where explanations for not yet explained instances can be generated without retraining the explanation model. This improves the generalizability compared to previous works, particularly the GNNExplainer by Ying et al. [72] and focuses on explaining graph structure rather than graph features.

We follow the structure of the original paper [43] and start by describing the learning objective in Section 4.1.1, the utilized reparameterization trick in Section 4.1.2, the idea of global explanations in Section 4.1.3 and finally the applied regularization terms in Section 4.1.4.

4.1.1 Learning Objective

To explain the predictions made by a target GNN model for an original input graph G_o with m edges, Luo et al. [43] first define the graph as a combination of two subgraphs: $G_o = G_s + \Delta G$. G_s represents the subgraph holding the most relevant information for the prediction of a GNN, referred to as explanatory graph. ΔG contains the remaining edges that are deemed irrelevant for the prediction of the GNN. Inspired by GNNExplainer [72], the PGExplainer then finds G_s by maximizing the mutual information between the predictions of the TM and the underlying G_s :

$$\max_{G_s} MI(Y_o; G_s) = H(Y_o) - H(Y_o|G = G_s), \quad (4.1)$$

where Y_o is the prediction of the TM with G_o as input and number of possible classes c . This quantifies the probability of prediction Y_o when the input graph is restricted to the explanatory graph G_s . In the case of $MI(Y_o; G_s) = 1$, knowing the explanatory graph G_s gives us complete information about Y_o , and vice versa.

Intuitively, if removing an edge (i, j) changes the prediction of a GNN drastically, this edge is considered important and should therefore be included in G_s . This idea originates from traditional forward propagation based methods for white-box explanations (see Dabkowski and Gal [12]). It is important to note that $H(Y_o)$ is only related to the TM with fixed parameters during the evaluation/explanation stage. This leads to the objective being equivalent to minimizing the conditional entropy $H(Y_o|G = G_s)$.

To optimize this function, a relaxation is applied for the edges, since normally there would be 2^m candidates for G_s . The explanatory graph is henceforth assumed to be a Gilbert random graph, where the selections of edges from G_o are conditionally independent to each other. However, Luo et al. [43] describe a random graph with each edge having its own probability, rather than a shared probability as described in Section 2.2, as follows: Let $e_{i,j} \in V \times V$ be the binary variable indicating whether the edge is selected, with $e_{i,j} = 1$ if edge (i, j) is selected to be in the graph, and 0 otherwise. For the random graph variable G the probability of a graph G can be factorized as

$$P(G) = \prod_{(i,j) \in E(G)} P(e_{i,j}). \quad (4.2)$$

$P(e_{i,j})$ is instantiated with the Bernoulli distribution $e_{i,j} \sim \text{Bern}(\theta_{ij})$, where $P(e_{i,j} = 1) = \theta_{ij}$ is the probability that edge (i, j) exists in G . This can be understood as the generative model in the context of PGExplainer.

After this relaxation the learning objective becomes

$$\min_{G_s} H(Y_o|G = G_s) = \min_{G_s} \mathbb{E}_{G_s}[H(Y_o|G = G_s)] \approx \min_{\Theta} \mathbb{E}_{G_s \sim q(\Theta)}[H(Y_o|G = G_s)], \quad (4.3)$$

where $q(\Theta)$ is the distribution of the explanatory graph that is parameterized by Θ 's.

4.1.2 Reparameterization Trick

As described in Section 3.1, a reparameterization trick can be utilized to relax discrete edge weights to continuous variables in the range $(0, 1)$. PGExplainer uses the reparameterizable Gumbel-Softmax estimator [33] to allow for efficiently optimizing the objective function with gradient-based methods. This method introduces the Gumbel-Softmax distribution, a continuous distribution used to approximate samples from a categorical distribution.

A temperature τ is used to control the smoothness of the approximation, usually starting from a high value and annealing to a small, non-zero value. Samples with $\tau > 0$ are not discrete, but are differentiable and therefore allow gradient-based optimization [1]. The sampling process $G_s \sim q(\Theta)$ of PGExplainer is therefore approximated with a determinant function of parameters Ω , a temperature τ and an independent random variable ϵ : $G_s \approx \hat{G} = f_{\Omega}(G_o, \tau, \epsilon)$.

The binary concrete distribution [47] is utilized as an instantiation for the sampling, yielding the weight $\hat{e}_{i,j} \in (0, 1)$ for edge (i, j) in \hat{G}_s , computed by

$$\epsilon \sim \text{Uniform}(0, 1), \quad \hat{e}_{i,j} = \sigma((\log \epsilon - \log(1 - \epsilon) + \omega_{ij}/\tau)), \quad (4.4)$$

where $\sigma(\cdot)$ is the Sigmoid function and $\omega_{ij} \in \mathbb{R}$ is an explainer parameter, more specifically a logit associated with the corresponding edge (see Section 4.1.3). When $\tau \rightarrow 0$, e.g. during the explanation stage, the weight $\hat{e}_{i,j}$ is binarized with the sigmoid function $\lim_{\tau \rightarrow 0} P(\hat{e}_{i,j} = 1) = \frac{e(\omega_{ij})}{1+e(\omega_{ij})}$. Since $P(e_{i,j} = 1) = \theta_{ij}$, choosing $\omega_{ij} = \log \frac{\theta_{ij}}{1-\theta_{ij}}$ leads to $\lim_{\tau \rightarrow 0} \hat{G}_s = G_s$ and justifies the approximation of the Bernoulli distribution with the binary concrete distribution. During training, when $\tau > 0$, the objective function in (4.3) is smoothed with a well-defined gradient $\frac{\partial \hat{e}_{i,j}}{\partial \omega_{ij}}$ and becomes

$$\min_{\Omega} \mathbb{E}_{\epsilon \sim \text{Uniform}(0,1)} H(Y_o|G = \hat{G}_s) \quad (4.5)$$

The authors follow the approach of GNNExplainer [72] and modify the objective by replacing the conditional entropy with cross entropy between the label class and the prediction of the TM. This is justified by the greater importance of understanding the model's prediction of a certain class, rather than providing an explanation based solely on its confidence.

With the modification to cross-entropy $H(Y_o, \hat{Y}_s)$, where \hat{Y}_s is the prediction of the TM given the input \hat{G}_s , and the adaption of Monte Carlo sampling, the learning objective becomes

$$\begin{aligned} \min_{\Omega} \mathbb{E}_{\epsilon \sim \text{Uniform}(0,1)} H(Y_o, \hat{Y}_s) &\approx \min_{\Omega} -\frac{1}{K} \sum_{k=1}^K \sum_{c=1}^C P(Y_o = c) \log P(\hat{Y}_s = c) \\ &= \min_{\Omega} -\frac{1}{K} \sum_{k=1}^K \sum_{c=1}^C P_{\Phi}(Y_o = c | G = G_o) \log P_{\Phi}(\hat{Y}_s = c | G = \hat{G}_s^{(k)}). \end{aligned} \quad (4.6)$$

Φ denotes the parameters in the TM, K is the number of total sampled graphs, C is the number of class labels, and $\hat{G}_s^{(k)}$ denotes the k -th graph sampled with Equation 4.4, parameterized by Ω .

4.1.3 Global Explanations

The novelty of PGExplainer [43] lies in the ability to generate explanations for graph data with a global perspective, that allow for understanding the general picture of a model across a population. This saves resources when analyzing large graph datasets, as new instances can be explained without retraining the model, and can also be helpful for establishing the users' trust in these explanations. To achieve this the authors propose the use of a parameterized network that learns to generate explanations from the TM, which also apply to not yet explained instances.

GNN models generally apply two functions to first learn node representations and utilize these in downstream tasks such as graph classification or node classification [35], [68]. Therefore, Luo et al. [43] define two general functions $\text{GNNE}_{\Phi_0}(\cdot)$ and $\text{GNNC}_{\Phi_1}(\cdot)$ for any target GNN in the context of PGExplainer. $\text{GNNE}_{\Phi_0}(\cdot)$ denotes a model of L stacked GNN layers that returns higher dimensional node representations of the input graph and its node features. These are used as input for both the downstream task $\text{GNNC}_{\Phi_1}(\cdot)$ and the explainer network (see Equation 4.8). For models without explicit classification layers the last layer is used instead. It follows

$$\mathbf{Z} = \text{GNNE}_{\Phi_0}(G_o, \mathbf{X}), \quad Y = \text{GNNC}_{\Phi_1}(\mathbf{Z}), \quad (4.7)$$

where $\mathbf{Z} \in \mathbb{R}^{n \times D}$ denotes a matrix of n node representations \mathbf{z} , referred to as node embeddings. $\mathbf{X} \in \mathbb{R}^{n \times d}$ denotes the d -dimensional node features of G_o . The general target GNN model is visualized in Figure 4.1. Note that \mathbf{Z} encapsulates both features and structure of the input graph and therefore serves as input for the explainer network g_{Ψ} , defined as

$$\Omega = g_{\Psi}(G_o, \mathbf{Z}). \quad (4.8)$$

Ψ denotes the parameters in the explanation network and the output Ω is treated as parameter in Equation 4.6. Since Ψ is shared by all edges among the population, PG-

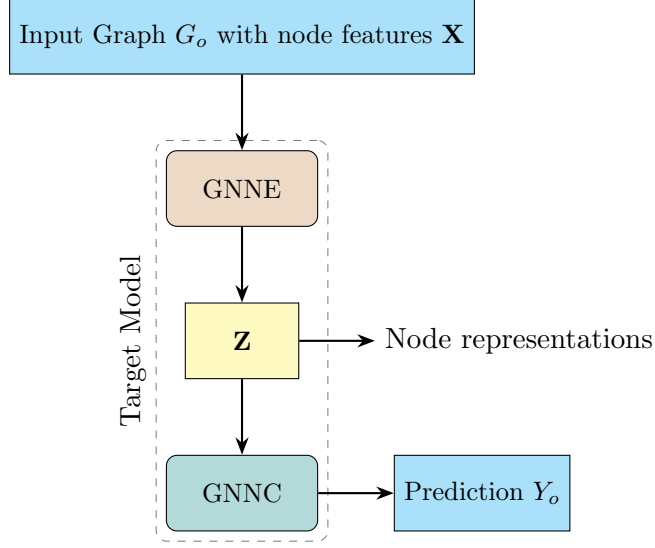


Figure 4.1: A black-box target model in the context of PGExplainer.

Explainer collectively provides explanations for multiple instances. Thus, the learning objective in a collective setting with \mathcal{I} being the set of instances becomes

$$\min_{\Psi} -\frac{1}{K} \sum_{i \in \mathcal{I}} \sum_{k=1}^K \sum_{c=1}^C P_{\Phi}(Y_o = c | G = G_o^{(i)}) \log P_{\Phi}(\hat{Y}_s = c | G = \hat{G}_s^{(i,k)}). \quad (4.9)$$

Consequently, $G_o^{(i)}$ and $\hat{G}_s^{(i,k)}$ denote the input graph and the k -th graph sampled with Equation 4.4, respectively, for instance i .

The authors propose two slightly different instantiations of Ω for node classification and graph classification tasks.

Explanation Network for Graph Classification

For graph level tasks, the authors consider each graph to be an instance, independent of specific nodes. The output Ω of the network (see Equation 4.8) is thus specified as:

$$\omega_{ij} = \text{MLP}_{\Psi}([\mathbf{z}_i \oplus \mathbf{z}_j]), \quad (4.10)$$

where MLP_{Ψ} is an MLP (see Section 4.3.1 for implementation details) parameterized with Ψ and \oplus denotes the concatenation operation. Effectively, for each edge in G_o a concatenation of both its nodes' embeddings is fed through the MLP. For the MLP used in both the original and this work the output ω_{ij} is an edge logit, which serves as a parameter in the sampling process.

Explanation Network for Node Classification

For node level tasks on the other hand, each prediction node is considered as an instance. Let an edge (i, j) be considered relevant for the prediction of a node u , but irrelevant for

the prediction of a node v . To explain the prediction of node v the authors specify the output Ω of the network in Equation 4.8 as:

$$\omega_{ij} = \text{MLP}_\Psi([\mathbf{z}_i \oplus \mathbf{z}_j \oplus \mathbf{z}_v]). \quad (4.11)$$

Thus, a concatenation of the node embeddings of nodes i, j and v is fed through the network. We denote this preprocessing step of creating edge embeddings from node embeddings as edge embedding transformation. The full pipeline of the PGExplainer can be observed in figure 4.2.

It is important to note, that for L -layer target GNNs utilizing a message passing mechanism, the prediction at node v is fully determined by its local computation graph [72]. The local computation graph of v is defined as its L -hop neighborhood $\mathcal{N}_L(v)$ (see Figure 2.5).

Collective and Inductive Setting

Due to the nature of its predecessor GNNExplainer [72], the main focus of the PGExplainer [43] was the application in a collective setting, where the goal is to explain a full population of instances by training on all these and thus being able to provide explanations for every single one. However, since the PGExplainer utilizes a deep neural network to parameterize the generation process of explanations for a population, it can be utilized in an inductive setting, unlike its predecessor.

This means that explanations can be generated for a set of instances from the same population, that have not been seen during training. Thus, it is not necessary to retrain the explainer for new instances of the same population, effectively reducing the computational complexity by the training time when compared to the GNNExplainer. Moreover, the number of parameters in the explainer does no longer depend on the size of the input graph

4.1.4 Regularization Terms

To enhance the preservation of desired properties of explanations the authors propose various regularization terms. These are added to the learning objective, depending on the specific downstream task at hand.

Size and Entropy Constraints

Inspired by GNNExplainer [72], to obtain compact and precise explanations, a constraint on the size of the explanations is added in the form of $\|\Omega\|_1$, the l_1 norm on latent variables Ω . Additionally, to encourage the discreteness of edge weights, element-wise entropy is added as a constraint:

$$H_{\hat{G}_s} = -\frac{1}{|E(\hat{G}_s)|} \sum_{(i,j) \in E(\hat{G}_s)} (\hat{e}_{i,j} \log \hat{e}_{i,j} + (1 - \hat{e}_{i,j}) \log(1 - \hat{e}_{i,j})), \quad (4.12)$$

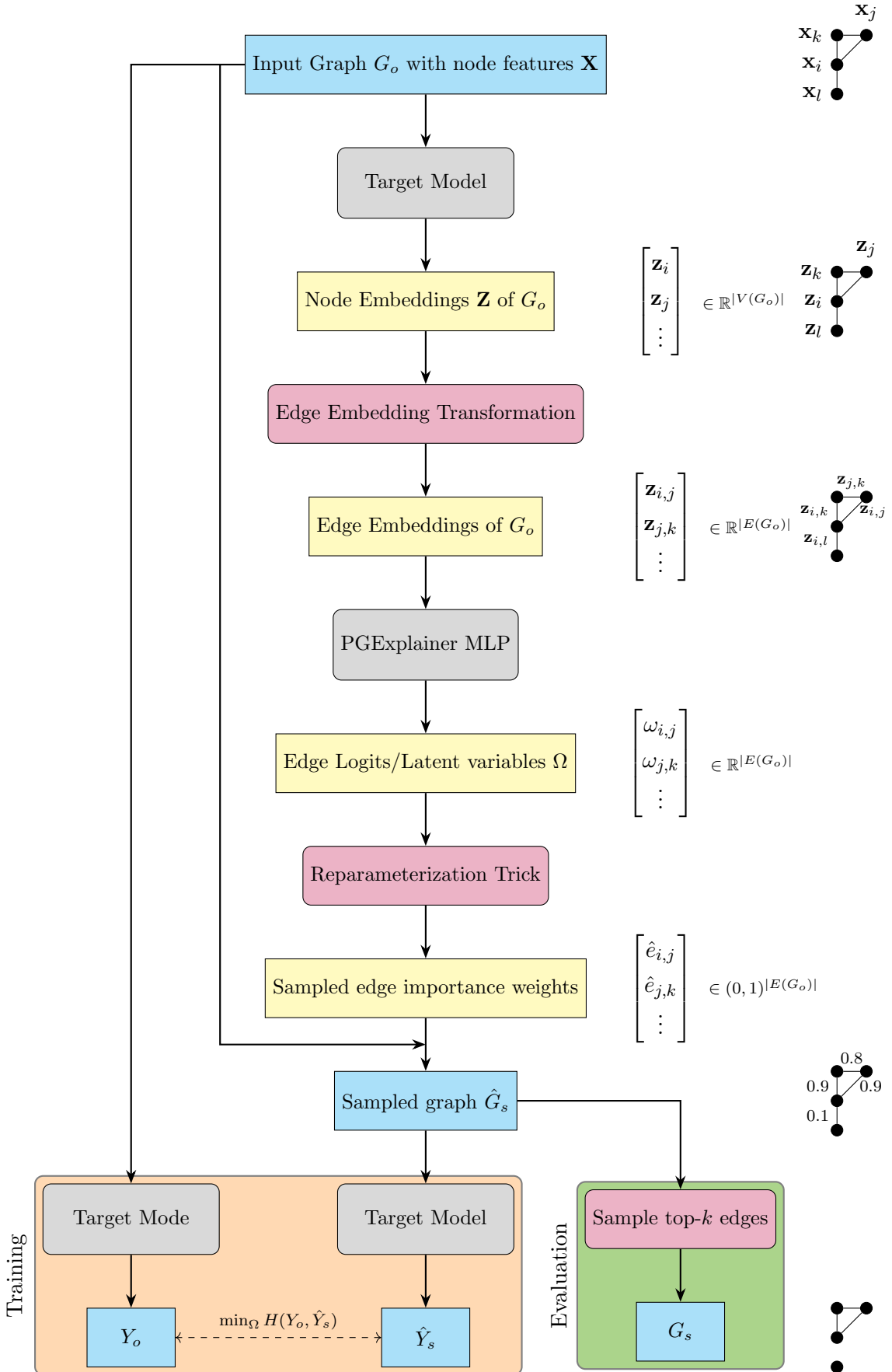


Figure 4.2: The complete pipeline of PGExplainer.

for each explanatory graph \hat{G}_s .

Note that the following two constraints are not used in the original experimental setup, but serve as inspiration for the constraints we introduce in our NeuroSAT application (see Section 4.2) and are therefore included.

Budget Constraint

The authors propose the modification of the size constraint to a budget constraint, for a predefined available budget B . Let $|E(\hat{G}_s)| \leq B$, then the budget regularization is defined as

$$R_b = \text{ReLU}\left(\sum_{(i,j) \in E(\hat{G}_s)} \hat{e}_{i,j} - B\right). \quad (4.13)$$

Note that $R_b = 0$ when the explanatory graph is smaller than the budget. When out of budget, the regularization is similar to that of the size constraint.

Connectivity Constraint

To enhance the effect of the explainer detecting a small, connected subgraph, motivated through real-life motifs being inherently connected, the authors suggest adding the cross-entropy of adjacent edges. Let (i,j) and (i,k) be two edges that both connect to the node i , then (i,k) should rather be included in the explanatory graph if the edge (i,j) is selected to be included. This is formally defined by Luo et al. [43] as

$$H(\hat{e}_{i,j}, \hat{e}_{i,k}) = -[1 - \hat{e}_{i,j} \log(1 - \hat{e}_{i,k}) + \hat{e}_{i,j} \log \hat{e}_{i,k}]. \quad (4.14)$$

We note that in practice this is implemented only for the two highest edge weights for each edge. The definition therefore would change to (i,j) and (i,k) being the edges carrying the top two edge weights from all nodes connecting to node i .

4.2 Extension to Application on NeuroSAT

In this section we propose additional restraints to fit the explanations of PGExplainer to the structure of SAT formulae. We start by giving a short introduction to NeuroSAT[64] and how it may function as a TM.

Proposed by Selsam et al. [64], NeuroSAT utilizes a MPNN, generally utilized to express GNNs, to solve SAT formulae. It is able to generalize in the sense that it may solve substantially larger and more difficult formulae than seen during training by running for more iterations. Though it may be used to calculate variable assignments that satisfy a formula, it is unable to provide proofs for predictions of formulae that are unsatisfiable.

In a separate experiment the authors were able to make NeuroSAT identify specific unsatisfiable cores. This is assumed to be due to the network memorizing the subgraphs rather

than learning a generic procedure that proves unsatisfiability. To support and validate the predictions of unsatisfiability, we aim to generate global, generalized explanations for unsatisfiable formulae using the PGExplainer, trained on predictions of a trained NeuroSAT model.

We test the quality and "human-understandability" of an explanation by comparing it to a MUS of the input problem, since the prediction of an unsatisfiable SAT instance can in theory be reduced to the prediction of said MUS. Furthermore, the fundamental idea of perturbing edges, or sets of edges, to learn explanations is analogous to the process of deleting clauses from a problem until a minimal unsatisfiable core is attained, as done in deletion-based MUS extractors (see Marques-Silva [48]). Thus, we test whether PGExplainer is able to generate explanations for NeuroSAT that align with MUSes.

Since the following restraints are tailored to the application on bipartite graphs representing SAT formulae, we have to define the specifics of the input LCG in this context. A formula is encoded as an undirected bipartite graph G_b , with bipartition (L, C) . It contains one node for every literal $l \in L$, one for every clause $c \in C$, and an edge for every pair (l, c) where l appears in clause c .

Additionally, in the context of NeuroSAT connections exist between each literal and its negation, since messages are also passed along these. Note that these edges are not present in the biadjacency matrix $\mathbf{B} \in \{0, 1\}^{L \times C}$. \mathbf{B} is used as input for the NeuroSAT model, without explicit node features. In the following definitions we let G_b be the original input graph for the PGExplainer, completely defined by its biadjacency matrix \mathbf{B} .

Since PGExplainer generates edge wise explanations, and we want to explain the SAT instance predictions with unsatisfiable cores as GT, we need to adapt the framework to account for the definition of unsatisfiable cores. Since a core is a subset of clauses, predicting singular edges that represent literals being present in a clause, may not provide sufficient results in the sense of human understandable explanations. Therefore, we propose a soft and a hard restraint that encourage the explainer to predict "sets" of edges that connect to the same node c , approximating the prediction of a complete clause.

The remainder of the explainer pipeline stays identical. The target model - NeuroSAT - calculates hidden node representations \mathbf{h}^t for the input graph G_b , now modeling a SAT instance, at each iteration t . The representations in the last iteration T are extracted as node embeddings \mathbf{z} for clause and literal nodes respectively, and transformed into edge embeddings (see Equation 4.10). Though this is only done for node level tasks in the original, we also consider using a concatenation of multiple hidden representations $\mathbf{h}^{\frac{1}{2}T} \oplus \mathbf{h}^{\frac{3}{4}T} \oplus \mathbf{h}^T$ as node embeddings \mathbf{z} . These serve as the input of the explainer MLP and are processed as usual, with either of the following additional limitations.

Soft Modified Connectivity Constraint

To account for the definition of unsatisfiable cores - a subset of clauses in the original formula whose conjunction is still unsatisfiable - we add a constraint that reinforces the prediction of complete clauses. Therefore, if the explainer assigns a high score to an edge (l_1, c) , all edges $(l_k, c) \in E(c)$ that also connect to the clause node c should receive a high score. Therefore, we introduce a soft constraint that punishes varying edge weights for the same clause. For our sampled bipartite Graph \hat{G}_s with node sets L and C containing literal nodes and clause nodes respectively, we define

$$R_C = \sum_{c \in C} \text{Var}(\hat{E}_c) = \sum_{c \in C} \frac{1}{|E(c)|} \sum_{(l,c) \in E(c)} (\hat{e}_{l,c} - \bar{E}_c)^2, \quad (4.15)$$

where

$$\hat{E}_c = \{\hat{e}_{l,c} \mid (l, c) \in E(\hat{G}_s)\} \quad (4.16)$$

denotes the set of edge weights corresponding to edges incident to c and

$$\bar{E}_c = \frac{1}{|\hat{E}_c|} \sum_{\hat{e}_{l,c} \in \hat{E}_c} \hat{e}_{l,c} \quad (4.17)$$

denotes the mean of \hat{E}_c . This is added to our objective function during training.

Hard Constraint

Since the soft constraint only encourages the prediction of entire clauses but does not enforce it, we also propose a hard constraint that modifies the prediction process. We restrain the edge logits $\omega_{i,j}$ calculated by the MLP to be identical for all edges that connect to the same clause. For all clause nodes $c \in C$, we calculate the mean logit μ_c of all edges incident to c with

$$\mu_c = \frac{1}{|E(c)|} \sum_{(l,c) \in E(c)} \omega_{l,c}. \quad (4.18)$$

The update rule is then defined as

$$\omega'_{l,c} \leftarrow \mu_c, \quad (4.19)$$

since edges in the biadjacency matrix are from literals to clauses at all times.

The reparameterization trick is still applied for each edge, but ϵ_c is sampled per clause instead of per edge, so that all edges that connect to a clause are forced to not only bear the same logit, but also the same importance score. The Equation 4.4 thus changes to:

$$\epsilon_c \sim \text{Uniform}(0, 1), \quad \hat{e}_{l,c} = \sigma((\log \epsilon_c - \log(1 - \epsilon_c) + \omega_{l,c}/\tau). \quad (4.20)$$

4.3 Implementation Details

In the following, we provide the implementation details needed to reproduce our results. This includes the general replication of the PGExplainer [43] with the adapted TMs in Section 4.3.1 and the specifics for the application on NeuroSAT [64] in Section 4.3.2.

4.3.1 Replication of PGExplainer

For our replication we try to implement the methods and details as close to the original paper as possible. Thus, we follow the general pseudocode algorithms presented by the authors (see Appendix A.1). Since the paper differs from the original codebase and is imprecise about certain descriptions, as found by Holdijk et al. [29], we aim to give a thorough description. This includes the tools we used, resulting changes regarding the data processing, the general architecture and hyperparameters of the TMs, the architecture and hyperparameters of the explainer model, as well as concrete methods implemented in the model.

Libraries

To reimplement the framework, we utilize a couple of libraries that we introduce shortly. Most notably, we use PyTorch Geometric [17], a library built upon PyTorch [54], that provides methods to create and train GNNs. For evaluation of the explainer model, specifically for calculating the AUROC score, we use TorchEval, a model evaluation library that is part of PyTorch. Furthermore, we integrate WandB [7] to monitor model performance and allow for easy hyperparameter searches. To visualize the graphs and their explanations we employ NetworkX [25]. Lastly, we utilize seaborn [69] to plot loss curves and other metrics.

Preprocessing

We use the original datasets that are provided in the PGExplainer codebase¹. We transform the data to fit our PyTorch Geometric framework. Each graph is stored as a torch-geometric Data object. This holds the d -dimensional node features as a tensor, the graph-level label index or alternatively all node-level labels as a tensor of class indices, a GT edge mask that contains the edges belonging to the motif, as well as boolean node masks for training, evaluating and testing the TM.

In PyTorch Geometric edges are stored in the edge-index format as a COO tensor - a PyTorch coordinate format that stores tuples of element indices and their corresponding values. In the context of graph edges in PyTorch Geometric, for an edge (i, j) the element index is the starting node i and the corresponding value its incident node j . This is computed from the adjacency matrix A as $A.\text{nonzero}().\text{t}().\text{contiguous}()$. First, the matrix indices or coordinates of the edges - non-zero elements - are extracted. These are then transposed and lastly stored in contiguous memory. The resulting shape of the edge-index is $[2, E]$, where E denotes the number of edges in the graph. Therefore, we only transform the data without changing its content.

¹<https://github.com/flyingdoog/PGExplainer>

Reproducibility

Inspired by Holdijk et al. [29] we implement the ability to seed the experiments performed on PGExplainer. PyTorch Geometric provides a way of seeding all modules that generate random numbers during the training process, including torch and python random. To further increase reproducibility, we utilize PyTorch’s `use_deterministic_algorithms`, forcing the learning algorithm to only use deterministic algorithms. For the dataset splits we use a separate fixed seed that consistently creates the same instance sets across all explainer training runs and experiments.

Target Model Specifications

In PGExplainer two slightly different architectures of GNNs for node classification and graph classification are introduced. We recreate these in PyTorch Geometric, while changing the exact layers used in the network to test whether the claim that the explainer does apply to any target GNN model holds. These models implement the same downstream classification tasks on the given datasets that achieve accuracies of at least 85%, a baseline set in GNNExplainer [72]. The datasets as well as the exact accuracies of each of the models are presented in the experimental setup (see Section 5.1).

Our model for both node- and graph classification consist of 3 `GraphConv` layers, a PyTorch Geometric implementation of the stacked GNN by Morris et al. [52] (see Equation 2.28). Since this layer allows for the passing of edge weights, weights of one are passed by default to simply maintain the discrete adjacency matrix, e.g., during training of the TM. Each of these layers has 20 hidden units and is followed by a ReLU activation function. The first layer processes the d -dimensional input node features, while the remaining layers retain the hidden dimensionality of 20.

Holdijk et al. [29] found that the original code wrongfully uses undocumented batch normalization layers in training mode during evaluation, which leads to a deviation in results, and thus completely omit the use of batch normalization. We choose to add batch normalization between the first two layers and their activation functions for both models, similar to the original codebase, without the training mode error. Additionally, we add an optional dropout layer after each activation function to improve the generalizability on more difficult tasks.

Note that in their codebase the authors use a concatenation of the hidden representations at each layer instead of solely the final layer representation as node embeddings for node level tasks. This leads to $\mathbf{Z} \in \mathbb{R}^{n \times (LD)}$ being the matrix of node embeddings \mathbf{z} that are computed as:

$$\mathbf{z}_i = \mathbf{h}_i^{(1)} \oplus \mathbf{h}_i^{(2)} \oplus \mathbf{h}_i^{(3)}, \quad (4.21)$$

with $\mathbf{h}_i^{(l)} \in \mathbb{R}^D$ denoting the hidden representations of node i in layer l for the specified $L = 3$ layer network with constant embedding dim $D = 20$.

Thus, the node embeddings used in the explainer as well as in the downstream classification task each have a shape of $\mathbb{R}^{3(20)}$. For the classification a final linear layer is added to the model that maps each 60-dimensional node embedding to C classes. A softmax is applied to the model output to get class probabilities for each node. We also adopt this in our implementation.

The softmax function is defined as follows [22]: Given a vector $\mathbf{z} = [z_1, z_2, \dots, z_K] \in \mathbb{R}^K$, the softmax function maps \mathbf{z} to a probability distribution over K classes:

$$\text{softmax}(\mathbf{z})_i = \frac{e^{z_i}}{\sum_{j=1}^K e^{z_j}} \quad \text{for } i = 1, 2, \dots, K, \quad (4.22)$$

where e denotes the exponential function.

The model used for graph tasks differs slightly, in the sense that only the hidden embeddings of the last `GraphConv` layer are treated as node embeddings. In addition, before the final linear layer used for classification, both a max pooling and mean pooling operation are performed on the embeddings of each graph and the results concatenated to get a representation of a complete graph. Note that the paper only states to use max pooling, while in practice a concatenation of the max pooling and sum pooling is used. We adopt the combination of mean pooling and max pooling from the replication study [29], as this has been used in recent graph neural networks [45], [65], [76].

The max pooling operation extracts the maximum value of each feature dimension across the nodes of a graph, while the mean pooling extracts the mean value of each feature dimension across all nodes of a graph. Since the results of both pooling operations are in \mathbb{R}^{20} , the resulting 40-dimensional graph embedding is fed into the linear layer, again mapping to C classes, and a softmax is applied to get probabilities of a graph belonging to each class. Figure 4.3 visualizes both described models.

Furthermore, following the original paper, all layer weights are initialized with Xavier initialization [21], while biases are initialized with 0. The datasets are split into training, testing and validation sets with an 80/10/10 split ratio. The models are trained for 1000 epochs, with a learning rate of 1.0×10^{-3} and Adam [34] is used as an optimizer. The loss is defined as the PyTorch `CrossEntropyLoss()` between the GNN prediction and the actual label of the input.

Note that the main differences between our TM and the model described in PGExplainer [43] lie in the used graph layer, as well as the addition of dropout, two batch normalizations before the activations, rather than after activations, and the usage of a slightly different global pooling.

We want to stress that though not documented in the paper, early stopping is utilized in the TM training and the model state with the highest validation accuracy is selected. For models that achieve the highest accuracy at multiple epochs, the model state with the

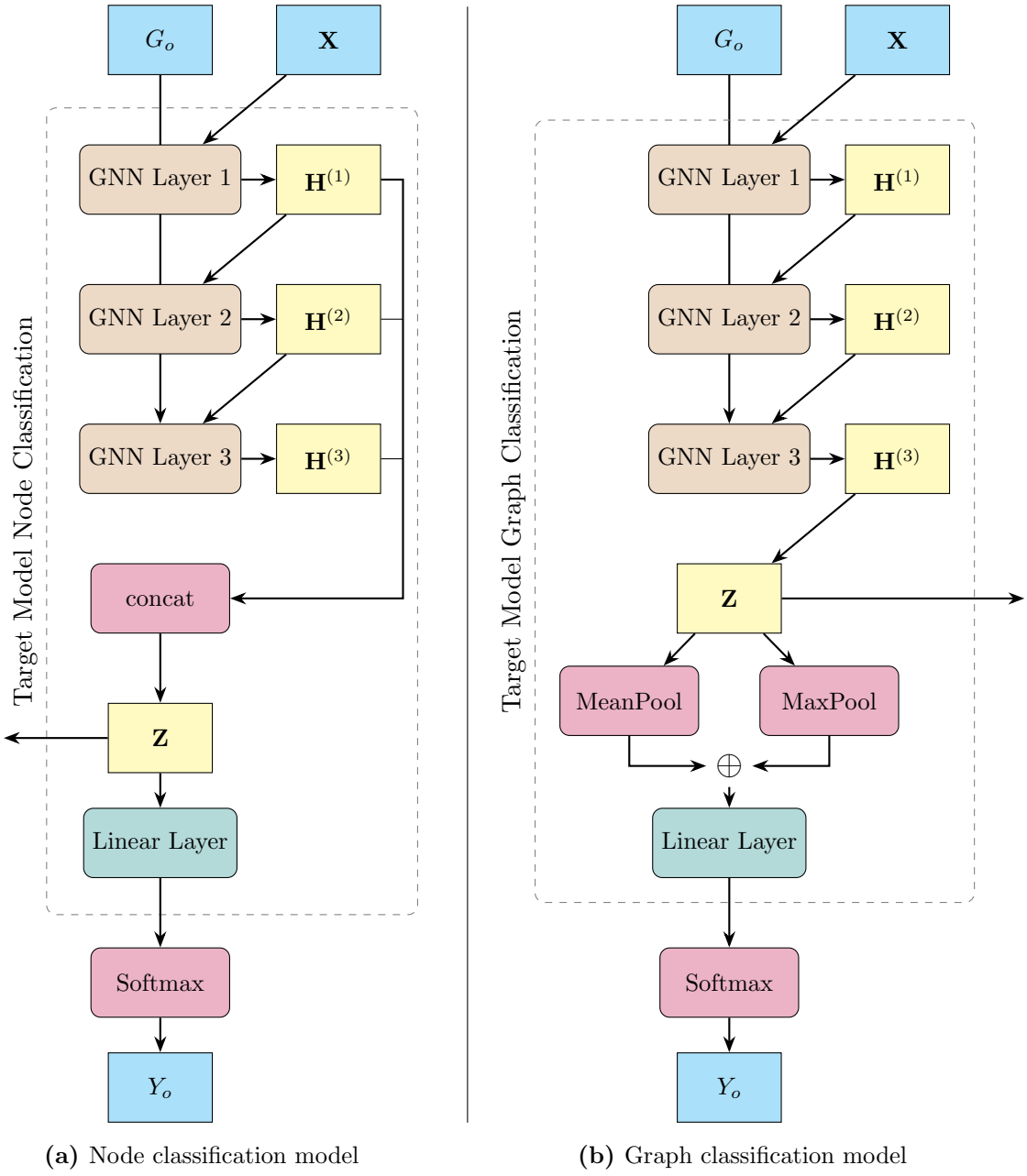


Figure 4.3: Visualizations of the two target GNN models used for node classification (a) and graph classification (b). "concat" denotes the row-wise concatenation along the feature dimension.

lowest validation loss is chosen. If the validation loss does not decrease below the minimum for 500 epochs, the training is stopped early. This is very important for a fair comparison of the models, as we found that the explanations of an overfit TM differ significantly from those of the best performing one.

In a more recent version of the PGExplainer [44], the authors add a formal description of the TM layer used in their framework. The used GNN layer is defined as:

$$f(\mathbf{H}^{(l)}, \mathbf{A}) = \sigma(\mathbf{W}^{(l)} \mathbf{A} \mathbf{H}^{(l)}), \quad (4.23)$$

where A is the normalized Laplacian matrix.

Note that a PyTorch Geometric implementation of the GCN layer described in equation 2.27 is used in the replication paper [29] with a ReLU activation function. Thus, the sole difference between the two is the order of the matrix multiplication.

We use a PyTorch Geometric implementation of the stacked GNN layer with a ReLU activation function, as defined in Equation 2.28. On the one hand, it works on bipartite graphs by definition. On the other hand, it explicitly allows for edge weights to be passed, which is essential for applying the sampled, approximate discrete explanation mask to the input graph during training. This is necessary since in practice, applying a hard mask to the input graph would prevent the computation of gradients during backpropagation.

Thus, instead of actually removing edges of the graph, the edge importance scores that are learned by the MLP are treated as edge weights in the prediction process of the TM, with higher scores indicating edges being more relevant for the prediction. During training, the prediction for the original input graph is computed from the graph defined by its node features and edge-index alone, while for the sampled graph the edge weights are passed additionally and internally multiplied with the edge-index.

Explainer Architecture

We implement the explainer MLP architecture described in the paper. It consists of two linear layers, with a ReLU activation function applied after the first. The first layer maps the input edge embedding dimension to 64 hidden units, and the second maps the hidden units to a single output scalar. The input edge embeddings for the MLP are calculated as described in Section 4.1.3.

For the described TMs, the resulting MLP input - a concatenation of the node embeddings - has a shape of $\mathbb{R}^{2 \cdot 20}$ for graph tasks and $\mathbb{R}^{3 \cdot 60}$ for node tasks. Again, this is taken from the original codebase, as the paper does not consider the node embeddings as a concatenation of all GNN layers for node tasks.

We implement the calculation of edge embeddings as seen in Listing 4.1.

```

1  def getEdgeEmbeddings(self, modelGNN, x, edge_index, nodeToPred=None):
2      emb = modelGNN.getNodeEmbeddings(x, edge_index)
3      i, j = edge_index[0], edge_index[1]

```

```

4
5     if nodeToPred is not None:
6         node_emb = emb[nodeToPred].repeat(len(i), 1)
7         embCat = torch.cat([emb[i], emb[j], node_emb], dim=1)
8     else:
9         embCat = torch.cat([emb[i], emb[j]], dim=1)
10    return embCat

```

Listing 4.1: Implementation of edge embedding calculation.

The trained, fixed TM `modelGNN` is passed to the explainer and returns its node embeddings for the input graph, defined by its node features `x` and the `edge_index`. Depending on the task at hand, the node embeddings of each two connected nodes, as well as the node embeddings of the node to be predicted `nodeToPred` in the case of a node task, are concatenated and returned as edge embeddings.

Explainer Training Specifications

We initialize all linear layer weights of the explainer with He initialization [27], which is used by default for linear layers with ReLU activation in PyTorch. We also test the effect of adopting the initializations from the TMs and initializing all layer weights with Xavier [21] (see Section 5.1.2). Biases are generally initialized with zero. During training, the Adam [34] optimizer is used to update the model parameters based on gradients. Additionally, gradients are clipped during training using PyTorch’s `clip_grad_norm_` with a maximum norm of 2. The authors define the temperature used in the reparameterization trick (see Equation 4.4) with an annealing temperature schedule, as proposed by Abid et al. [1]:

$$\tau^{(t)} = \tau_0 \left(\frac{\tau_T}{\tau_0} \right)^{\frac{t}{T}}, \quad (4.24)$$

where t is the current epoch and T is the total number of epochs. τ_0 and τ_T are hyperparameters that define the initial and final temperature, respectively. The reason for this is that small temperatures tend to generate more discrete graphs, as they more closely approximate samples from the binary concrete distribution. While this is desirable at convergence, it may hinder the optimization early in training due to a reduced gradient signal. It should be noted that in the original codebase t is initialized with 0, leading to a temperature $\tau^{(0)} = \tau_0$ in the first epoch, and $\tau^{(T-1)} = \tau_0 \left(\frac{\tau_T}{\tau_0} \right)^{\frac{T-1}{T}}$ in the last epoch. We initialize t with 1 to get a temperature of $\tau^{(T)} = \tau_T$ in the last epoch, as we believe this to be more inline with the proposition by Abid et al. [1].

As established in Section 4.1.3, the node prediction of an L -layer GNN is completely determined by its local computation graph, defined as its L -hop neighborhood [72]. This is capitalized on during explainer training by computing the neighborhood graphs of each input node and treating this subgraph as a base for the node predictions, rather than using the full graph (see Algorithm 1). Since the TMs for node tasks consist of three

graph layers, the 3-hop subgraph of each node is computed. We implement this using the `k_hop_subgraph()` function from PyTorch Geometric.

We compute the loss as described in Equation 4.9, with each regularization term being added according to a regularization coefficient hyperparameter. It is noteworthy that the loss function used in the original codebase can formally be defined as:

$$\min_{\Psi} \frac{1}{K} \sum_{i \in \mathcal{I}} \sum_{k=1}^K -\log P_{\Phi}(\hat{Y}_s = c_i | G = \hat{G}_s^{(i,k)}), \quad (4.25)$$

where c_i denotes the class label according to the prediction on the original graph $G_o^{(i)}$ and $K = 1$. However, this is not mentioned in the paper and therefore not adopted.

A further undocumented specification is that for TMs that perform node tasks, only node instances that belong to the "motif classes" are selected for training and evaluation, since for nodes that do not belong to these classes there does not exist a specific GT motif that may serve as an explanation. This is only documented for one graph classification dataset, where only one of two possible classes has a dedicated motif. The specific node sets used for each dataset vary as well and are presented in Section 5.1.

In the PGExplainer paper, Luo et al. [43] propose the use of high temperatures, with $\tau_0 = 5.0$ and $\tau_T = 2.0$. Holdijk et al. [29] found that all hyperparameters described in the paper are overly simplified and in practice, different parameters are used for each dataset. Therefore, we conduct hyperparameter searches for each task in 5.1. We add that the number of sampled graphs K is not defined in the original work, and the codebase suggests the use of $K = 1$. We implement the ability to sample multiple graphs as described in the pseudocode (see Appendix A.1) and also consider this in our hyperparameter searches.

Extension Description

This is not described in the original paper, but since undirected graphs contain bidirectional edges, effectively each edge carries two importance scores. The authors alleviate this in the code by symmetrizing the edge weight matrix, corresponding to the adjacency matrix of the graph. We propose meaning the logits of each pair of bidirectional edges after the MLP output has been calculated. We implement the logic of meaning each edge's logits as seen in Listing 4.2.

```

1  edge_pairs = edge_index.t()
2  # Sort node pairs so that (i, j) and (j, i) are treated the same
3  canonical_pairs, _ = edge_pairs.sort(dim=1)
4  # Find unique undirected edges and get mapping indices
5  unique_pairs, inverse_indices = torch.unique(canonical_pairs, dim=0)
6
7  # Average weights for duplicate edges
8  for i in range(unique_pairs.size(0)):

```

```

9     mask = inverse_indices == i
10    mean_weight = torch.mean(w_ij[mask])
11    w_ij[mask] = mean_weight

```

Listing 4.2: Implementation of meaning bidirectional edge weights.

All edge pairs from the edge-index that connect the same two nodes, e.g. (i, j) and (j, i) , are treated as a unique pair. For each of these unique pairs the mean of the logits $\omega_{i,j}$ and $\omega_{j,i}$ corresponding to its two edges is calculated and used to update each of the two logits. To account for this in the reparameterization trick, the unique pairs are further passed there to sample ϵ for each edge pair, rather than each edge. This process guarantees edge pairs that connect the same two nodes to always carry identical importance scores.

Evaluation Implementation

To quantitatively evaluate the explanations of each prediction (see Section 5.1), the authors utilize the ROC-AUC as a metric to compare the predicted importance scores of the edges to the GT edges. Since the exact procedure is not further described by the authors, we extract it from the codebase as far as possible.

For graph tasks the metric is computed globally, meaning that for all graph instances the edge predictions and GTs are gathered, and the global thresholds are computed, while for node tasks the metric is computed locally for the 3-hop subgraph of each node instance and a mean is calculated later on. Since a reason for this difference in calculation is not provided, we choose to only consider the mean of the local values, regardless of task, to get a uniform procedure. Additionally, we believe that this is more in line with the inductive setting, where individual unseen instances can be explained.

It is notable that motif nodes may be selected for explanation, where the local computation graph only consist of motif nodes and consequently only GT edges. Since the local AUROC score is not computable for these binary cases with only one class present, it is explicitly disregarded and skipped for these nodes in the evaluation process. Note that these node instances are not disregarded during training.

We implement this calculation using the `BinaryAUROC` from TorchEval, which operates identical to the `roc_auc_score` from scikit-learn [55] in the binary case, used in PGExplainer [43].

The qualitative explanations provided by the explainer are implemented as a NetworkX visualization of the graph instance in the case of graph tasks, or a visualization of the 3-hop subgraph of the instance node in the case of node tasks. Only the edges with the top- $2k$ importance scores are drawn, where k equals #motif-edges, since edges are bidirectional and guaranteed to carry identical weights. k can therefore be understood as a needed parameter for qualitative evaluation [29].

The inference time is measured as the time it takes to generate an explanation for any instance. This starts with the computation of node embeddings from the TM and ends

after the reparameterization trick - the simple application of a Sigmoid to the edge logits during evaluation - that returns the edge importance scores. This process is illustrated in Figure 4.2, starting from input graph G_o and ending at the sampled graph \hat{G}_s .

4.3.2 Application on NeuroSAT

In this section we describe the necessary changes for explaining predictions of NeuroSAT [64] with our PGExplainer framework. We want to stress that the NeuroSAT codebase was provided by a fellow student and only the changes mentioned in this section are part of our work. The source code for NeuroSAT is publicly available.²

Since NeuroSAT can be regarded as a black box MPNN in the context of our work, we only describe how it passes messages superficially. In each iteration, each clause receives messages from its neighboring literals to update its embedding. Then, each literal receives messages not only from its neighboring clauses, but also from its complementary literal, to update its embedding. The number of iterations is set to 26 for the model used, which was trained in the standard manner on both satisfiable and unsatisfiable SAT problems - formulae in CNF with the goal of determining whether they are satisfiable. The downstream task of NeuroSAT can hence be understood as a graph classification task.

Besides the prediction of satisfiability, NeuroSAT returns the node embeddings of both clauses and literals at each iteration. We use these to generate edge embeddings for all edges in the biadjacency matrix as input for the explainer MLP (see Section 4.2), using the same procedure as in the previous replication study (see Section 4.3.1). Since the SAT instances are defined as biadjacency matrices, edges only exist in one direction - from literals to clauses. Thus, we dismiss the meaning of edge logits and qualitatively evaluate using the top- k edges, rather than the previous top-2 k .

The only change we have to make is allowing the NeuroSAT forward pass to receive edge weights as a parameter. If no edge weights are passed, the forward pass behaves as usual and the biadjacency matrix contains discrete values of 0 or 1. When predicting sampled graphs from the explainer, we pass the sampled edge weights and multiply these with the biadjacency matrix, to receive a weighted biadjacency matrix. NeuroSAT then calculates the prediction for the weighted matrix. This change is implemented as seen in Listing 4.3.

```

1 connections = torch.sparse_coo_tensor(
2     indices=edges,
3     values=torch.ones(problem.n_cells, device=self.device)
4     if edge_weights is None else edge_weights,
5     size=torch.Size([n_literals, n_clauses])
6 ).to_dense()

```

Listing 4.3: Adaptation of NeuroSAT.

²Daniel Selsam et al. “NeuroSAT” (2018). URL: <https://github.com/dselsam/neurosat>

Usually, the `connections` tensor - a biadjacency matrix - is initialized with ones at the coordinates of the edge-index tensor `edges`, containing `problem.n_cells` edges of a SAT problem batch. However, when `edge_weights` is passed into the function, the edge weights are used as initialization, rather than ones. This can be understood as a multiplication of the edge weights with the ones representing edges.

Furthermore, the input of the explainer pipeline changes to a SAT problem instance, containing only the edge-index representation of a SAT formula, as well as a label 1 or 0, denoting satisfiability or unsatisfiability, respectively. Node features are not used in NeuroSAT and therefore irrelevant for the explainer.

The hard constraint described in Section 4.2 is implemented as seen in Listing 4.4.

```

1  batch_clauses = torch.tensor(problem.batch_edges[:, 1])
2  clauses, inverse_indices = torch.unique(batch_clauses, dim=0,
3      return_inverse=True)
4
5  for clause_id in clauses:
6      mask = batch_clauses == clause_id
7      clause_edge_probs = w_ij[mask]
8
9      if len(clause_edge_probs) > 1:
10          clause_mean_weight = torch.mean(clause_edge_probs)
11          w_ij[mask] = clause_mean_weight
12
13  if self.training:
14      rand_vals = torch.rand(len(clauses), device=w_ij.device) + 1e-8
15      epsilon = rand_vals[inverse_indices].reshape(w_ij.shape)
16
17      trick = (torch.log(epsilon)-torch.log(1-epsilon)+w_ij)/temp
18      edge_ij = nn.Sigmoid()(trick)
19  else:
20      edge_ij = nn.Sigmoid()(w_ij)
```

Listing 4.4: Implementation of Hard Constraint.

First, all clauses are extracted from an edge index batch `problem.batch_edges`. Since these appear in the edge index for each literal that connects to it, we need to calculate the `torch.unique` clauses. For each `clause` in this list of unique `clauses` we create a mask that stores its appearance in the `batch_clauses` and extract the masked edge logits `w_ij` that have the same shape as `batch_clauses`. For all clause logits `clause_edge_probs` the mean is calculated and the logits `w_ij` are updated accordingly. The unique `clauses` are further used in the reparameterization trick to sample a unique `epsilon` for each clause rather than for each edge.

The soft constraint uses the same idea of iterating over the unique `clauses` in a batch. Instead of calculating the `torch.mean` it calculates the `torch.var` and adds this to the loss after multiplication with a fixed connectivity coefficient hyperparameter.

To evaluate the explanations provided by the PGExplainer, we require GTs to calculate the AUROC score and understand the visualizations of explanations. Since our goal is testing whether the explanations of unsatisfiable problems, based on NeuroSAT predictions, align with human-understandable concepts, we propose the use of MUSes as GT. Therefore, we utilize the deletion-based MUS extractor `MUSX` from PySAT [31] to generate a MUS for each unsatisfiable problem. This MUS is transformed into a mask matching the corresponding edges in its problem’s graph representation, and treated as expected GT. This allows us to calculate the local AUROC for each SAT problem as described in Section 4.3.1. We visualize the provided explanations and GTs as a `pyvis` [56] Network for qualitative evaluation.

We adopt the MLP architecture described in Section 4.3.1, but also perform experiments with a more complex architecture (see Section 5.2). This introduces two additional hidden layers, leading to the architecture described in Listing 4.5.

```

1   self.model = nn.Sequential(
2       nn.Linear(self.inputSize, 256),
3       nn.ReLU(),
4       nn.Linear(256, 64),
5       nn.ReLU(),
6       nn.Linear(64, 20),
7       nn.ReLU(),
8       nn.Linear(20, 1)
9   )

```

Listing 4.5: Implementation of extended MLP architecture.

The `inputSize` depends on whether the node embeddings \mathbf{z} are used from the last iteration or if a concatenation of the states at multiple iterations shall be used. Since the embedding size of NeuroSAT is 128, this leads to an edge embedding `inputSize` of either 256 or 768, respectively. Besides these changes, the explainer operates as previously explained.

Chapter 5

Experiments and Results

In this chapter we introduce all performed experiments. This includes a general experimental setup, as well as more detailed experiment settings including their results.

Since our work is twofold, we start with the experiments regarding the replication of the PGExplainer with a changed TM architecture and a focus on the inductive setting in Section 5.1. Next, we describe the experiments performed on the adapted explainer framework to generate explanations for the NeuroSAT model predictions of unsatisfiable problems in Section 5.2.

5.1 Replication of PGExplainer

In this section we present all experiments regarding the replication of the presented explainer model. We first put forward the common experimental setup, including the datasets, corresponding TMs and hyperparameter searches (see Section 5.1.1). In Section 5.1.2 we replicate the experiments in the inductive setting from the original paper with our adapted TMs. Furthermore, in Section 5.1.3 we perform the original quantitative experiment in the collective setting for better comparability, as this was the core study of the original paper. We also include a study on the effect of using a larger set of training data, as the original proposes that only few training instances are necessary for the explainer to generalize well (see Section 5.1.4). In Section 5.1.5 we run an experiment specific to the BA-2Motif dataset, as we found that it behaves opposite to the expectations. Later, we study the effects of the specific node sets that were used in the original codebase in Section 5.1.6. Lastly, we qualitatively evaluate the explanations provided by our reimplemented model (see Section 5.1.7).

5.1.1 Common experimental setup

In this section we describe the common setup for the experiments that we perform on PGExplainer. We follow the experimental setup from the PGExplainer as closely as possible. Since the textual description refers to the setup from GNNExplainer and is lacking

in some aspects, we mostly extract the missing information from the codebase. As the hyperparameters are unclear or not comprehensible for some tasks we also draw information from the settings used in the replication by Holdijk et al. [29].

Datasets

We perform the experiments on the same datasets used in the original. These were constructed by the authors similarly to the ones used in the baseline GNNExplainer. Four synthetic datasets were used for the node classification tasks. For the graph classification task the authors provide one synthetic dataset as well as the real-world dataset MUTAG. The synthetic datasets are constructed by creating a base graph and attaching motifs to random nodes of the base graph. These motifs determine the labels of the nodes or graphs, depending on the task at hand, and therefore serve as the GT explanations that the explainer shall detect. Statistics of each dataset can be found in Table 5.1 and a visualization in Section A.2. We will give a short description of each dataset.

Since three of the synthetic datasets use a Barabási-Albert (BA) graph as a base, we briefly introduce the BA model [2]. The BA model generates scale-free networks that grow over time. Starting with an initialization network of $m_0 \geq m$ nodes, at each step a new node is added and connected to m of the nodes already existing in the graph. The probability for each node to be selected as a neighbor depends on its degree, leading to a higher probability for nodes that already have a high degree rather than nodes with a low degree.

BA-Shapes is the first node dataset that consists of a single BA-graph with 300 nodes and 80 house motifs - five nodes resembling the shape of a house (see Figure 5.1a). Base graph nodes are labeled with 0 while nodes at the top/middle/bottom of the "house" are labeled with 1,2,3, respectively. The top node of each house motif is attached to a random base graph node. Additional edges are added for perturbation. Each node is assigned a 10-dimensional feature vector of 1s.

BA-Community consists of two unified BA-Shapes graphs. The features of the nodes are sampled from two Gaussian distributions. Nodes are labeled according to the house motif scheme for each community respectively, leading to 8 classes in total.

Tree-Cycles uses an 8-level balanced binary tree as a base graph. 80 cycle motifs, consisting of a 6 node cycle (see 5.1b), are attached to random nodes from the base graph. Node features are assigned as a 10-dimensional vector of 1s. A node of the base graph is labeled as 0 and a motif node is labeled as 1.

The Tree-Grid dataset is assembled in the same way as Tree-Cycles, with the difference that the motifs are 3-by-3 grids (see 5.1c). Node features and labels also follow the same procedure.

BA-2Motif is the first graph-level dataset with 800 graphs. Each of these graphs is obtained by attaching either a house or a cycle as a motif to a base BA graph of 20 nodes. According

to the attached motif the graphs are assigned one of two labels, with 0 or 1 implying a house or circle, respectively. Node features are represented as 10-dimensional vectors with elements equal to 0.1, instead of 1.

The real-world dataset MUTAG contains 4,337 molecule graphs that are assigned to one of 2 classes, depending on the molecules mutagenic effect [59], [72]. Node features are assigned as a one-hot encoding in $\{0, 1\}^{14}$, representing the chemical group of a node out of 14 possible ones. Following [13], [72], carbon rings with chemical groups NH_2 or NO_2 are known to be mutagenic, with carbon rings in general existing in both mutagenic and non-mutagenic graphs. The authors thus propose treating the carbon ring as a shared base graph and NH_2 and NO_2 as motifs for mutagenic graphs (see 5.1d). Since there are no explicit motifs for the non-mutagenic graphs, these graphs are not considered in PGExplainer.

	Node Classification				Graph Classification	
	BA-Shapes	BA-Community	Tree-Cycles	Tree-Grid	BA-2Motifs	MUTAG
#graphs	1	1	1	1	1,000	4,337
#nodes	700	1,400	871	1,231	25,000	131,488
#edges	4,110	8,920	1,950	3,410	51,392	266,894
#labels	4	8	2	2	2	2

Table 5.1: Dataset statistics for Node and Graph Classification tasks, reprinted from [43].

Note that in the collective setting used in the original paper the explainer is trained and evaluated on the same data. This data is further reduced by only using graphs and nodes that contain a GT motif. This makes sense for evaluation, since the AUROC cannot be calculated for GTs with only one class present. However, the authors do not specify why the training is performed only on these instances. Therefore, only the 1,015 mutagenic graphs where either NH_2 or NO_2 are present are selected for the MUTAG experiment.

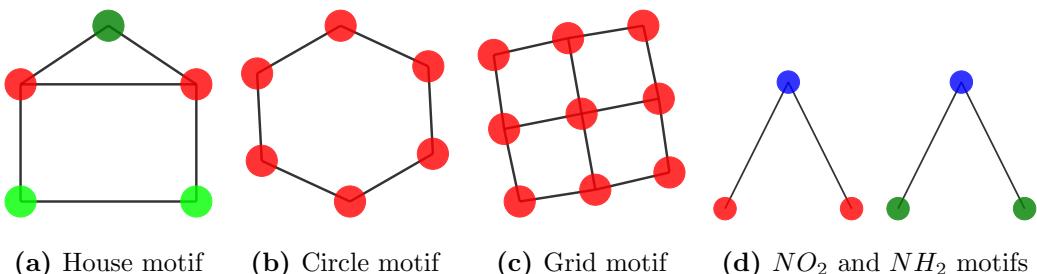


Figure 5.1: The different motifs used in the datasets.

In the node classification experiments the instance sets \mathcal{I} containing the nodes to be explained, used for both training and evaluation, were further finetuned per dataset. This

leads to a selection of either all nodes that are part of a motif, or only one node per motif. This inconsistency is also left unexplained by the authors and extracted from the codebase. It is likely adapted from the GNNExplainer [72], where single-instance and multi-instance explanations are differentiated. We perform an experiment on the effects of these node selections in 5.1.6.

For the instance set \mathcal{I} used in BA-community multiple configurations exist in the PGExplainer codebase. One is extracted from the GNNExplainer [72] and consists of the same nodes used for the BA-Shapes dataset, which seems unjustified and is not addressed in the paper. Another setting uses all motif nodes of both communities - effectively all nodes that do not belong to the two community base graphs. We select this setting for our replication, as this makes more sense than using the arbitrary indices from BA-Shapes.

The selection of instances for the remaining dataset is as follows: In BA-Shapes one "middle" node from each motif in the graph is selected as instance. A similar selection is used in Tree-Cycles, where the "first" motif node connected to the base graph is chosen for each motif. For Tree-Grid all motif nodes in the graph are selected as instances, similar to BA-Community. For the graph dataset BA-2Motif all graphs are used as instances, since each one explicitly contains one of the two motifs. The consequential number of instances N used for each dataset are listed in Table 5.2. Note that these instance sets are only considered in the explainer and not during TM training.

	Node Classification				Graph Classification	
	BA-Sh.	BA-Community	Tree-Cycles	Tree-Grid	BA-2M.	MUTAG
#total motif instances	300	800	360	289	1,000	1,015
#used motif instances N	60	800	60	289	1,000	1,015

Table 5.2: Amount of possible and actually used motif instances per dataset, as found in the original codebase.

The fixed TM that we use for each dataset is trained as described in Section 4.3.1. Since we use a different GNN layer, we try to achieve accuracies above 85%, similar to the original. The accuracies can be seen in Table 5.3 and are slightly higher than in the original for four of the datasets, except for BA-Community and MUTAG. We add a dropout layer with a probability of $p = 0.1$ to the latter two models to improve their generalizability and achieve testing scores closer to the original. The exact downstream task accuracies achieved in PGExplainer [43] can be seen in Table A.1.

Accuracy	BA-Shapes	BA-Community	Tree-Cycles	Tree-Grid	BA-2Motif	MUTAG
Training	1.00	0.92	1.00	0.99	1.00	0.86
Validation	1.00	0.87	1.00	0.99	1.00	0.86
Testing	0.97	0.89	0.99	0.99	1.00	0.82

Table 5.3: Accuracy table for node and graph classification downstream tasks from our reimplementations using a slightly adapted GNN.

Evaluation Metrics

Following Luo et al. [43], the explanation problem is considered a binary classification of edges for quantitative evaluation. Edges that appear in a motif are positive targets, and negative otherwise. The edge importance weights of each explained instance are treated as prediction scores.

Since the original paper does not specify the exact calculation of the AUROC score, we use the approach described in Section 4.3.1 for a standardized procedure. Thus, we conduct the mean over the local AUROC scores of all instances as the metric for quantitative evaluation. Node instances with a local computation graph of only motif nodes are skipped in the calculation due to having only positive targets. We calculate the mean local AUROC on the training-, validation and test sets individually. The validation set is used to evaluate the hyperparameter search, while the results of the following inductive experiments usually consider the score on the test set. For the collective setting we only consider a singular instance set that is used for both training and evaluation.

To qualitatively evaluate the explanations we visualize the top- k explanation mask edges with the highest prediction scores, following Luo et al. [43]. The parameter k for each dataset is extracted from the original codebase, and is set to include at least the number of GT motif edges in the explanation. For node classification tasks the visual explanations only include the nodes inside the local computation graph of the prediction node, as only these are relevant for the prediction [72].

We perform the efficiency evaluation as described by Holdijk et al. [29]. The average inference time needed to generate an explanation for any instance is calculated over the test set for each run individually (see Section 4.3.1). We include the mean of these averages for the inductive replication experiment only.

Hyperparameter Search

Most details on the training procedure of the explainer have been established in Section 4.3.1. As found by Holdijk et al. [29] the PGExplainer is very sensitive to hyperparameter settings on each dataset. Therefore, we conduct hyperparameter searches for the explainer model on each of the datasets to obtain the best performing explainers. We follow Liashchynskyi and Liashchynskyi [39] to perform grid searches over the parameter

space that we define as an extended combination of the setting used in the original [43], as well as the configs provided in Replication study [29].

For our hyperparameters $\lambda_1, \lambda_2, \dots, \lambda_n$ we define corresponding sets S_1, S_2, \dots, S_n of possible values. The grid search finds the best model with respect to the mean of the local AUROC scores on all validation instances over all combinations $(\lambda_1, \lambda_2, \dots, \lambda_n) \in S_1 \times S_2 \times \dots \times S_n$. Additionally, we consider that the predicted edge importance scores shall not be exactly 0 or 1 for all edges. Although the theory defines the importance score to be in (0,1), in practice scores of 0 and 1 are possible due to floating point precision limits. Since we found that some datasets behave unexpectedly regarding the evaluation metric, we may choose to optimize in the opposite direction, which we will further discuss in Section 5.1.2. All experiments and training were conducted on an AMD Ryzen 7 2700X processor.

The hyperparameters tested consist of the learning rate $\eta \in \mathbb{R}^+$, the number of epochs $E \in \mathbb{N}$ used to train the explainer, the number of sampled graphs $K \in \mathbb{N}$, the initial and final temperatures $\tau_0, \tau_T \in \mathbb{R}^+$, as well as two coefficients $\alpha_e \in \mathbb{R}^+$ and $\alpha_s \in \mathbb{R}^+$ to control the entropy regularization and the size regularization, respectively. For the BA-Community explainer we also test a sample bias $b = 0.5$, that restricts the ϵ in Equation 4.4 to $\epsilon \sim \text{Uniform}(0 + b, 1 - b)$. This is also extracted from the original codebase of PGExplainer [43] and leads to a constant $\epsilon = 0.5$. We further define a set of fixed seeds used during each grid search as $S = \{74, 75, 76\}$, since we found that the performance of the explainer is highly dependent on the seed for some of the datasets.

Since we care about the inductive performance and Luo et al. [43] demonstrate that the explainer performs well on few training instances, we set the number of training instances $a = 30$ for graph tasks and $a = 0.08N$ for node tasks during the searches. We choose a percental split for the node tasks, since the node sets used in the original experiment highly vary in size and generally contain fewer instances than the graph sets. The resulting absolute number of training instances for the node tasks, as well as the specifics of each search can be seen in Section A.3. Following PGExplainer [43], the resulting validation set and test set each have a size of $\frac{(N-a)}{2}$, where N denotes the number of used instances in each dataset. The optimal hyperparameter values used for the following experiments are listed in Table 5.4.

Baselines

We compare our work to both the collective and inductive results from the original PG-Explainer paper, as well as the results from the collective PyTorch replication study by Holdijk et al. [29] (see Table 5.5). Since the inductive results of PGExplainer are only provided as plots, we approximate the numeric values.

Experimental Protocol

We follow the general experimental setup used in the baselines [43], [29], originally proposed in [72]. We train a PGExplainer model on a fixed TM with a specified seed, with

	K	b	E	η	α_e	α_s	τ_0	τ_T
BA-Shapes	1	0.0	10	0.003	0.1	0.05	5.0	1.0
BA-Community	5	0.0	20	0.003	1.0	0.1	1.0	5.0
Tree-Cycles	5	0.0	20	0.0003	1.0	0.0001	1.0	1.0
Tree-Grid	5	0.0	30	0.003	1.0	0.5	5.0	2.0
BA-2Motif	10	0.0	20	0.01	0.1	0.03	5.0	1.0
MUTAG	10	0.0	20	0.01	1.0	0.005	5.0	1.0

Table 5.4: The best-performing parameter values for each dataset based on the performed grid searches (see Section A.3).

	Node Classification				Graph Classification	
	BA-Shapes	BA-Community	Tree-Cycles	Tree-Grid	BA-2Motif	MUTAG
Explanation AUROC						
PGExplainer	0.963±0.011	0.945±0.019	0.987±0.007	0.907±0.014	0.926±0.021	0.873±0.013
RE-PGExplainer	0.999±0.000	0.825±0.040	0.760±0.014	0.679±0.008	0.133±0.046	0.843±0.084
PGExplainer (inductive)	~0.98	~0.99	~0.99	~0.88	~0.84	-
Inference Time (ms)						
<i>PGExplainer</i>	10.92	24.07	6.36	6.72	80.13	9.68
<i>RE-PGExplainer</i>	3.58	5.23	0.45	0.54	0.33	2.05

Table 5.5: PGExplainer performance baselines.

the hyperparameter values listed in Table 5.4. This process is repeated 10 times for each dataset over a set of seeds $S_e = \{0, 1, \dots, 9\}$. The models are evaluated quantitatively using the AUROC metric and qualitatively for select experiments, in the sense of comparing visualizations of explanations to the GT motifs. We provide the quantitative results as the mean and standard deviation over 10 runs for all experiments.

5.1.2 Inductive Setting

Experimental Setup

In this experiment we evaluate the quantitative performance of PGExplainer in the inductive setting on our slightly adapted TMs. Since Luo et al. [43] showed that the PGExplainer can achieve good results with only few training instances, we aim to replicate this for $a = 30$ training instances, one of the original experiment settings. Since the exact instance sets used are not further specified in the paper, we treat the motif node sets described in Section 5.1.1 as the instance sets of size N for node task.

We repeat this experiment with Xavier [21] used as initialization for the explainer MLP weights, opposed to the He [27] initialization standard to PyTorch linear layers with ReLU activations. This is done since the grid searches showed that the performance is heavily

dependent on the used seed for some datasets, which mainly controls the initializations. Xavier is used by default in the original TensorFlow [50] implementation.

Additionally, we measure the average inference time to explain any instance and compare it to both baselines.

Results

Table 5.6 shows the quantitative results, as well as the inference time for all datasets. First, BA-Shapes is the only experiment that comes close to the originally recorded scores. It is notable, that both Tree-Cycles and BA-2Motif achieve an AUROC score far below 0.5, indicating that the opposite of the GT expectations is predicted. Though the variance of Tree-Cycles is quite high, the figures 5.2a and 5.2b show that this is mostly caused by a singular outlier run. Both the losses and AUROC scores are decreasing steadily, illustrating a stable learning process.

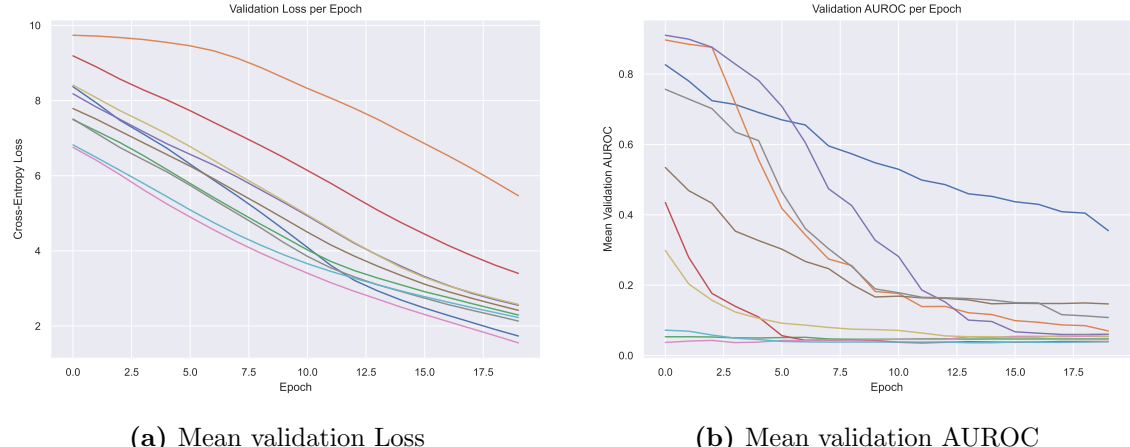


Figure 5.2: Validation metrics for Tree-Cycles over 10 runs in inductive setting.

We were unable to determine a reason for the unexpected opposite classification of select tasks, but highlight that this can also be observed for BA-2Motif in the replication study [29] (see Table 5.5). To validate this, we perform an experiment with flipped GT edges in Section 5.1.5.

When considering that AUROC scores close to 0 also indicate learning, Tree-Grid is the worst performing dataset, converging to a metric score close to random guessing. We note that the loss does converge as expected in all runs, but the model seems to be unable to generalize well.

It is notable that the Xavier initialized model achieves worse results across the board. Though the mean values are higher for most of the datasets, the variance is also much higher, suggesting less stability. Since we care for stable models we only consider He initialization for the following experiments.

	Node Classification				Graph Classification	
	BA-Shapes	BA-Community	Tree-Cycles	Tree-Grid	BA-2Motif	MUTAG
Explanation AUROC						
PGExplainer	~0.98	~0.99	~0.99	~0.88	~0.84	-
Our work (He)	0.994±0.001	0.754±0.013	0.106±0.104	0.537±0.081	0.017±0.006	0.874±0.009
Our work (Xavier)	0.995±0.002	0.779±0.036	0.467±0.316	0.551±0.119	0.035±0.05	0.834±0.04
Inference Time (ms)						
<i>PGExplainer</i>	10.92	24.07	6.36	6.72	80.13	9.68
<i>RE-PGExplainer</i>	3.58	5.23	0.45	0.54	0.33	2.05
<i>Our work</i>	37.0±1.4	24.8±0.1	3.0±0.2	2.7±0.1	4.0±0.3	4.0

Table 5.6: Inductive performance of PGExplainer ($a = 30$).

Our implementation improves the inference time of the original explainer for 4 datasets, but is notably slower for BA-Shapes. We report considerably lower times than the replication study, which we primarily attribute to our limited hardware.

5.1.3 Collective Setting

Experimental Setup

To allow for a better comparison with both baselines we perform an experiment in the collective setting. Therefore, both the training and evaluation are performed on the complete set of motif instances. This is the setting that can be found in the original codebase. It is noteworthy that we use the hyperparameters found in an inductive setting (see Section 5.1.1), which should allow for good generalization. We also include our results obtained in the inductive setting, to evaluate the difference between the settings.

Results

We are unable to reproduce the scores achieved in the original work for most of the datasets, as seen in Table 5.7. BA-Shapes achieves a higher score than the original in both settings, while MUTAG comes close to the original baseline and even obtains a higher score in the inductive setting. The other scores do not come close when considering the scores as they are without flipped GTs. It is notable that we are able to match the results achieved in the replication baseline in all but the Tree-Cycles experiment. This validates that the PGExplainer achieves similar results for different target GNN layers. However, the actual difference in the models is hard to measure since GNNs operate very similarly.

5.1.4 Inductive Setting with More Training Instances

Experimental Setup

	Node Classification				Graph Classification	
	BA-Shapes	BA-Community	Tree-Cycles	Tree-Grid	BA-2Motif	MUTAG
Explanation AUROC						
PGExplainer	0.963±0.011	0.945±0.019	0.987±0.007	0.907±0.014	0.926±0.021	0.873±0.013
RE-PGExplainer	0.999±0.000	0.825±0.040	0.760±0.014	0.679±0.008	0.133±0.046	0.843±0.084
Our work (collective)	0.993±0.001	0.831±0.009	0.084±0.078	0.679±0.032	0.018±0.004	0.833±0.006
Our work (inductive)	0.994±0.001	0.754±0.013	0.106±0.104	0.537±0.081	0.017±0.006	0.874±0.009

Table 5.7: Collective PGExplainer performance ($a = N$).

Luo et al. [43] show that the inductive performance of PGExplainer improves with the number of instances used for training. To validate this we perform an inductive experiment with an increased number of training instances $a = 60$. Since the motif instance sets of BA-Shapes and Tree-Cycles in the original setting only consist of 60 instances, we use a split ratio of 80/10/10. This leads to $a = 48$ for these two tasks. We compare the results to our original inductive experiment (see Section 5.1.2).

Results

The results for this experiment are found in Table 5.8. The graph tasks see a slight improvement, while the node tasks all seem to perform worse with more training instances. While the variance decreases for both tree tasks, the mean moves toward the value indicating random predictions. We observe that BA-Community reaches a peak in AUROC early but steadily decreases afterward, as opposed to the setting with $a = 30$ where the AUROC rises steadily and converges strongly. This result suggests that the hyperparameters have to be retuned for this setting, which significantly limits the generalizability of the explainer. We are unable to confirm that the PGExplainer generally achieves better results when more instances are seen during training.

	Node Classification				Graph Classification	
	BA-Shapes	BA-Community	Tree-Cycles	Tree-Grid	BA-2Motif	MUTAG
Explanation AUROC						
Inductive ($a = 30$)	0.994±0.001	0.754±0.013	0.106±0.104	0.537±0.081	0.017±0.006	0.874±0.009
More instances	0.987±0.002	0.641±0.045	0.144±0.096	0.495±0.052	0.017±0.004	0.895±0.009

Table 5.8: Inductive PGExplainer performance with more training instances where a is either 48 or 60.

5.1.5 BA-2Motif with Inverted Ground Truth

Experimental setup

Since we found that the AUROC score for BA-2Motif decreases rather than increases over the training epochs, converging near zero, we run an additional experiment with inverted

GT. Since both the loss and AUROC curves decrease steadily and flatten in the original inductive experiment (see Figure 5.3), we consider this experiment an additional validation to highlight that the explainer does learn the motifs.

The mean individual AUROC is calculated identical to before, but the GT mask of each graph is inverted, meaning that edges in the motif now carry a label of 0 and all other edges a label of 1. Note that the GT does not affect the training procedure in any way and merely changes the metric evaluation.

AUROC	BA-2Motif
PGExplainer	0.926 ± 0.021
RE-PGExplainer	0.133 ± 0.046
Our work	0.017 ± 0.006
Inverted GT	0.985 ± 0.006

Table 5.9: Explanation AUROC for BA-2Motif with inverted GT.

Results

As expected, the AUROC score for BA-2Motif is nearly perfect in this experiment, even surpassing the original baseline, as seen in Table 5.9. It is notable that the results by Holdijk et al. [29] suggest a similar observation, but the authors do not expand on this. We are unable to identify an explanation for this behavior, since no consistent differences in comparison to the other experiments were observed. However, in principle, this signals that the explainer learns to predict the edges that are unimportant to the prediction, rather than the important ones. Further investigation of this behavior is necessary to determine its cause.

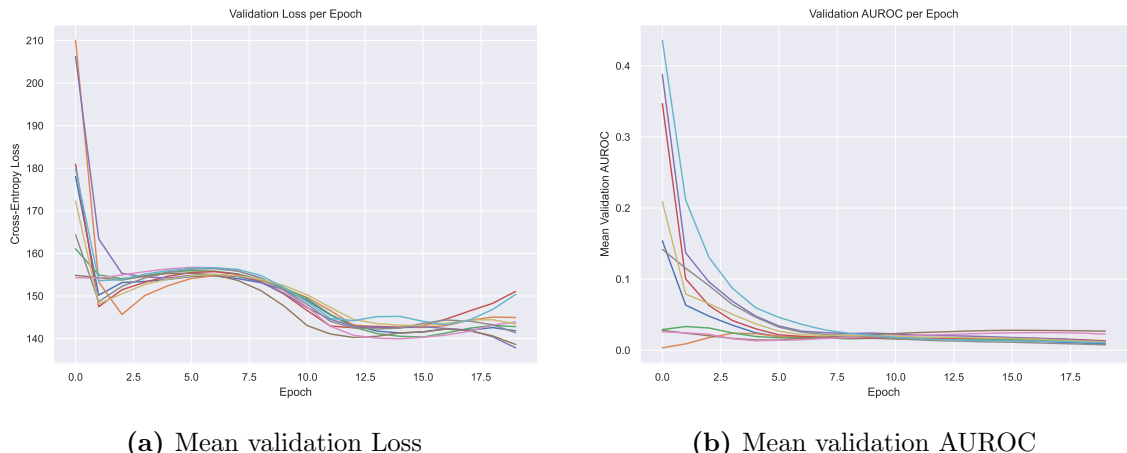


Figure 5.3: Validation metrics for BA-2Motif over 10 runs in inductive setting.

5.1.6 Effects of Used Motif Instances for Node Tasks

Experimental Setup

As presented in 5.1.1 the motif instances used in PGExplainer [43] for different node level tasks are not defined consistently. This is likely related to their direct comparison to GNNExplainer [72] and the adaptation of their dataset settings. Nevertheless, since the PGExplainer claims to generalize well and be able to provide explanations for any downstream GNN task, a uniform procedure for providing explanations is necessary.

Evidently, different nodes in a motif have different local computation graphs, containing different motif- and non-motif nodes. The 3-hop graph computed from a corner node of a grid motif may for example never contain the complete motif. If such a node is commonly selected during training, it is reasonable to believe that the explainer may learn the "sub-motif" consisting of three squares, rather than the complete motif. A 3-layer GNN may therefore not be ideal for learning the grid motif. We evaluate the effect of using all motif nodes or a singular node from each motif as instances in this experiment.

We suggest changing the instance sets \mathcal{I} used for training and evaluation to include either all or one select motif node of each motif, depending on the dataset. The hyperparameters used for the previous experiments are retained. Besides this change, we follow the general experimental setup in the inductive setting with $a = 30$ to evaluate whether a reasoning behind the node selection can be made out.

Since BA-Shapes and Tree-Cycles originally use a singular node from each motif, we evaluate the effect of using all nodes in each motif and refer to this as All-Motif-Nodes. Accordingly, we select one fixed node from each motif for the BA-Community and Tree-Grid tasks, similar to the original BA-Shapes and Tree-Cycles task. For BA-Community we choose one of the two "middle" nodes in the house motif, similar to BA-Shapes. For Tree-Grid we select the "second" node, starting from the corner node attached to the base graph, as the 3-hop graph from this node contains all motif nodes as well as the most nodes from the base graph. We call this experiment One-Motif-Node. The exact number of instances used in this experiment can be seen in Table 5.10.

It is noteworthy that using singular corresponding topological nodes across motifs restricts the explanation task in terms of generalizability, since only the explanations of these nodes are learned.

	All-Motif-Nodes		One-Motif-Node	
	BA-Shapes	Tree-Cycles	BA-Community	Tree-Grid
#total motif instances	300	360	800	289
#used motif instances N	300	360	160	32

Table 5.10: Amount of possible and actually used motif instances in the experiments with adapted instance sets.

Results

We present the results of the All-Motif-Nodes experiment compared to our results achieved in the inductive setting in Table 5.11 and for One-Motif-Node in Table 5.12. It is most notable that the Tree-Grid experiment achieves perfect edge classification accuracy in the One-Motif-Node experiment. BA-Community also reports a significant increase in AUROC score.

The All-Motif-Nodes experiment leads to a slight deterioration in score for BA-Shapes, which is still better than the scores achieved on the other node tasks in our inductive experiment. The explainer’s performance on Tree-Cycles deteriorates in both variance and mean score, particularly in terms of its distance from a random AUROC score.

This indicates that the different settings lead to vastly different results, highlighting the need of a general setup procedure when explaining node instances with PGExplainer. Furthermore, it suggests that the explainer is able to reliably explain unseen node instances with identical topological information of the motif. Nonetheless, the ability of generally learning motif structures from different motif notes and generalizing this to unsee instances lacks, as indicated by the All-Motif-Nodes results of Tree-Cycles, Tree-Grid and BA-Community.

AUROC	BA-Shapes	Tree-Cycles
Our work	0.994±0.001	0.106±0.104
All-Motif-Nodes	0.959±0.004	0.204±0.162

Table 5.11: Explanation AUROC for All-Motif-Nodes.

AUROC	BA-Community	Tree-Grid
Our work	0.754±0.013	0.537±0.081
One-Motif-Node	0.951±0.007	1.0±0.0

Table 5.12: Explanation AUROC for One-Motif-Node.

5.1.7 Qualitative Analysis

Experimental setup

For the qualitative analysis the best performing explainer model for each TM is selected, and random explanations are sampled. For the explainer models with AUROC scores below 0.5, we select the model that achieves the lowest score and visualize the top- k lowest edges accordingly. Following the approach of the original, we present instance explanations that highlight the successful detection of motifs. We additionally include sample grids of 16 random graphs in the Appendix.

Following Luo et al. [43], we select dataset-specific values of k : BA-Shapes, BA-Community and Tree-Cycles use $k = 6$; Tree-Grid uses $k = 12$; BA-2Motif uses $k = 5$ and MUTAG

uses $k = 10$. These represent the lower bound of the number of edges needed to visualize a full motif, except for MUTAG where more edges are selected to show the additional prediction of base carbon rings.

Results

The visualized explanations generated for each TM show that the GT motifs are detected (see Figure 5.4). We found that the MUTAG explainer detects the chemical combinations that cause the mutagenicity as the highest edges regularly, but the shared base carbon ring is not detected at all. More qualitative random samples for each dataset can be seen in Appendix A.4. The qualitative explanations of BA-Community rarely contain all connected motif edges, as seen in Figure A.3. Note that due to the setting of $k = 5$ for BA-2Motif the house motif is never detected completely, but it is clearly visible that the additional house edge is detected.

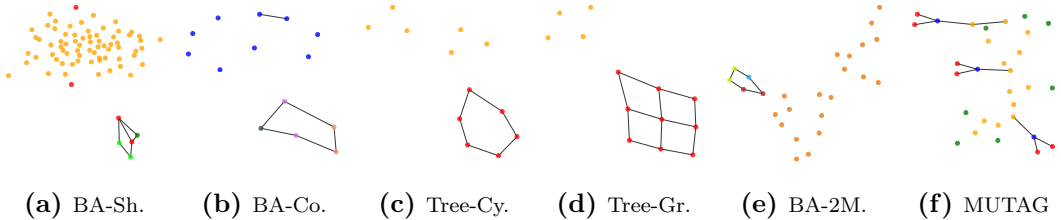


Figure 5.4: Explanations for a singular instance of each dataset.

5.2 Generating Bipartite Explanations for NeuroSAT

In this section we present the experiments for generating bipartite explanations for unsatisfiable SAT problems evaluated by NeuroSAT [64]. We describe the general procedure in Section 5.2.1, followed by the results using the PGExplainer with a soft constraint in Section 5.2.2, as well as the hard constraint experiment in Section 5.2.3.

5.2.1 Common Experimental Setup

NeuroSAT [64] uses a distribution $\mathbf{SR}(n)$ that creates pairs of SAT problems on n variables, which are satisfiable and unsatisfiable, only differing in a singular negated literal. These are created by randomly sampling subclauses of k variables, where each variable is negated with a probability of 50%. These subclauses are added to the problem until a SAT solver [16] finds it to be unsatisfiable.

We adapt this to only contain singular unsatisfiable problems, rather than pairs of problems, since unsatisfiable cores only appear in unsatisfiable problems. The difficulty of the problems is slightly reduced by using $n = 8$, to allow for the explainer to run on NeuroSAT on our limited hardware. We create a dataset of 100 problems. The expected GT

is generated with the deletion-based MUS extractor `MUSX` from PySAT [31], as described in section 4.3.2.

The quantitative evaluation is adopted from Section 5.1.1, with the positive targets being the edges that appear in the corresponding GT MUS of each problem. We additionally evaluate the test instance that achieves the highest individual AUROC score and visualize it. Since the qualitative evaluation relies on knowing k , we calculate this dynamically during evaluation from the GT of the current problem. Clause nodes are drawn in red, while nodes representing literals are drawn in magenta.

The NeuroSAT model trained on a **SR**(40) distribution was provided by a fellow student. It achieves an accuracy of 1.0 on the dataset we created.

We apply PGExplainer in the inductive setting, using a 50/25/25 split for training, evaluating and testing the NeuroSAT explainer.

Hyperparameter Search

We perform a hyperparameter search for both the explainer with the soft constraint, and the explainer with the applied hard constraint. We follow the general grid search procedure used for the previous experiments, but introduce 4 new hyperparameters, 1 exclusive to the hard constraint and 2 exclusive to the soft constraint.

$\alpha_{arch} \in \{0, 1\}$, exclusive to the hard constraint, denotes whether a more complex MLP architecture is used in the explainer (see Listing 4.5). The second introduced hyperparameter $\alpha_{concat} \in \{0, 1\}$ controls whether the node embeddings \mathbf{z} are used from the last iteration of NeuroSAT or if a concatenation of the states at multiple iterations shall be used (see Section 4.2). For the soft constraint, we also try using the AdamW [42] optimizer from PyTorch with an internal weight decay of 0.01, denoted by $\alpha_{AdamW} \in \{0, 1\}$. Lastly, the coefficient $\alpha_c \in \mathbb{R}^+$ controls the effect of the soft constraint R_C (see Equation 4.15) on the loss. This is disregarded in the hard constraint experiment, as the hard constraint replaces the soft constraint.

The sample bias b used in PGExplainer is disregarded completely. We evaluate the search with respect to the validation AUROC score, as well as the validation loss. The specification of both grid searches can be found in Appendix A.5.

5.2.2 Soft Constraint Experiment

Experimental Setup

In this experiment we apply the soft constraint introduced in Section 4.2 to the PGExplainer to generate explanations for unsatisfiable SAT problems learned from NeuroSAT predictions. After performing the grid search, we utilize the optimal parameters to evaluate the test AUROC over 10 seeded runs. Additionally, we provide qualitative explanations in comparison to the GT MUS for the problem that results in the highest individual AUROC.

Results

We found that the grid search resulted in a maximum average validation AUROC of 0.5248 and a minimal score of 0.4726. This can be seen in Figure A.8. All runs achieved results in this interval, indicating completely random edge predictions on average. It seems that regardless of the tested hyperparameters the general explanations of unsatisfiable problems, as learned from NeuroSAT, do not align with MUSes.

We note that a low size regularization has the highest impact on the mean AUROC score, since a high value leads to uniform edge importance scores of 0. This is followed by a high consistency regularization, as well as a low learning rate. The other hyperparameters are not as decisive. We select the hyperparameter combination that maximizes the validation AUROC, as highlighted in Table A.8.

The mean test AUROC score achieved over 10 runs is listed in Table 5.13.

Over all runs, the highest individual test AUROC score of 0.711 is achieved for seed 4 (see Figure 5.5). As seen in Figure 5.5b, only 2 edges are identified correctly and no full clause is predicted. Since this does not correspond with the relatively high AUROC score, we stress that the AUROC might not be an ideal metric for evaluation in this context. Nevertheless, we did not find a visualization that shared significantly more edges with its GT or indicated a better learning of the MUS motif.

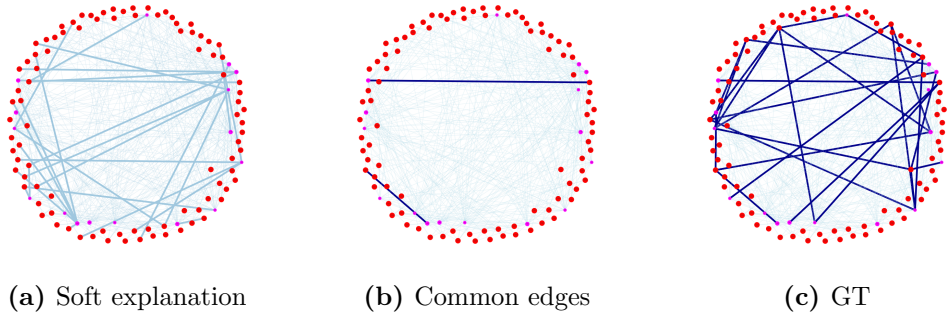


Figure 5.5: Visualization of the soft constraint explanation that achieves the highest individual test AUROC score when compared to its corresponding GT MUS.

5.2.3 Hard Constraint Experiment

Experimental Setup

In this experiment we apply the hard constraint introduced in Section 4.2 to the PGExplainer to generate explanations for unsatisfiable SAT problems learned from NeuroSAT predictions. The experimental setup is adopted from Section 5.2.2.

Results

The grid search revealed that none of the parameter configurations achieves an AUROC score above 0.5 and below 0.44. Since 0.5 equals random guessing and is usually caused

by all edges being predicted with a uniform score of 0, we select the hyperparameter combination that achieves the highest score, while maintaining edge weights unequal to 0. We found that a low learning rate is important to keep the edge predictions from reaching 0, as these steadily decrease over training time. $\alpha_s = 1.0$ further enhanced this unwanted behavior. The resulting combination used for the experiment is highlighted in Table A.9.

AUROC	NeuroSAT
Soft Constraint	0.512 ± 0.023
Hard Constraint	0.528 ± 0.013

Table 5.13: Inductive explanation AUROC for NeuroSAT predictions of unsatisfiable SAT problems.

5.2.4 Qualitative Analysis

Using a concatenation of the embeddings at multiple iterations achieved worse results than the usual graph task procedure when considering the highest individual AUROC of validation instances. However, this does not consider whether a general procedure is learned. It is important to note that the average of the lowest absolute edge importance score per run is 0.34, while the average of the highest score is 0.44. This indicates a reasonable span of importance scores, but may still lack in the sense of resembling approximated discrete masks.

We found that the run on seed 0 achieves the highest individual test AUROC of 0.776 (See Figure 5.6). It is notable that 2 out of 6 full clauses are predicted correctly. Nevertheless, the mean test AUROC only sees a slight increase as presented in Table 5.13.

We present an additional evaluation of the satisfiability of a singular explanation in Appendix A.6.

Furthermore, we found that running the training on seed 0 for 500 epochs resulted in a converging loss, as well as a converging metric score close to 0.46. A local score minimum is reached in epoch 60 with a value of 0.44. Since this is very close to a score indicating randomness, we conclude that the post-hoc explanations provided by our modified version of PGExplainer for NeuroSAT do not align with MUSes.

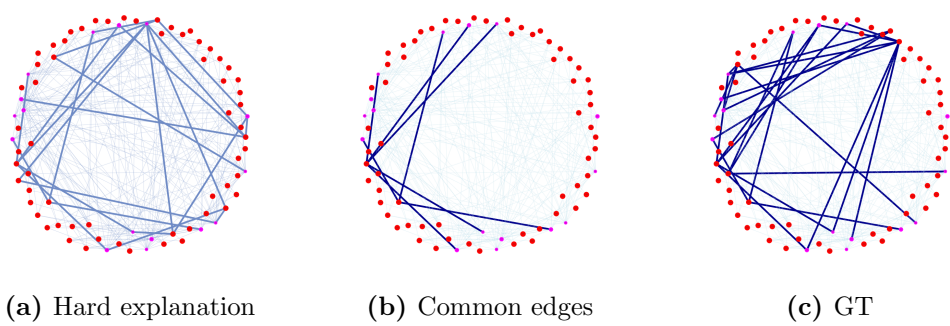


Figure 5.6: Visualization of the hard constraint explanation that achieves the highest individual test AUROC score when compared to its corresponding GT MUS.

Chapter 6

Discussion

In the following chapter we discuss our results regarding the general reproducibility of the PGExplainer [43] when using modified TMs in an inductive setting (see Section 6.1). Moreover, we elaborate on the explanations provided for the NeuroSAT [64] model and their alignment with the human-understandable concept of MUSes in Section 6.2.

6.1 Generalizability of PGExplainer

When taking a closer look at the simplicity of replicating the PGExplainer, we share the concerns highlighted by Holdijk et al. [29]. The many inconsistencies between paper and codebase, as well as the lackluster documentation of experiments hinder the implementation. However, we are able to achieve results comparable to the existing replication baseline, accentuating the explainer’s functionality on modified TMs. Furthermore, we were able to achieve promising results in simplified experiment settings, highlighting the general ability to explain instances. The explainer’s generalization and global understanding of TMs were not sufficient, and we cannot confirm these claims at this point.

We stress the necessity of a general setting for evaluating explanations of node instances, as well as the importance of a stable explainer setup, to evaluate the actual explanations using any GNN rather than the performance of the explainer. We were unable to generalize the setup, which results in the explainer requiring a lot of fine-tuning to achieve consistent results. This in itself is impeded by slightly different TMs resulting in vastly different explanations.

Further research is required regarding the reason for opposite classification of selected tasks, to confirm whether this can be understood as an improvement in performance.

6.2 Explanations for Unsatisfiable SAT Problems

It seems that the PGExplainer is unable to learn the important edges for unsatisfiable problems well with regard to our assumed GT. Though we were able to obtain a range

of importance scores comparable to the replication experiments, the explanations did ultimately not align with MUSes. We believe that a drawback in our approach may lie in the introduced evidence problem of edge weights, due to not knowing how weighted edges affect the predictions of NeuroSAT internally. Moreover, our GT assumption may not be ideal, since multiple MUSes may exist for each instance, though these are not unlikely to share detected clauses. The constraints introduced by us may also be lacking or too restrictive for the PGExplainer.

Furthermore, our perturbation approach only modifies edges between literals and clauses, which essentially define a sub problem, but we do not consider the connections between a literal and its negation. These may play a substantial role in the NeuroSAT predictions of unsatisfiability, which may hinder the learning process of the explainer if disregarded in the masking process. Lastly, since the NeuroSAT model is far more complex than the classification models used in the replication, the explanation networks tested may not be complex enough to capture the general features of MUSes or unsatisfiable cores in general.

It is important to note that our idea considers unsatisfiable cores as a conceptual motif, rather than a strict topological motif in the sense of a specific subgraph of nodes aligned in a fixed way. Though the MUS of a singular problem can be understood as a fixed subgraph, this cannot be generalized to other sub problems by its topological information alone. Thus, the approach of using the PGExplainer may not be sufficient, since it focuses on graph structure rather than graph features. However, the replication of MUTAG achieved promising results and was partially reliant on features, indicating that further features may be necessary for the representation of unsatisfiable problems.

Ultimately, we believe that explainability methods can provide important insights into the functionality of GNNs, and are essential for supporting predictions of message passing networks such as NeuroSAT. This also suggests many possibilities for future work, including the application of different explainer models and evaluation of feature importance to explain unsatisfiable problems using machine learning methods. Other directions may focus on explaining singular instances of said problems, as well as rethinking the evaluation methods, especially in regard to GT motifs.

Chapter 7

Conclusion

To conclude this work we highlight our key findings and incentivize future work on the subject. Though the replication of PGExplainer came with many inconsistencies and proved to be not as general as originally claimed, our results suggest that the method is able to explain instances inductively, as long as the instances used share the same topological information regarding the motifs. Generally explaining different unexplained node instances from the same motif proved to be more difficult and requires more investigation. In addition, further experiments regarding the observable flipped explanations are necessary to better understand and leverage this behavior.

In brief, our work presents the PGExplainer in a more general context, seeking to pave the way for more universal approaches to evaluating GNN explanations.

Moreover, we were able to apply the PGExplainer to a NeuroSAT model and generate limited bipartite explanations for unsatisfiable problems in the form of subclauses. However, these do not meet our assumption of aligning with MUSes and did not prove unsatisfiable themselves, limiting the significance of these explanations.

We are optimistic that further work may allow for creating explanations that support NeuroSAT predictions.

Bibliography

- [1] Abubakar Abid, Muhammad Fatih Balin, and James Zou. “Concrete autoencoders for differentiable feature selection and reconstruction”. In: *arXiv preprint arXiv:1901.09346* (2019).
- [2] Réka Albert and Albert-László Barabási. “Statistical mechanics of complex networks”. In: *Reviews of modern physics* 74.1 (2002), p. 47.
- [3] Hesham Ali. *Graph Neural Networks (GNNs) and Its Applications*. Feb. 2023. URL: <https://mlarchive.com/deep-learning/graph-neural-networks-gnns-and-its-applications/> (visited on 05/09/2025).
- [4] A.S. Asratian, T.M.J. Denley, and R. Häggkvist. *Bipartite Graphs and their Applications*. Cambridge Tracts in Mathematics. Cambridge University Press, 1998. ISBN: 9781316582688. URL: <https://books.google.de/books?id=18fLCgAAQBAJ>.
- [5] Gilles Audemard and Laurent Simon. “Predicting Learnt Clauses Quality in Modern SAT Solvers.” In: *IJCAI*. Vol. 9. Citeseer. 2009, pp. 399–404.
- [6] Federico Baldassarre and Hossein Azizpour. “Explainability techniques for graph convolutional networks”. In: *arXiv preprint arXiv:1905.13686* (2019).
- [7] Lukas Biewald. *Experiment Tracking with Weights and Biases*. Software available from wandb.com. 2020. URL: <https://www.wandb.com/>.
- [8] Hongyun Cai, Vincent W Zheng, and Kevin Chen-Chuan Chang. “A comprehensive survey of graph embedding: Problems, techniques, and applications”. In: *IEEE transactions on knowledge and data engineering* 30.9 (2018), pp. 1616–1637.
- [9] Augustin Cauchy et al. “Méthode générale pour la résolution des systemes d’équations simultanées”. In: *Comp. Rend. Sci. Paris* 25.1847 (1847), pp. 536–538.
- [10] Stephen A Cook. “The complexity of theorem-proving procedures”. In: *Logic, automata, and computational complexity: The works of Stephen A. Cook*. 2023, pp. 143–152.

- [11] T.M. Cover and J.A. Thomas. “Entropy, Relative Entropy, and Mutual Information”. In: *Elements of Information Theory*. John Wiley & Sons, Ltd, 2005, pp. 13–55. ISBN: 9780471748823. DOI: <https://doi.org/10.1002/047174882X.ch2>. eprint: <https://onlinelibrary.wiley.com/doi/pdf/10.1002/047174882X.ch2>. URL: <https://onlinelibrary.wiley.com/doi/abs/10.1002/047174882X.ch2>.
- [12] Piotr Dabkowski and Yarin Gal. “Real time image saliency for black box classifiers”. In: *Advances in neural information processing systems* 30 (2017).
- [13] Asim Kumar Debnath et al. “Structure-activity relationship of mutagenic aromatic and heteroaromatic nitro compounds. correlation with molecular orbital energies and hydrophobicity”. In: *Journal of medicinal chemistry* 34.2 (1991), pp. 786–797.
- [14] Nachum Dershowitz, Ziyad Hanna, and Alexander Nadel. “A scalable algorithm for minimal unsatisfiable core extraction”. In: *Theory and Applications of Satisfiability Testing-SAT 2006: 9th International Conference, Seattle, WA, USA, August 12-15, 2006. Proceedings* 9. Springer. 2006, pp. 36–41.
- [15] Reinhard Diestel. “Random Graphs”. In: *Graph Theory*. Berlin, Heidelberg: Springer Berlin Heidelberg, 2017, pp. 323–345. ISBN: 978-3-662-53622-3. DOI: 10.1007/978-3-662-53622-3_11. URL: https://doi.org/10.1007/978-3-662-53622-3_11.
- [16] Niklas Eén and Niklas Sörensson. “An extensible SAT-solver”. In: *International conference on theory and applications of satisfiability testing*. Springer. 2003, pp. 502–518.
- [17] Matthias Fey and Jan E. Lenssen. “Fast Graph Representation Learning with PyTorch Geometric”. In: *ICLR Workshop on Representation Learning on Graphs and Manifolds*. 2019.
- [18] Hongyang Gao and Shuiwang Ji. “Graph u-nets”. In: *international conference on machine learning*. PMLR. 2019, pp. 2083–2092.
- [19] Edgar N Gilbert. “Random graphs”. In: *The Annals of Mathematical Statistics* 30.4 (1959), pp. 1141–1144.
- [20] Justin Gilmer et al. “Neural message passing for quantum chemistry”. In: *International conference on machine learning*. PMLR. 2017, pp. 1263–1272.
- [21] Xavier Glorot and Yoshua Bengio. “Understanding the difficulty of training deep feedforward neural networks”. In: *Proceedings of the thirteenth international conference on artificial intelligence and statistics*. JMLR Workshop and Conference Proceedings. 2010, pp. 249–256.
- [22] Ian Goodfellow, Yoshua Bengio, and Aaron Courville. *Deep Learning*. <http://www.deeplearningbook.org>. MIT Press, 2016.

- [23] Marco Gori, Gabriele Monfardini, and Franco Scarselli. “A new model for learning in graph domains”. In: *Proceedings. 2005 IEEE international joint conference on neural networks, 2005*. Vol. 2. IEEE. 2005, pp. 729–734.
- [24] Wenxuan Guo et al. “Machine learning methods in solving the boolean satisfiability problem”. In: *Machine Intelligence Research* 20.5 (2023), pp. 640–655.
- [25] Aric A. Hagberg, Daniel A. Schult, and Pieter J. Swart. “Exploring Network Structure, Dynamics, and Function using NetworkX”. In: *Proceedings of the 7th Python in Science Conference*. Ed. by Gaël Varoquaux, Travis Vaught, and Jarrod Millman. Pasadena, CA USA, 2008, pp. 11–15.
- [26] William L Hamilton, Rex Ying, and Jure Leskovec. “Representation learning on graphs: Methods and applications”. In: *arXiv preprint arXiv:1709.05584* (2017).
- [27] Kaiming He et al. “Delving deep into rectifiers: Surpassing human-level performance on imagenet classification”. In: *Proceedings of the IEEE international conference on computer vision*. 2015, pp. 1026–1034.
- [28] Geoffrey E Hinton et al. “Improving neural networks by preventing co-adaptation of feature detectors”. In: *arXiv preprint arXiv:1207.0580* (2012).
- [29] Lars Holdijk et al. “[Re] Parameterized Explainer for Graph Neural Network”. In: *ML Reproducibility Challenge 2020*. 2021.
- [30] Qiang Huang et al. “Graphlime: Local interpretable model explanations for graph neural networks”. In: *IEEE Transactions on Knowledge and Data Engineering* 35.7 (2022), pp. 6968–6972.
- [31] Alexey Ignatiev, Antonio Morgado, and Joao Marques-Silva. “PySAT: A Python Toolkit for Prototyping with SAT Oracles”. In: *SAT*. 2018, pp. 428–437. DOI: 10.1007/978-3-319-94144-8_26. URL: https://doi.org/10.1007/978-3-319-94144-8_26.
- [32] Sergey Ioffe and Christian Szegedy. “Batch normalization: Accelerating deep network training by reducing internal covariate shift”. In: *International conference on machine learning*. pmlr. 2015, pp. 448–456.
- [33] Eric Jang, Shixiang Gu, and Ben Poole. “Categorical reparameterization with gumbel-softmax”. In: *arXiv preprint arXiv:1611.01144* (2016).
- [34] Diederik P Kingma and Jimmy Ba. “Adam: A method for stochastic optimization”. In: *arXiv preprint arXiv:1412.6980* (2014).
- [35] Thomas N Kipf and Max Welling. “Semi-supervised classification with graph convolutional networks”. In: *arXiv preprint arXiv:1609.02907* (2016).
- [36] Alex Krizhevsky, Ilya Sutskever, and Geoffrey E Hinton. “Imagenet classification with deep convolutional neural networks”. In: *Advances in neural information processing systems* 25 (2012).

- [37] Y. Lecun et al. “Gradient-based learning applied to document recognition”. In: *Proceedings of the IEEE* 86.11 (1998), pp. 2278–2324. DOI: 10.1109/5.726791.
- [38] Yujia Li et al. “Gated graph sequence neural networks”. In: *arXiv preprint arXiv:1511.05493* (2015).
- [39] Petro Liashchynskyi and Pavlo Liashchynskyi. “Grid search, random search, genetic algorithm: a big comparison for NAS”. In: *arXiv preprint arXiv:1912.06059* (2019).
- [40] Mark H Liffiton and Karem A Sakallah. “Algorithms for computing minimal unsatisfiable subsets of constraints”. In: *Journal of Automated Reasoning* 40 (2008), pp. 1–33.
- [41] Zhiyuan Liu and Jie Zhou. “Introduction”. In: *Introduction to Graph Neural Networks*. Cham: Springer International Publishing, 2020, pp. 1–3. ISBN: 978-3-031-01587-8. DOI: 10.1007/978-3-031-01587-8_1. URL: https://doi.org/10.1007/978-3-031-01587-8_1.
- [42] Ilya Loshchilov and Frank Hutter. “Decoupled weight decay regularization”. In: *arXiv preprint arXiv:1711.05101* (2017).
- [43] Dongsheng Luo et al. “Parameterized explainer for graph neural network”. In: *Advances in neural information processing systems* 33 (2020), pp. 19620–19631.
- [44] Dongsheng Luo et al. “Towards Inductive and Efficient Explanations for Graph Neural Networks”. In: *IEEE Transactions on Pattern Analysis and Machine Intelligence* 46.8 (2024), pp. 5245–5259. DOI: 10.1109/TPAMI.2024.3362584.
- [45] Tengfei Ma and Jie Chen. “Unsupervised learning of graph hierarchical abstractions with differentiable coarsening and optimal transport”. In: *Proceedings of the AAAI conference on artificial intelligence*. Vol. 35. 10. 2021, pp. 8856–8864.
- [46] Yao Ma and Jiliang Tang. *Deep learning on graphs*. Cambridge University Press, 2021.
- [47] Chris J Maddison, Andriy Mnih, and Yee Whye Teh. “The concrete distribution: A continuous relaxation of discrete random variables”. In: *arXiv preprint arXiv:1611.00712* (2016).
- [48] Joao Marques-Silva. “Minimal Unsatisfiability: Models, Algorithms and Applications (Invited Paper)”. In: *2010 40th IEEE International Symposium on Multiple-Valued Logic*. 2010, pp. 9–14. DOI: 10.1109/ISMVL.2010.11.
- [49] Joao P Marques-Silva and Karem A Sakallah. “GRASP: A search algorithm for propositional satisfiability”. In: *IEEE Transactions on Computers* 48.5 (1999), pp. 506–521.
- [50] Martín Abadi et al. *TensorFlow: Large-Scale Machine Learning on Heterogeneous Systems*. Software available from tensorflow.org. 2015. URL: <https://www.tensorflow.org/>.

- [51] Tomonori Masui. *Graph Neural Networks with PyG on Node Classification, Link Prediction, and Anomaly Detection*. Oct. 2022. URL: <https://medium.com/datascience/graph-neural-networks-with-pyg-on-node-classification-link-prediction-and-anomaly-detection-14aa38fe1275> (visited on 05/17/2025).
- [52] Christopher Morris et al. “Weisfeiler and leman go neural: Higher-order graph neural networks”. In: *Proceedings of the AAAI conference on artificial intelligence*. Vol. 33. 01. 2019, pp. 4602–4609.
- [53] Mohd Halim Mohd Noor and Ayokunle Olalekan Ige. “A Survey on State-of-the-art Deep Learning Applications and Challenges”. In: *arXiv preprint arXiv:2403.17561* (2024).
- [54] A Paszke. “Pytorch: An imperative style, high-performance deep learning library”. In: *arXiv preprint arXiv:1912.01703* (2019).
- [55] Fabian Pedregosa et al. “Scikit-learn: Machine learning in Python”. In: *Journal of machine learning research* 12.Oct (2011), pp. 2825–2830.
- [56] Giancarlo Perrone, Jose Unpingco, and Haw-minn Lu. “Network visualizations with Pyvis and VisJS”. In: *arXiv preprint arXiv:2006.04951* (2020).
- [57] Marco Tulio Ribeiro, Sameer Singh, and Carlos Guestrin. “” Why should i trust you?” Explaining the predictions of any classifier”. In: *Proceedings of the 22nd ACM SIGKDD international conference on knowledge discovery and data mining*. 2016, pp. 1135–1144.
- [58] Eve Richardson et al. “The receiver operating characteristic curve accurately assesses imbalanced datasets”. In: *Patterns* 5.6 (2024), p. 100994. ISSN: 2666-3899. DOI: <https://doi.org/10.1016/j.patter.2024.100994>. URL: <https://www.sciencedirect.com/science/article/pii/S2666389924001090>.
- [59] Kaspar Riesen and Horst Bunke. “IAM graph database repository for graph based pattern recognition and machine learning”. In: *Structural, Syntactic, and Statistical Pattern Recognition: Joint IAPR International Workshop, SSPR & SPR 2008, Orlando, USA, December 4-6, 2008. Proceedings*. Springer. 2008, pp. 287–297.
- [60] Frank Rosenblatt. “The perceptron: a probabilistic model for information storage and organization in the brain.” In: *Psychological review* 65.6 (1958), p. 386.
- [61] David E Rumelhart, Geoffrey E Hinton, and Ronald J Williams. “Learning representations by back-propagating errors”. In: *nature* 323.6088 (1986), pp. 533–536.
- [62] Franco Scarselli et al. “The Graph Neural Network Model”. In: *IEEE Transactions on Neural Networks* 20.1 (2009), pp. 61–80. DOI: [10.1109/TNN.2008.2005605](https://doi.org/10.1109/TNN.2008.2005605).
- [63] Bart Selman, Henry A Kautz, Bram Cohen, et al. “Local search strategies for satisfiability testing.” In: *Cliques, coloring, and satisfiability* 26 (1993), pp. 521–532.

- [64] Daniel Selsam et al. “Learning a SAT solver from single-bit supervision”. In: *arXiv preprint arXiv:1802.03685* (2018).
- [65] Martin Simonovsky and Nikos Komodakis. “Dynamic edge-conditioned filters in convolutional neural networks on graphs”. In: *Proceedings of the IEEE conference on computer vision and pattern recognition*. 2017, pp. 3693–3702.
- [66] Hanqing Sun et al. “Supervised biadjacency networks for stereo matching”. In: *Multimedia Tools and Applications* 83 (June 2023), pp. 1–26. DOI: 10.1007/s11042-023-15362-5.
- [67] Emina Torlak, Felix Sheng-Ho Chang, and Daniel Jackson. “Finding Minimal Unsatisfiable Cores of Declarative Specifications”. In: *FM 2008: Formal Methods*. Ed. by Jorge Cuellar, Tom Maibaum, and Kaisa Sere. Berlin, Heidelberg: Springer Berlin Heidelberg, 2008, pp. 326–341. ISBN: 978-3-540-68237-0.
- [68] Petar Veličković et al. “Graph attention networks”. In: *arXiv preprint arXiv:1710.10903* (2017).
- [69] Michael L. Waskom. “seaborn: statistical data visualization”. In: *Journal of Open Source Software* 6.60 (2021), p. 3021. DOI: 10.21105/joss.03021. URL: <https://doi.org/10.21105/joss.03021>.
- [70] Keyulu Xu et al. “How powerful are graph neural networks?” In: *arXiv preprint arXiv:1810.00826* (2018).
- [71] Rex Ying et al. “Graph convolutional neural networks for web-scale recommender systems”. In: *Proceedings of the 24th ACM SIGKDD international conference on knowledge discovery & data mining*. 2018, pp. 974–983.
- [72] Zhitao Ying et al. “Gnnexplainer: Generating explanations for graph neural networks”. In: *Advances in neural information processing systems* 32 (2019).
- [73] Hao Yuan et al. “Explainability in graph neural networks: A taxonomic survey”. In: *IEEE transactions on pattern analysis and machine intelligence* 45.5 (2022), pp. 5782–5799.
- [74] Hao Yuan et al. “On explainability of graph neural networks via subgraph explorations”. In: *International conference on machine learning*. PMLR. 2021, pp. 12241–12252.
- [75] Muhan Zhang and Yixin Chen. “Link prediction based on graph neural networks”. In: *Advances in neural information processing systems* 31 (2018).
- [76] Tianxiang Zhao et al. “Faithful and consistent graph neural network explanations with rationale alignment”. In: *ACM Transactions on Intelligent Systems and Technology* 14.5 (2023), pp. 1–23.

Appendix A

Supplementary Material

A.1 Material from original PGExplainer

This section contains the reprinted pseudocode by Luo et al. [43] in algorithms 1 and 2, as well as the accuracies achieved by their used target models in Table A.1.

Algorithm 1 Training Algorithm for Explaining Node Classification from [43].

Require: Input graph $G_o = (\mathcal{V}, \mathcal{E})$, node features X , node labels Y , set of instances to be explained \mathcal{I} , trained GNN model: $\text{GNNE}_{\Phi_0}(\cdot)$ and $\text{GNNC}_{\Phi_1}(\cdot)$, parameterized explainer MLP Ψ .

```
1: for each node  $i \in \mathcal{I}$  do
2:    $G_o^{(i)} \leftarrow$  extract the computation graph for node  $i$ .
3:    $Z^{(i)} \leftarrow \text{GNNE}_{\Phi_0}(G_o^{(i)}, X)$ .
4:    $Y^{(i)} \leftarrow \text{GNNC}_{\Phi_1}(Z^{(i)})$ .
5: end for
6: for each epoch do
7:   for each node  $i \in \mathcal{I}$  do
8:      $\Omega \leftarrow$  latent variables calculated with (10).
9:     for  $k \leftarrow 1$  to  $K$  do
10:       $G_s^{(i,k)} \leftarrow$  sampled from (4).
11:       $\hat{Y}_s^{(i,k)} \leftarrow \text{GNNC}_{\Phi_1}(\text{GNNE}_{\Phi_0}(G_s^{(i,k)}, X))$ .
12:    end for
13:  end for
14:  Compute loss with (9).
15:  Update parameters  $\Psi$  with backpropagation.
16: end for
```

Algorithm 2 Training Algorithm for Explaining Graph Classification from [43].

Require: A set of input graphs with i -th graph represented by $G_o^{(i)}$, node features $X^{(i)}$, label $Y^{(i)}$, trained GNN model: $\text{GNNE}_{\Phi_0}(\cdot)$ and $\text{GNNC}_{\Phi_1}(\cdot)$, parameterized explainer MLP Ψ .

```

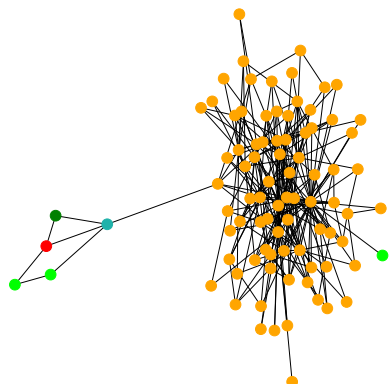
1: for each graph  $G_o^{(i)}$  do
2:    $Z^{(i)} \leftarrow \text{GNNE}_{\Phi_0}(G_o^{(i)}, X^{(i)})$ .
3:    $Y^{(i)} \leftarrow \text{GNNC}_{\Phi_1}(Z^{(i)})$ .
4: end for
5: for each epoch do
6:   for each graph  $G_o^{(i)}$  do
7:      $\Omega \leftarrow$  latent variables calculated with (11).
8:     for  $k \leftarrow 1$  to  $K$  do
9:        $G_s^{(i,k)} \leftarrow$  sampled from (4).
10:       $\hat{Y}_s^{(i,k)} \leftarrow \text{GNNC}_{\Phi_1}(\text{GNNE}_{\Phi_0}(G_s^{(i,k)}, X^{(i)}))$ .
11:    end for
12:   end for
13:   Compute loss with (9).
14:   Update parameters  $\Psi$  with backpropagation.
15: end for

```

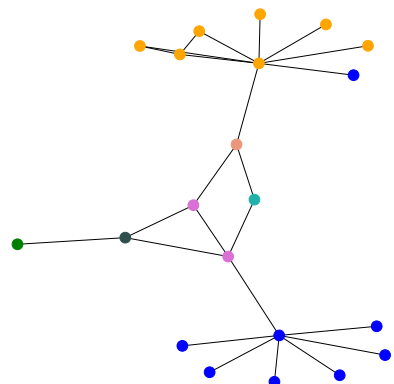
Accuracy	BA-Shapes	BA-Community	Tree-Cycles	Tree-Grid	BA-2Motif	MUTAG
Training	0.98	0.99	0.99	0.92	1.00	0.87
Validation	1.00	0.88	1.00	0.94	1.00	0.89
Testing	0.97	0.93	0.99	0.94	1.00	0.87

Table A.1: Accuracy table for Node and Graph Classification. Reprinted from [43].

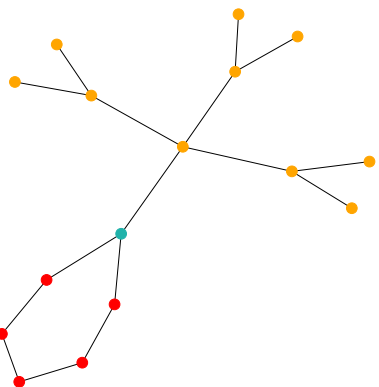
A.2 Data Visualization



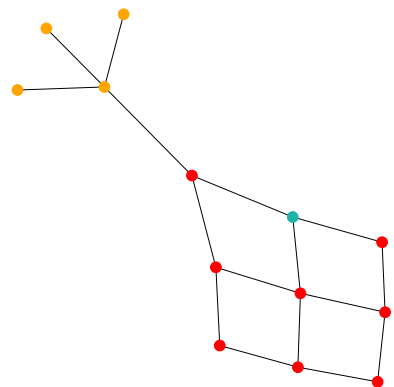
(a) BA-Shapes



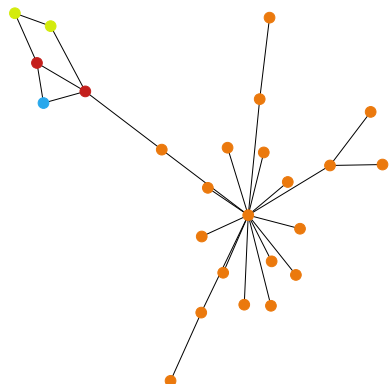
(b) BA-Community



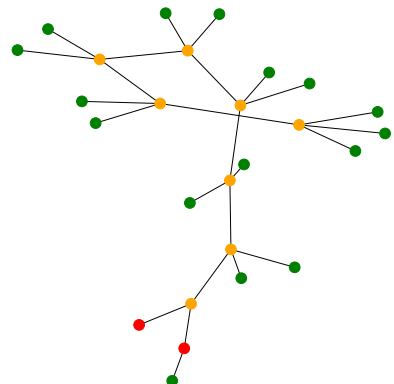
(c) Tree-Cycles



(d) Tree-Grid



(e) BA-2Motif



(f) MUTAG

Figure A.1: Visualization of all six datasets. For node datasets (a-d) the target prediction node where the computational graph is computed from is colored in light blue.

A.3 Replication Hyperparameter Searches

The following tables contain the grid search configurations for the explainer on each target model. The first row includes the configuration used in the original codebase [43] and the second row contains the configurations used in [29]. For BA-Community (see Table A.3) both configurations are identical, and the second row is thus omitted. The last section of each table contains the set of the values that we tested for each parameter. The optimal settings for our explainer implementation are highlighted in each column. Note that we optimize Tree-Cycles (see Table A.4) and BA-2Motif (see Table A.6) towards a minimal metric score, as discussed in Section 5.1.2.

BA-Shapes									
a	K	b	E	η	S	α_e	α_s	τ_0	τ_T
N	1	0.0	10	0.003	-	1.0	0.05	1.0	0.05
N	1	0.0	10	0.003	-	1.0	0.05	5.0	2.0
5	1	0.0	10	0.0003	74	0.1	0.005	5.0	1
	5			0.003	75	0.5	0.05		2
	10			0.03	76	1.0	0.1		5

Table A.2: First two rows show hyperparameter settings used in [43] and [29], respectively. Last section contains our grid search configuration. Bolded values indicate the best performance.

BA-Community									
a	K	b	E	η	S	α_e	α_s	τ_0	τ_T
N	1	0.5	20	0.003	-	1.0	0.05	1.0	1.0
64	1	0.0	20	0.003	74	1.0	0.05	1.0	1.0
	5	0.5		0.0003	75	0.1	0.1		5.0
	10				76				

Table A.3: First row shows hyperparameter settings used in [43] and [29]. Last section contains our grid search configuration. Bolded values indicate the best performance.

Tree-Cycles									
a	K	b	E	η	S	α_e	α_s	τ_0	τ_T
N	1	0.0	20	0.003	-	0.01	0.0001	5.0	5.0
N	1	0.0	20	0.003	-	10.0	0.1	1.0	5.0
5	1	0.0	20	0.0003	74	0.01	0.0001	1.0	1.0
	5			0.003	75	1.0	0.05		5.0
	10				76	10.0	0.1		

Table A.4: First two rows show hyperparameter settings used in [43] and [29], respectively. Last section contains our grid search configuration. Bolded values indicate the best performance.

Tree-Grid									
a	K	b	E	η	S	α_e	α_s	τ_0	τ_T
N	1	0.0	30	0.01	-	1.0	0.01	5.0	5.0
N	1	0.0	30	0.003	-	1.0	1.0	5.0	2.0
24	1	0.0	30	0.0003	74	0.1	0.01	5.0	2.0
	5		30	0.003	75	1.0	0.5		5.0
	10		30	0.01	76	10	1.0		
				0.05					

Table A.5: First two rows show hyperparameter settings used in [43] and [29], respectively. Last section contains our grid search configuration. Bolded values indicate the best performance.

BA-2Motif									
a	K	b	E	η	S	α_e	α_s	τ_0	τ_T
N	1	0.0	10	0.003	-	0.0	0.00	1.0	0.0
N	1	0.0	20	0.005	-	0.01	0.03	5.0	1.0
30	1	0.0	10	0.0003	74	0.01	0.03	5.0	1.0
	5		20	0.003	75	0.1			5.0
	10			0.005	76				
				0.01					

Table A.6: First two rows show hyperparameter settings used in [43] and [29], respectively. Last section contains our grid search configuration. Bolded values indicate the best performance.

MUTAG									
a	K	b	E	η	S	α_e	α_s	τ_0	τ_T
N	1	0.0	10	0.01	-	1.0	0.01	5.0	5.0
N	1	0.0	30	0.0003	-	1.0	0.005	5.0	5.0
30	1	0.0	10	0.0003	74	0.1	0.01	5.0	1.0
	5		20	0.003	75	1.0	0.005		5.0
	10		30	0.01	76				

Table A.7: First two rows show hyperparameter settings used in [43] and [29], respectively. Last section contains our grid search configuration. Bolded values indicate the best performance.

A.4 Multiple Explanation Visualizations

The following figures A.2, A.3, A.4, A.5, A.6, A.7 contain 16 randomly sampled explanations for the best explainer model of every dataset. For graph tasks all nodes of the input graph are included, while for node tasks only the nodes of the local computation graph from the prediction motif node are shown.

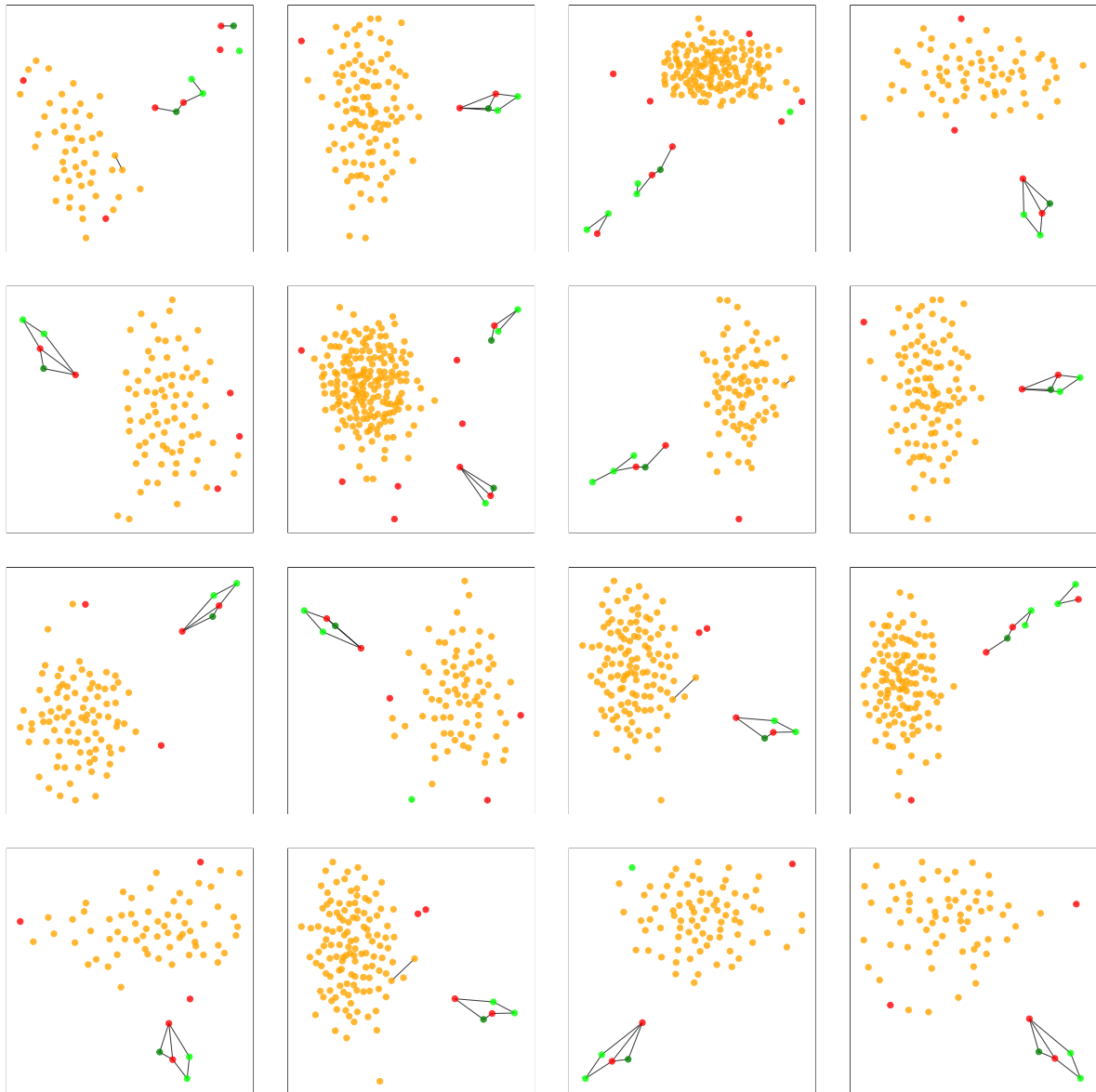


Figure A.2: Grid of BA-Shapes explanations (top-6 edges).

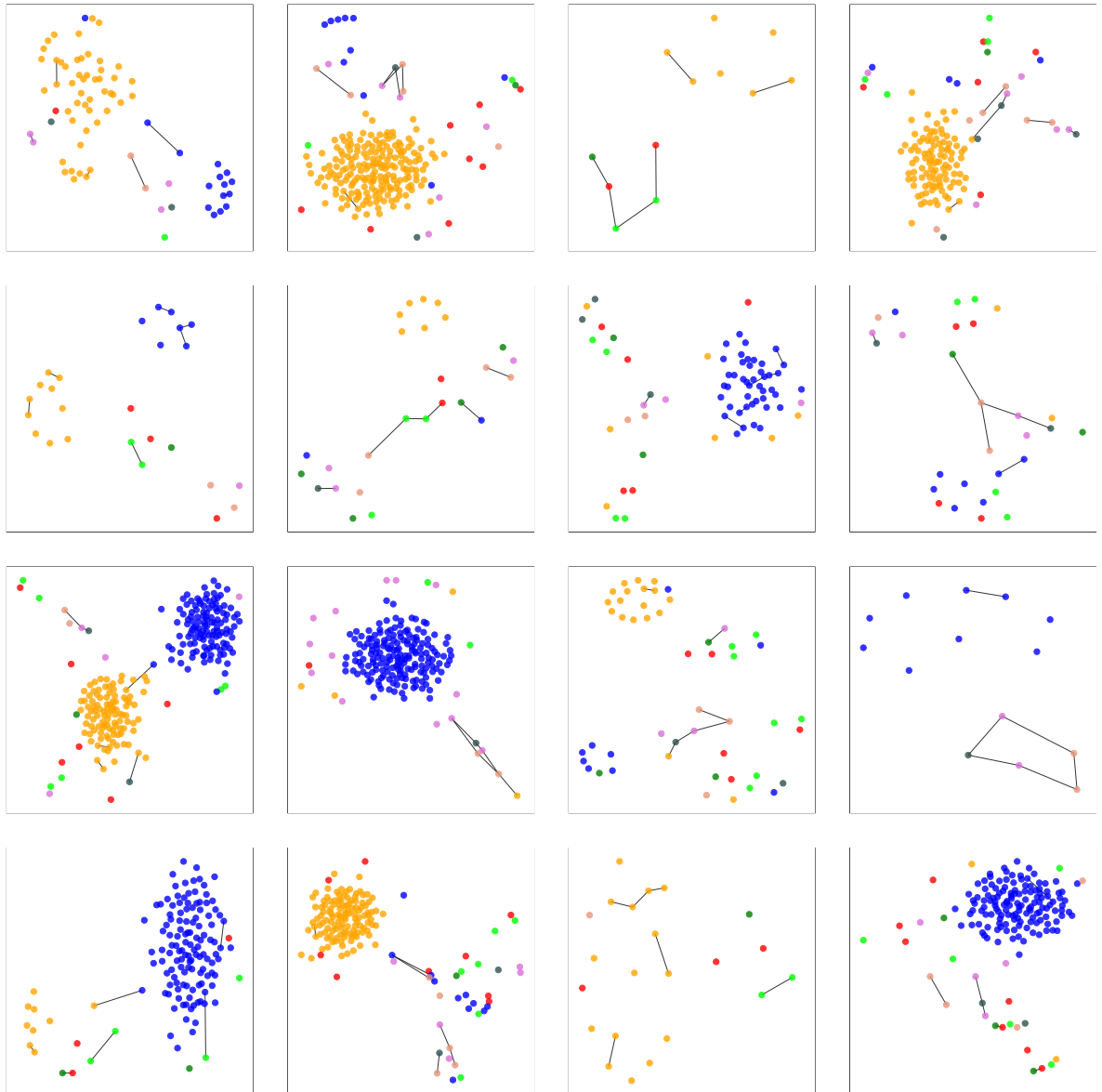


Figure A.3: Grid of BA-Community explanations (top-6 edges).

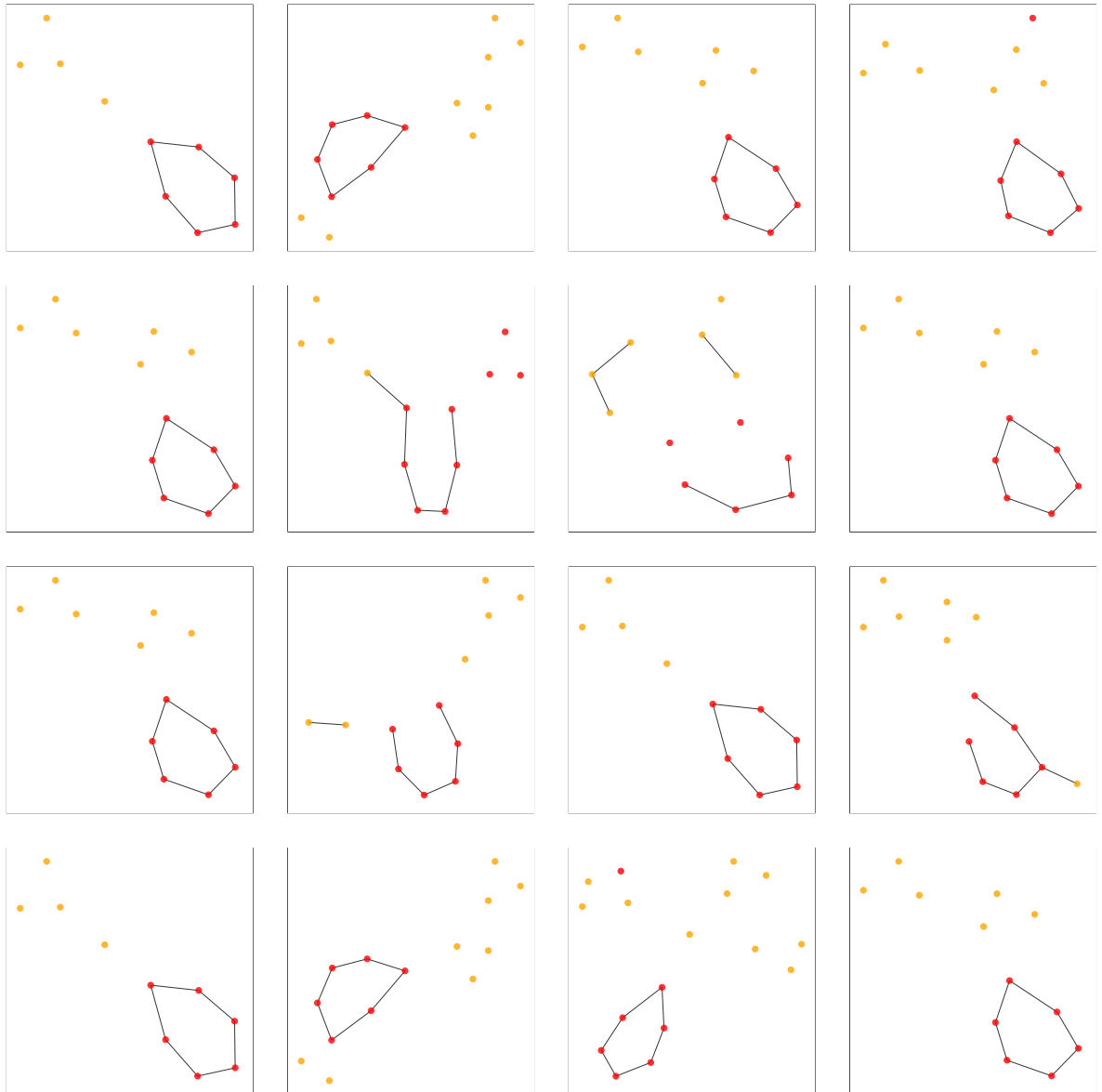


Figure A.4: Grid of Tree-Cycles explanations (top-6 edges).

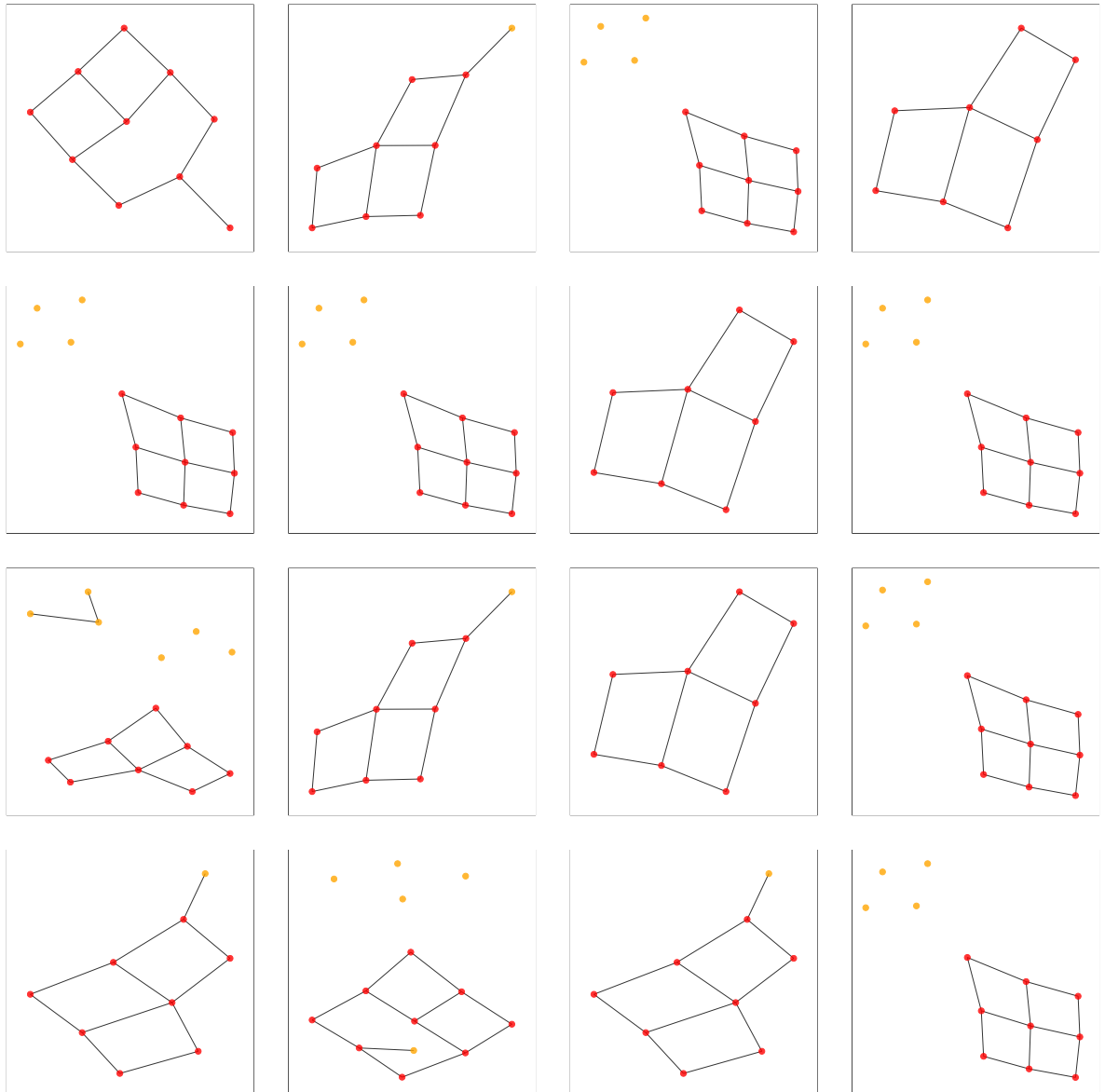


Figure A.5: Grid of Tree-Grid explanations (top-12 edges).

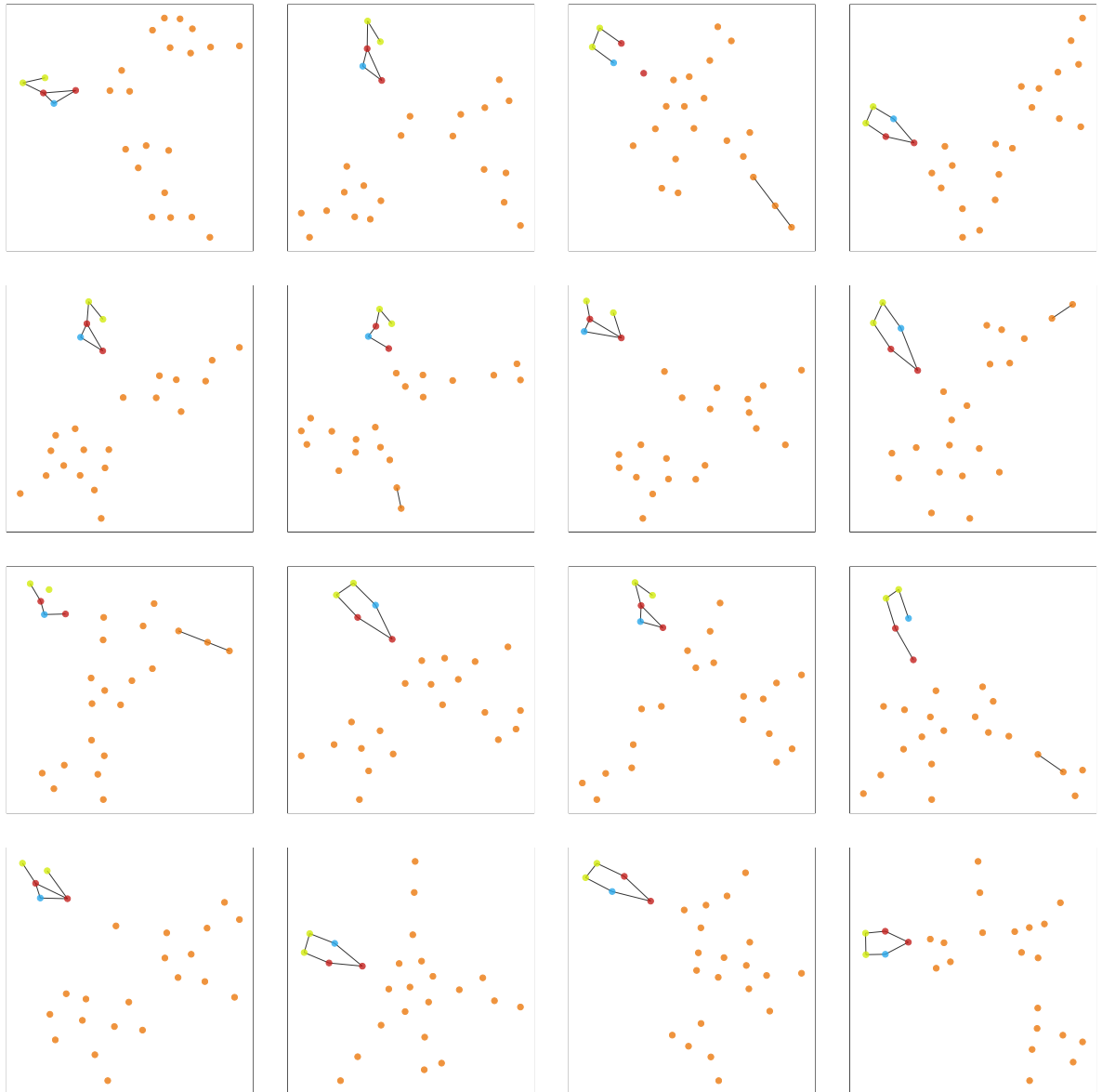


Figure A.6: Grid of BA-2Motif explanations (top-5 edges).



Figure A.7: Grid of MUTAG explanations (top-10 edges).

A.5 NeuroSAT Explainer Hyperparameter Searches

The following tables contain the grid search configurations for the NeuroSAT explainer models with either the soft constraint (see Table A.8) or the hard constraint (see Table A.9) applied. The columns contain the values tested for the corresponding hyperparameter. The optimal settings for each explainer implementation are highlighted. Figure A.8 shows the AUROC range of all runs performed in the grid search for the soft constraint explainer.

Soft Constraint Explainer										
K	E	η	S	α_e	α_s	τ_0	τ_T	α_{concat}	α_C	α_{AdamW}
1	20	0.0003	75	0.1	0.001	5.0	1.0	False	0.1	False
5	30	0.003	76	1.0	0.01		5.0	True	1.0	True
	50	0.01			0.1				10.0	

Table A.8: Grid search results over the defined hyperparameter space for the NeuroSAT explainer that uses a soft constraint. Bolded values indicate the best performance.

Hard Constraint Explainer									
K	E	η	S	α_e	α_s	τ_0	τ_T	α_{concat}	α_{arch}
1	20	0.00003	75	0.1	0.01	5.0	1.0	False	False
5	30	0.0003	76	1.0	0.1		5.0	True	True
	50	0.003			1.0				
		0.01							

Table A.9: Grid search results over the defined hyperparameter space for the NeuroSAT explainer that uses a hard constraint. Bolded values indicate the best performance.

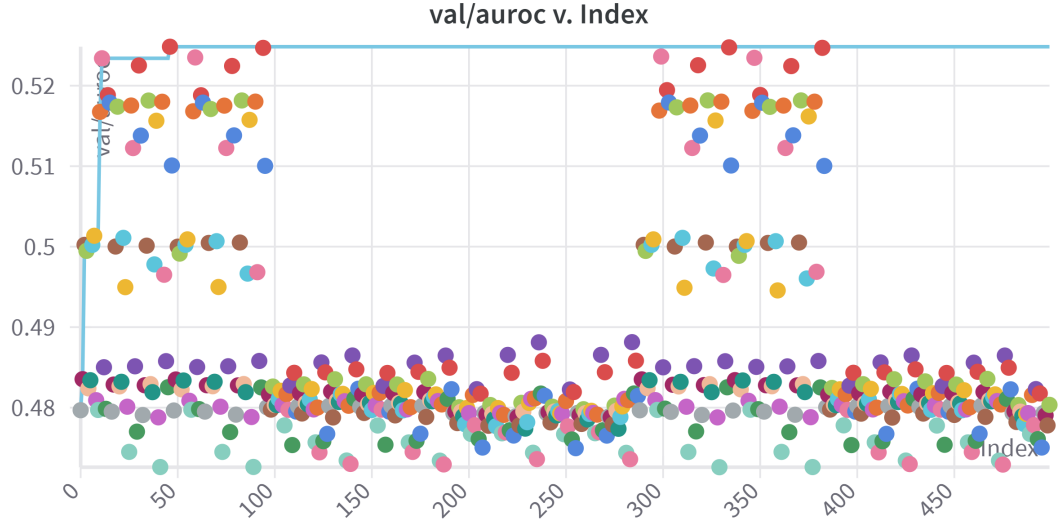


Figure A.8: Grid search results of all runs on the soft constraint explainer using WandB [7].

A.6 Satisfiability of a Hard Constraint Explanation

The SAT formula represented by the top- k edges of the validation problem that achieved the highest individual AUROC score for the seed 0 run, with k being the number of edges in its corresponding MUS, is defined as:

$$\begin{aligned}
 & (174 \vee 175 \vee 173 \vee 169) \wedge \\
 & (171 \vee 170 \vee 173) \wedge \\
 & (171 \vee 175 \vee 168 \vee 173) \wedge \\
 & (172 \vee 174 \vee 171) \wedge \\
 & (171 \vee 169 \vee 168 \vee 174) \wedge \\
 & (\neg 170) \wedge \\
 & (170 \vee 173 \vee 168) \wedge \\
 & (\neg 168 \vee 171) \wedge \\
 & (172 \vee \neg 168 \vee \neg 170) \wedge \\
 & (169 \vee 171 \vee 172 \vee \neg 174) \wedge \\
 & (175 \vee 173 \vee 168)
 \end{aligned}$$

We note that this subset of clauses is satisfiable and therefore not an unsatisfiable core. It is important to note that setting k as the number of edges in its corresponding MUS only makes sense if the MUS is known to be the GT. Since we do not know this, this selection of k can be seen as arbitrary. However, a selection is necessary in the context of

PGExplainer, since a dynamic way of getting the most important explanation edges was not provided in the original.

Eidesstattliche Versicherung

(Affidavit)

Schulz, Tristan Martin Lewin

Name, Vorname
(surname, first name)

Bachelorarbeit
(Bachelor's thesis)

Titel
(Title)

Providing Bipartite GNN Explanations with PGExplainer

221803

Matrikelnummer
(student ID number)

Masterarbeit
(Master's thesis)

Ich versichere hiermit an Eides statt, dass ich die vorliegende Abschlussarbeit mit dem oben genannten Titel selbstständig und ohne unzulässige fremde Hilfe erbracht habe. Ich habe keine anderen als die angegebenen Quellen und Hilfsmittel benutzt sowie wörtliche und sinngemäße Zitate kenntlich gemacht. Die Arbeit hat in gleicher oder ähnlicher Form noch keiner Prüfungsbehörde vorgelegen.

I declare in lieu of oath that I have completed the present thesis with the above-mentioned title independently and without any unauthorized assistance. I have not used any other sources or aids than the ones listed and have documented quotations and paraphrases as such. The thesis in its current or similar version has not been submitted to an auditing institution before.

Dortmund, 19.05.2025

Ort, Datum
(place, date)

T. Schulz

Unterschrift
(signature)

Belehrung:

Wer vorsätzlich gegen eine die Täuschung über Prüfungsleistungen betreffende Regelung einer Hochschulprüfungsordnung verstößt, handelt ordnungswidrig. Die Ordnungswidrigkeit kann mit einer Geldbuße von bis zu 50.000,00 € geahndet werden. Zuständige Verwaltungsbehörde für die Verfolgung und Ahndung von Ordnungswidrigkeiten ist der Kanzler/die Kanzlerin der Technischen Universität Dortmund. Im Falle eines mehrfachen oder sonstigen schwerwiegenden Täuschungsversuches kann der Prüfling zudem exmatrikuliert werden. (§ 63 Abs. 5 Hochschulgesetz - HG -).

Die Abgabe einer falschen Versicherung an Eides statt wird mit Freiheitsstrafe bis zu 3 Jahren oder mit Geldstrafe bestraft.

Die Technische Universität Dortmund wird ggf. elektronische Vergleichswerkzeuge (wie z.B. die Software „turnitin“) zur Überprüfung von Ordnungswidrigkeiten in Prüfungsverfahren nutzen.

Die oben stehende Belehrung habe ich zur Kenntnis genommen:

Official notification:

Any person who intentionally breaches any regulation of university examination regulations relating to deception in examination performance is acting improperly. This offense can be punished with a fine of up to EUR 50,000.00. The competent administrative authority for the pursuit and prosecution of offenses of this type is the Chancellor of TU Dortmund University. In the case of multiple or other serious attempts at deception, the examinee can also be unenrolled, Section 63 (5) North Rhine-Westphalia Higher Education Act (*Hochschulgesetz, HG*).

The submission of a false affidavit will be punished with a prison sentence of up to three years or a fine.

As may be necessary, TU Dortmund University will make use of electronic plagiarism-prevention tools (e.g. the "turnitin" service) in order to monitor violations during the examination procedures.

I have taken note of the above official notification.*

Dortmund, 19.05.2025

Ort, Datum
(place, date)

T. Schulz

Unterschrift
(signature)

*Please be aware that solely the German version of the affidavit ("Eidesstattliche Versicherung") for the Bachelor's/ Master's thesis is the official and legally binding version.